ERDC TR-18-2

US Army Corps
of Engineers®
Engineer Research and
Development Center

ERDC
INNOVATIVE SOLUTIONS
for a safer, better world

Miter Gate Gap Detection Using Principal Component Analysis

Brian A. Eick, Zachary R. Treece, Billie F. Spencer Jr., Matthew D. Smith, Steven C. Sweeney, Quincy G. Alexander, and Stuart D. Foltz

April 2018

U.S. Army Engineer Research and Development Center

The U.S. Army Engineer Research and Development Center (ERDC) solves the nation's toughest engineering and environmental challenges. ERDC develops innovative solutions in civil and military engineering, geospatial sciences, water resources, and environmental sciences for the Army, the Department of Defense, civilian agencies, and our nation's public good. Find out more at www.erdc.usace.army.mil.

To search for other technical reports published by ERDC, visit the ERDC online library at http://acwc.sdp.sirsi.net/client/default.

ERDC TR-18-2
April 2018

Miter Gate Gap Detection Using Principal Component Analysis

Brian A. Eick, Zachary R. Treece, and Billie F. Spencer Jr.

Department of Civil and Environmental Engineering
University of Illinois, Urbana-Champaign
205 N. Mathews Ave.
Urbana, IL 61801-2352

Steven C. Sweeney, and Stuart D. Foltz

Construction Engineering Research Laboratory
U.S. Army Engineer Research and Development Center
2902 Newmark Drive
Champaign, IL 61822

Matthew D. Smith

Coastal and Hydraulics Laboratory
U.S. Army Engineer Research and Development Center
3909 Halls Ferry Road
Vicksburg, MS 39180-6199

Quincy G. Alexander

Information Technology Laboratory
U.S. Army Engineer Research and Development Center
3909 Halls Ferry Road
Vicksburg, MS 39180-6199

Final Report

Prepared for Headquarters, U.S. Army Corps of Engineers
Washington, DC 20314-1000

Under Navigation Systems Research Program

Abstract

The U.S. Army Corps of Engineers (USACE) operates and maintains 236 lock chambers at 191 lock sites on 41 waterways throughout the contiguous United States. Waterway navigational locks are important parts of the nation's infrastructure. Locks enable the flow of billions of dollars of commerce and support efforts for flood control. Proper maintenance of the locks and early detection of damage is crucial; however, due to shrinking budgets, adequate funding to apply traditional scheduled maintenance and visual inspection is not available. Structural health monitoring (SHM) systems have been considered to assist in establishing more efficient maintenance, repair, and replacement priorities for navigational locks. This work was undertaken to develop and implement a real-time methodology that provides lock operators with a robust, accurate warning system of gap(s) at the gate-to-wall interface. This initial effort, which focused on horizontally framed miter gates and on damage that is assumed to take the form of a gap at the gate/wall interface (quoin), developed a methodology to identify the occurrence of damage in miter gate structures using data from strain and water level gages that is collected continuously from the SHM system deployed by USACE.

Contents

Figures and Tables

Figures

Tables

Preface

This study was conducted for Headquarters, U.S. Army Corps of Engineers (HQUSACE) under the Navigation Systems Research Program, "Project Structural Monitoring System for Lock Structures to Prevent Failure." The Program Manager was Charles E. Wiggins (CEERD-HVT).

The work was performed under the direction of the Materials and Structures Branch (CFM) of the Facilities Division (CF), U.S. Army Engineer Research and Development Center – Construction Engineering Research Laboratory (ERDC-CERL). At the time of publication, Vicki VanBlaricum was Chief, CEERD-CFM; Donald Hicks was Chief, CEERD-CF; and W. Jeff Lillycrop (CEERD-HVT) was the Technical Director for Civil Works. The Interim Deputy Director of ERDC-CERL was Michelle Hanson, and the Interim Director was Dr. Kirankumar Topudurti.

COL Bryan S. Green was Commander of ERDC, and Dr. David W. Pittman was the Director.

THIS PAGE INTENTIONALLY LEFT BLANK

1 Introduction

1.1 Background

Waterway navigational locks are important parts of the nation's infrastructure. Locks enable the flow of billions of dollars of commerce and support efforts for flood control. For example, one modern 15 barge tow (a common mode of commercial transport on the Mississippi River) is capable of transporting upwards of 26,000 tons of goods, equivalent to 1050 semi-trucks or 240 rail cars. At Lock 26 on the Mississippi River alone, more than 60 million tons of goods passed through the locks in 2014 (USACE 2015). Due to the interconnected nature of inland waterways, downtime for routine maintenance or unexpected failure of one set of locks can cause extensive, costly delays to shipping through large parts of the waterway.

Proper maintenance of the locks and early detection of damage is crucial; however, due to shrinking budgets, adequate funding to apply traditional scheduled maintenance and visual inspection is not available. The U.S. Army Corps of Engineers (USACE 2015) estimated that an investment of $13 billion dollars in inland waterways would be required between 2013 and 2020 to keep delays on these waterways from growing beyond their current level; however, only $7 billion dollars has been projected to be budgeted during this time period (ASCE 2013). As a result of this shortfall in funding, inspection and maintenance of the nation's locks has fallen behind schedule. A consequent increased rate of unexpected failure and more extensive repairs can be expected in the future. Early evidence of failures due to delayed maintenance and inspection include the high profile unexpected failures at the Markland Lock and Dam in September of 2009 (Chapman 2010) and the Chickamauga Lock and Dam in October of 2014 (Murray 2014).

1.1.1 Overview of lock and dam sites

USACE operates and maintains 236 lock chambers at 191 lock sites on 41 waterways throughout the contiguous United States (USACE 2014). Before the construction of the lock and dam system present today, inland navigation was difficult and precarious due to rapids, waterfalls, and varying river channel location and depth resulting from sediment deposit and flow rate changes. A barge traveling from St. Paul, MN to St. Louis, MO along the

Mississippi River would have had to navigate a 400-ft elevation change during its journey. In 1933, work commenced to create a reliable method for inland waterway transportation via a lock and dam system (MDNR 2004).

A lock and dam site is an elevator for waterway traffic (Figure 1). A vessel enters the lock, the stern gate is closed, and depending on the direction of travel, the water in the lock is either raised or drained to match the water level opposite of the bow gate. Once the water levels align, the bow gate opens and the vessel proceeds on its route. In Figure 1, the bow gate is the upstream gate, and the stern gate is downstream.

Figure 1. Typical lockage procedure: (a) ship enters lock, (b) gates close and chamber water levels rise, and (c) ship leaves the lock.

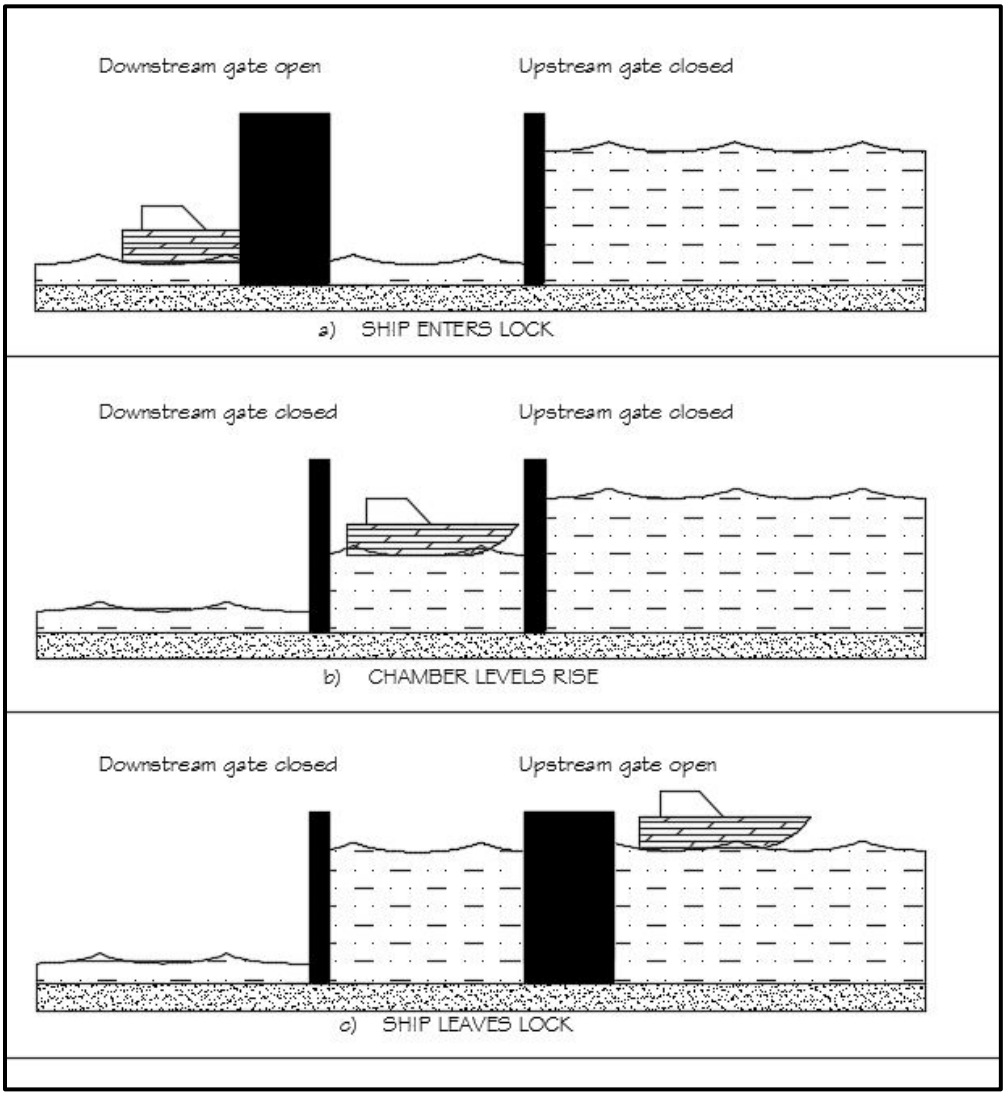

1.1.2 Miter gates

Miter lock gates are the most common gate type found at USACE lock and dam sites (USACE 2015). Characterized by their primary load carrying members, miter gates are either vertically framed (using vertical steel girders) or horizontally framed (using horizontal steel girders). A miter gate consists of two leaves, which, when closed, are referred to as "mitered" and dam the water on the upstream side. Figure 2 shows a typical elevation view of one leaf of a horizontally framed miter gate.*

During a lockage, when the gates are closed and the chamber filled, the lock gates form an angle of 60 to 70 degrees with the wall of the lock chamber resulting in an angle of approximately 126 degrees between the two intersecting gates (Figure 3).

Figure 2. Typical horizontally framed miter gate elevation (one leaf shown).

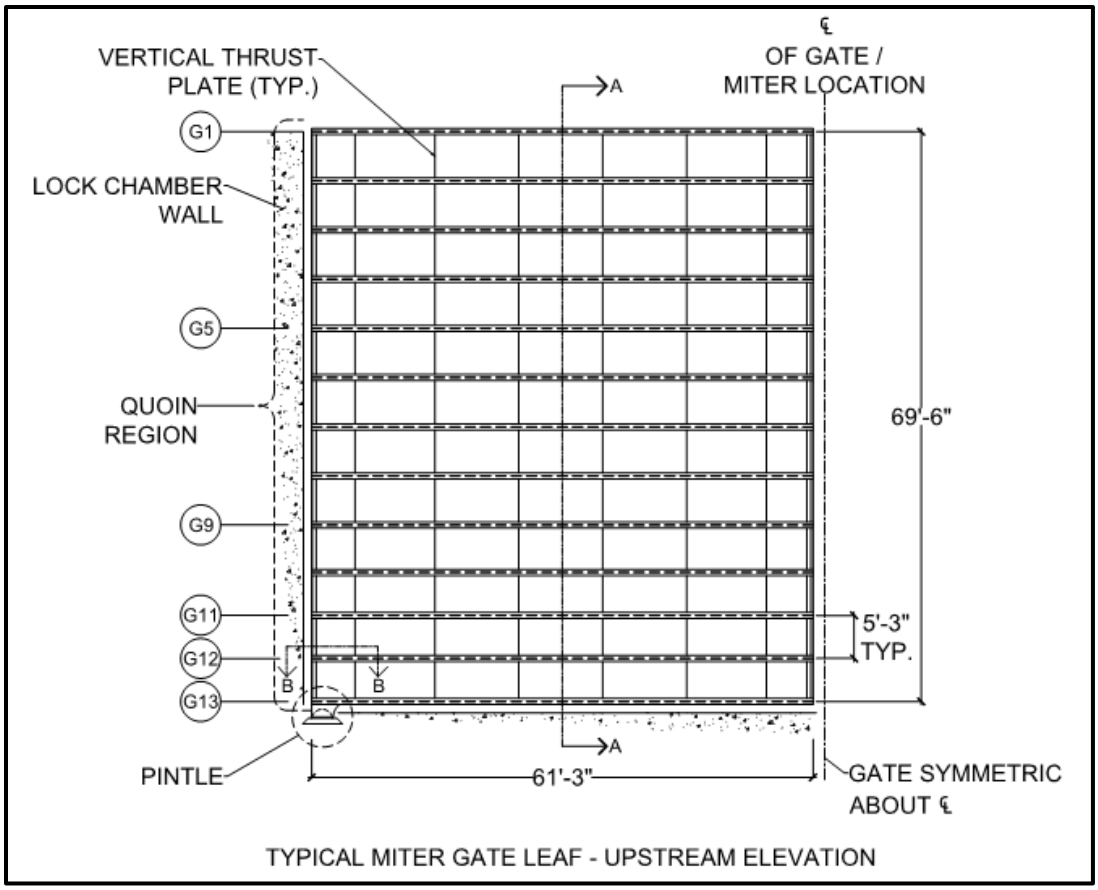

* The lock gates used as the case study for this report are horizontally framed, so the reader may assume throughout the report that the terms "lock gates" or "miter lock gates" refer to horizontally framed steel miter gates unless explicitly stated otherwise.

Figure 3. Typical miter gate plan view.

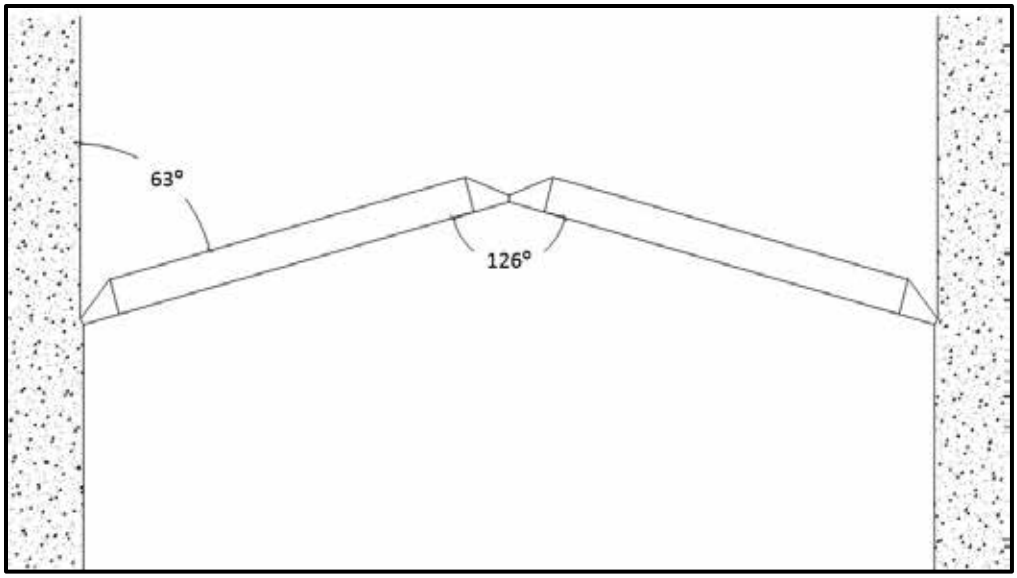

The boundary conditions at the gate-to-wall intersection (quoin) and between the two gates in the center of the chamber behave as pins, resulting in three-hinged arch behavior of the gates in their closed position. When the water level in the lock chamber differs from the water level outside the chamber, a load is placed on the gate that needs to be transferred to the lock wall. Under normal operating conditions, negligible moment is present at the ends of the gates, and the entire load transfers as axial compression through the girders and into the wall of the lock chamber. Figure 4 shows a schematic of the load transfer mechanism.

Figure 4. (a) Load scenario for miter gate; (b) Load path through girder to wall.

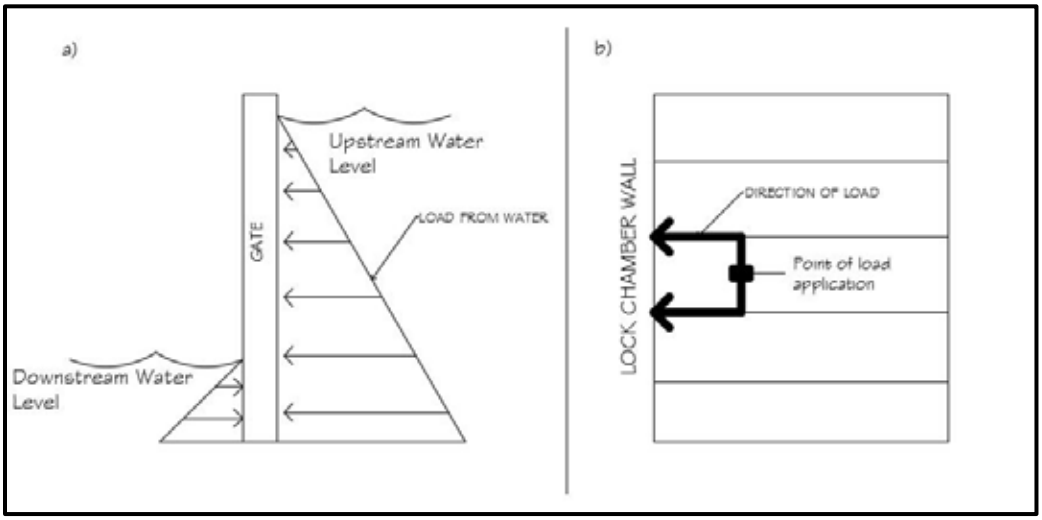

1.1.3 Problems associated with miter gates

Problems typically observed with miter gates during inspection include: fatigue cracking in the gate members, skin plate, and ball and socket joint (known as the pintle); damage from barge impact; corrosion; gate-misalignment caused by loss of tension in the diagonals; loss of contact or the formation of a gap at the gate/wall interface and the gate/gate interface; and general wear and deterioration of gate components (James and Zhang 1996).

The formation of a gap between the quoin of a miter gate and the wall of a lock chamber can occur as a discrete event, slowly over a period of weeks to months, or by some combination thereof. Gaps are different from other damage scenarios in that they themselves do not result in immediate damage to the gate in the same way, for instance, that a barge impact might. A gap changes the load path of the gate, forcing loads to redistribute, resulting in higher forces and stresses in other parts of the gate. The higher stresses become problematic, especially in the pintle region, which is prone to fatigue damage. The fatigue life of a structural component is dependent on both the number of loading cycles and the magnitude of the range of loads throughout each cycle, with the fatigue life declining as the stress range in the component increases. If a gap forms, it will result in higher stresses in fatigue prone structural components during loading, thereby shortening their fatigue life and in turn shortening the useful life of the gate unless repairs are made.

1.1.4 Current state of lock monitoring

Lock monitoring is generally done via visual inspection, either by dewatering or by sending divers to inspect. Dewatering consists of taking the lock out of service and draining the water. Figure 5 shows an example of dewatering. Due to high costs and funding availability, dewatering occurs less and less frequently (USACE 2016). Moreover, taking a lock out of service is estimated to cost the economy upwards of $3 million per day from goods not making it to market (Gillerman 2013). Sending divers has limited benefits, as underwater visibility conditions are generally poor, at best. As a result, divers are left with no choice but to feel for the presence of damage and then wait until they get back on land to sketch their findings. Moreover, the non-redundancy in the structure means that sending someone to inspect the gate without prior knowledge of the extent of damage can be a dangerous prospect (USACE 2016).

Figure 5. Maintenance worker inspecting a miter gate with the chamber dewatered.

Source: Rankin (2014).

The unreliable and often impractical nature of performing regular visual inspections of each gate provides the USACE with motivation to investigate alternative methodologies for assessing lock gates.

1.1.5 Structural health monitoring

Due to the need to efficiently allocate limited resources available for the maintenance and inspection of locks, structural health monitoring (SHM) systems have been considered to assist in establishing maintenance, repair, and replacement priorities for navigational locks. SHM is designed with the goal of moving away from a prescribed maintenance schedule to a system where maintenance decisions are made based on information gathered about the condition of the component from the SHM system, as well as limited use of formal visual inspections and assessment of other available information (e.g., perceptible vibrations or noises). These systems are also expected to detect any impending failures before their occurrence, as well as operational problems that acutely present themselves.

SHM is a process of detecting damage and characterizing the state of a structure by observing the structure over some period of time in the form of taking measurements at periodic intervals. A damage sensitive feature is extracted from the measurements, the statistics of which are analyzed to determine the health of the structure. The presence of damage in the structure will manifest itself as a change in the statistics of the damage

sensitive feature. A successful structural health monitoring program can be seen as having the goal of answering the following four questions (Farrar 2012):

1. Is there damage?
2. Where is the damage?
3. How much damage is there?
4. How much longer can the structure be used safely?

The implementation of an SHM plan requires data acquisition and processing, the selection of a damage sensitive feature, and appropriate statistical modeling to properly discriminate between true damage indicators and inherent random variations in the system. The discernment between true damage and system variability is critical to the success of an SHM program, because Type 1 and Type 2 errors (defined, respectively, as false positives and false negatives) need to be kept to an absolute minimum. Figure 6 shows a flowchart outlining the SHM process. The flowchart highlights the goals of continuous monitoring for SHM, as the program would continue without end for the life of the structure.

To date, SHM has found limited application to lock gates. Greimann, Stecker, and Rens (1991) implemented a simple monitoring procedure on lock gates in 1990. In the study, data from the gate were manually recorded during inspections and compared to the expected performance of the gate. An empirical condition index was developed to use as a decision making tool. As data were not collected continuously, this study can be seen as a precursor to SHM of lock gates.

Commander, Schulz, and Goble (1994) investigated detection of damage in miter gates by comparing strain measurements. The study was limited to types of damage that would lead to cross-section loss of structural members (e.g., cracks or corrosion), as the damage considered was simulated in a Finite Element Model (FEM) by reducing the Young's modulus of a member. The detection method relied heavily on manual inspection of data plots and on updating their FEM to match the damaged case. One of the metrics used in this study to detect damage is the correlation coefficient between monitored strain and the known undamaged strain. The correlation coefficient is measured on a strain-gage-by-strain-gage basis, and multivariate statistics were not considered. Finally, temperature effects on monitored strain values were not considered.

Figure 6. Flowchart of a structural health monitoring program.

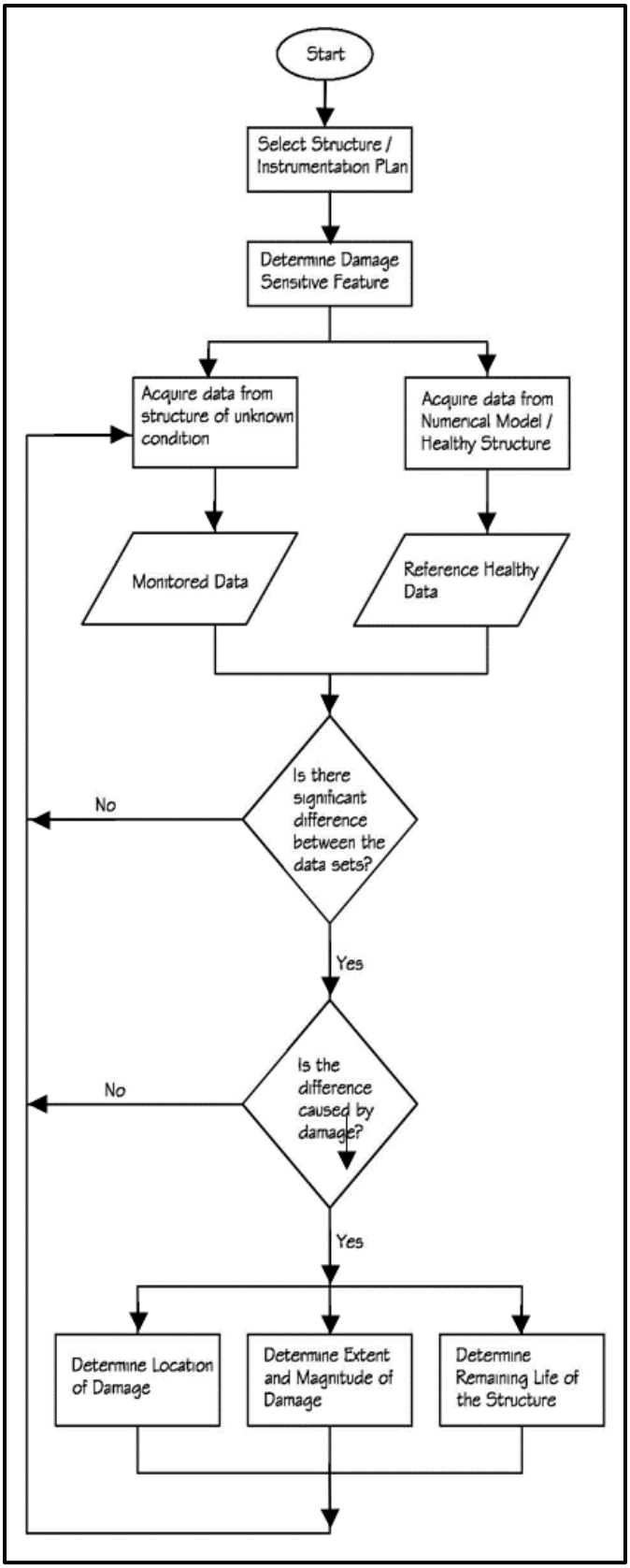

McAllister, et al. (2001) developed a reliability-based assessment method for existing miter gates calculating the probability of failure conditioned on detected flaw sizes. The study included uncertainty in strength, applied loads, flaw size, flaw detection, and flaw propagation. The goal of their study was to provide an estimate of the remaining life of a miter gate, given some detected flaws.

Estes, Frangopol, and Foltz (2004) implemented a Bayesian updating methodology to include data obtained in the field to reassess the reliability of a miter gate. Though these studies do not explicitly focus on damage detection, the concepts presented therein can be applied in a SHM program.

More research is required to take advantage of the potential offered by SHM for the USACE. The U.S. Army Engineering Research and Development Center (ERDC) intends to use SHM as one tool in a larger system-wide value and consequence modeling scheme. SHM is to be employed to provide data that will allow ERDC to characterize the current state of a structure. This current state of the structure is then used in conjunction with probabilistic models for future structural events to determine an expected remaining life of the structure. A consequence model is then developed to determine the effect of any action or inaction to remedy the damage detected from the SHM system, and a value is assigned to each action alternative to determine how each alternative meets USACE's mission. The value and consequence model framework will facilitate prioritization of maintenance and repairs and optimize the use of available funding. The research presented herein is intended to help USACE/ERDC toward achieving this vision of the future.

1.2 Objective

The objective of this study is to develop a methodology to identify the occurrence of damage in miter gate structures using data from strain and water level gages. For this initial effort, attention is focused on horizontally framed miter gates, where damage is assumed to be of the form of a gap at the gate/wall interface (quoin). The data investigated are collected continuously from the structural health monitoring system deployed by the USACE. The ultimate goal is to implement a robust and accurate warning system that, based on the methodology developed herein, provides a real-time alert of the presence of an unacceptable gap at the quoin.

1.3 Approach

The damage detection methodology is developed using statistical methods that incorporate data from multiple locations on the gate, and combines them into a single, statistically significant metric used to evaluate structural health and condition. The explicit intention of the approach described in this report was to develop a fully automated process.

Chapter 2 provides the necessary mathematical background required for this research. Appropriate data classification schemes are introduced, and the concept of data stationarity is explained. The statistical methods used to analyze the data in the study are then presented, with a specific focus on principal component analysis (PCA). The chapter concludes with a method for reducing the occurrence of false positive damage identification by use of the probability of consecutive observations above a specific damage threshold, given no damage is present.

Chapter 3 provides an overview of the structural health monitoring program developed by the USACE for lock gates, known as SMART (Structural Monitoring and Analysis in Real Time) Gate. The type of data collected by the system is explored and a selection is made for the ideal candidate for gap detection; namely, strain. The problems with strain, by itself, as a damage indicator are subsequently discussed (e.g., temperature sensitivity and long periods of gate inactivity, etc.).

Chapter 4 describes the proposed damage detection methodology, including applying the methods discussed in Chapter 2 to the data collected from the lock gates. A new damage sensitive feature, defined as the derivative of the strain with respect to the water height, herein referred to as slope, is introduced and is shown to be stationary, nominally free from environmental effects. The use of slope is additionally seen to effectively remove the long periods of gate inactivity from the data, increasing the computational efficiency of data processing.

Chapter 5 validates the proposed method through an example employing data collected at the Greenup lock and dam site. An overview of the instrumentation at the Greenup site is first presented, along with the data acquisition parameters. The assumptions of stationarity and temperature independence of slopes are further confirmed with the measured data at Greenup. A method for damage simulation using results from a finite ele-

ment model is explained, as is the method of imposing the damaged response onto the measured data. The chapter concludes with the presentation of a successful application of PCA to detect the presence of the simulated gap.

Chapter 6 summarizes the research detailed in this report, and Chapter 7 presents recommendations for future research on SHM of locks that builds on the research reported herein. Future research efforts on SHM of locks are expected to take the form of the remaining three steps of the SHM process namely, localize the damage, quantify the damage, and determine the remaining life of the structure. These are logical next steps in the process to develop practical, deployable, structural health monitoring systems for miter gates operated by USACE.

1.4 Scope

For this study, the change in strain resulting from a redistribution of load caused by the gap to be detected is used as the quantity to investigate. Changes in strain caused by temperature are specifically identified and addressed. Though this study focuses on the detection of gate/wall interface gaps, the methodology developed herein is expected to be readily extendable to detect other types of damage as well.

2 Mathematical Preliminaries

Implementation of an SHM program by the USACE will result in large amounts of data to be processed and analyzed. This chapter provides the background needed to analyze the available data. First, it introduces the ways that data are classified with a focus on the notions of time series and stationarity. Then, with the data appropriately classified, it discusses methods to analyze the data, with a particular focus on a technique known as PCA. Finally, it examines methods for discriminating outliers in the data.

2.1 Data classification

For this study, the collected data take the form of time series, which is a discrete sequence of data points sampled on a continuous time interval that may have equal spacing between samples. Prado and West (2010) provide a good introduction on time series notation and definitions; their conventions will be used in this report. For the case of a time series with equally spaced samples, a common notation for the observations of the time series is $\bar{A}_{\bar{A}}$ with $(\bar{A}=\ldots,-1,0,1,2,\ldots)$. For the case where samples are not taken with equal spacing, the notation is $\bar{A}_{\bar{A}_{\bar{A}}}$ with $\bar{A}_{\bar{A}}-\bar{A}_{\bar{A}-1}$ not necessarily equal to one. A time series process is a collection of random variables $\bar{A}_{\bar{A}}$ indexed in time and is represented as $\{\bar{A}_{\bar{A}}, \bar{A}\in \bar{A}\}$, or simply $\{\bar{A}_{\bar{A}}\}$ where *T* is an index set of real integers. A time series process is described by the joint cumulative distribution of the sequence of random variables $\{\bar{A}_{\bar{A}}\}$, given by:

$$\bar{A}_{\bar{A}_{\bar{A}}}\left(\bar{A}_1,\bar{A}_2,\ldots,\bar{A}_{\bar{A}_{\bar{A}}}\right)=\bar{A}\left\{\bar{A}_1\le\bar{A}_1,\bar{A}_2\le\bar{A}_2,\ldots,\bar{A}_{\bar{A}_{\bar{A}}}\le\bar{A}_{\bar{A}_{\bar{A}}}\right\} \tag{2-1}$$

Where $\bar{A}_1$ is the first sample of the realization of $\{\bar{A}_{\bar{A}}\}$, $\bar{A}_2$ is the second sample, and so on, and $\bar{A}_{\bar{A}}$ are the number of samples taken. The marginal cumulative distribution function of each individual random variable is also frequently specified, i.e.:

$$\bar{A}_{\bar{A}_{\bar{A}}}(\bar{A})=\bar{A}\{\bar{A}_{\bar{A}}\le\bar{A}\} \tag{2-2}$$

or equivalently, the marginal density function:

$$\bar{A}_{\bar{A}_{\bar{A}}}(\bar{A})=\frac{\bar{A}\bar{A}_{\bar{A}_{\bar{A}}}(\bar{A})}{\bar{A}\bar{A}} \tag{2-3}$$

The set of all possible realizations of the random process is called the ensemble. The ensemble average of the random process, or the mean, is written as:

$$\bar{A}_{\bar{A}_{\bar{A}}}=\bar{A}[\bar{A}_{\bar{A}}]=\int_{-\infty}^{\infty}\bar{A}\bar{A}_{\bar{A}_{\bar{A}}}(\bar{A})\bar{A}\bar{A} \tag{2-4}$$

where $\bar{A}[\cdot]$ is the expectation operator. Similarly, the variance of the random process at time t is:

$$\bar{A}^2_{\bar{A}_{\bar{A}}} = \bar{A}\left[\{\bar{A}_{\bar{A}} - \bar{A}_{\bar{A}_{\bar{A}}}\}^2\right] = \int_{-\infty}^{\infty}\{\bar{A} - \bar{A}_{\bar{A}_{\bar{A}}}\}^2 \bar{A}_{\bar{A}_{\bar{A}}}(\bar{A})\bar{A}\bar{A} \quad (2\text{-}5)$$

The ensemble average of $\bar{A}_{\bar{A}}$ can be better understood by examining the sample mean value of $\bar{A}_{\bar{A}}$. Consider the time series process $\{\bar{A}_{\bar{A}}\}$ sampled N_p times under identical conditions such that there were N_p realizations of each random variable $\bar{A}_{\bar{A}}$. The sample mean is given by:

$$\overline{\bar{A}_{\bar{A}}} = \frac{1}{\bar{A}_{\bar{A}}}\sum_{\bar{A}=1}^{\bar{A}_{\bar{A}}} \bar{A}_{\bar{A}}^{(\bar{A})} \quad (2\text{-}6)$$

where $\bar{A}_{\bar{A}}^{(\bar{A})}$ is the i^{th} realization of x at time t. The auto-covariance of $\{\bar{A}_{\bar{A}}\}$ is formally defined as:

$$\bar{A}_{\bar{A}}(\bar{A},\bar{A}) = \bar{A}\bar{A}\bar{A}\left(\bar{A}_{\bar{A}}, \bar{A}_{\bar{A}}\right) = \bar{A}\left[\left(\bar{A}_{\bar{A}} - \bar{A}_{\bar{A}_{\bar{A}}}\right)\left(\bar{A}_{\bar{A}} - \bar{A}_{\bar{A}_{\bar{A}}}\right)\right] \quad (2\text{-}7)$$

Much of the theory of time series is built under two important assumptions, stationarity and ergodicity. Determining these features will allow selection of an appropriate method for analyzing the data.

2.1.1 Stationary processes

Often times, the probability distribution of the stochastic process $\{\bar{A}_{\bar{A}}\}$ changes with time, and so the mean, variance, and autocorrelation are a function of time. However, many situations occur where the probability density function (pdf) of a stochastic process does not change with time. When the pdf of a stochastic process does not change with time, the process is said to be stationary. Formally, let $\bar{A}_{\bar{A}_{\bar{A}}}(\bar{A})$ be the joint cumulative distribution of the time series. Then, $\{\bar{A}_{\bar{A}}\}$ is said to be a strictly stationary process if this joint probability distribution does not change with an arbitrary shift in the time axis, τ, i.e.:

$$\bar{A}_{\bar{A}_{\bar{A}}}\left(\bar{A}_1, \bar{A}_2, \ldots \bar{A}_{\bar{A}_{\bar{A}}}\right) = \bar{A}_{\bar{A}_{\bar{A}}}\left(\bar{A}_{1+\bar{A}}, \bar{A}_{2+\bar{A}}, \ldots \bar{A}_{\bar{A}_{\bar{A}}+\bar{A}}\right) \quad (2\text{-}8)$$

Strict stationarity is often difficult to demonstrate for engineering applications, and so the concept of weak stationarity is frequently used synonymously with stationarity in the time-series analysis literature. A process is said to be weakly stationary if the mean value is independent of time, and the auto-covariance is dependent only on the time interval between the

two points considered. Formally, a process is weakly stationary if the following hold true:

$$\bar{A}(\bar{A}_{\bar{A}}) = \bar{A}_{\bar{A}} \tag{2-9}$$

$$\bar{A}\bar{A}\bar{A}\left(\bar{A}_{\bar{A}}\bar{A}_{\bar{A}+\bar{A}}\right) = \bar{A}[(\bar{A}_{\bar{A}} - \bar{A}_{\bar{A}})(\bar{A}_{\bar{A}+\bar{A}} - \bar{A}_{\bar{A}})] = \bar{A}_{\bar{A}} \tag{2-10}$$

where:

$\bar{A}_{\bar{A}}$ = the mean value of $\bar{A}_{\bar{A}}$
$\bar{A}_{\bar{A}}$ = the autocovariance of $\bar{A}_{\bar{A}}$
τ = time interval between two points.

2.1.2 Ergodicity

In time series analysis, only one realization of a time series process is usually available, for example, the Gross Domestic Product (GDP) of the United States in the 20th century, or the annual rainfall in a region. These processes can only be measured once, and thus, taking an ensemble average is not possible; however, a temporal average of the single realization can still be found. Consider the temporal average, $\bar{\bar{A}}_{\bar{A}}$, of all points in the realization such that:

$$\bar{\bar{A}}_{\bar{A}} = \frac{1}{\bar{A}_{\bar{A}}}\sum_{\bar{A}=1}^{\bar{A}_{\bar{A}}} \bar{A}_{\bar{A}} \tag{2-11}$$

Processes in which the temporal average is equal to the ensemble average are called ergodic. An intuitive definition of an ergodic process is one where the statistical properties can be determined from a sufficiently long sample (Farrar 2012). This study had only one record of data for each strain gage, so ergodicity is an important assumption and the measured data will be shown to be well approximated as ergodic for the mean.

2.1.3 Order of integration

Time series can be further classified by what is known as the order of integration (Hamilton 1994). The order of integration of a time series is defined by how many times the series must be differenced before it becomes stationary. Differencing a time series is the process of subtracting two consecutive observations in the time series to form a new series. That is, the differenced time series $\Delta\bar{A}_{\bar{A}}$ is defined as follows:

$$\Delta\bar{A}_{\bar{A}} = \bar{A}_{\bar{A}} - \bar{A}_{\bar{A}-1} \tag{2-12}$$

If a time series is stationary, the series is said to be integrated to order zero and denoted I(0). Similarly, a time series that becomes stationary after differencing once is said to be integrated of order one, or I(1). The determination of the classification of a time series is critical to selecting an appropriate method for analyzing the data. Thus, before exploring the methods for analyzing time series, tests for whether or not a time series is stationary are introduced in the next section. For this study, a time series that can be shown to be approximately stationary will also be assumed to be ergodic.

2.2 Tests for stationarity

To proceed with analyzing the data, the time series of interest must be classified as stationary or nonstationary. The most basic way to assess stationarity is by visual inspection. If the data display obvious trends, such as growth or decay in time, the data are nonstationary. To further quantify a visual inspection, the statistical quantities from Equations 2-9 and 2-10 are investigated. If the mean value is seen to not change over time, and the autocovariance at two equal length intervals are not different, this will provide evidence that process is stationary. However, for many practical applications, the stationarity of data does not manifest itself readily through visual inspection. Accordingly, a more rigorous, statistics-based hypothesis testing is used to determine whether or not a time series is stationary.

2.2.1 Unit roots and the Augmented Dickey-Fuller Test

Tests for stationarity generally take the form of a unit-root test. For this study, the Augmented Dickey-Fuller (ADF) test is used. The ADF test is briefly introduced here for completeness. For a more in-depth treatment, see Hamilton (1994). The first step of the ADF test is to fit the time series to an autoregressive (AR) model of the following form:

$$\bar{A}_{\bar{A}} = \bar{A}\bar{A}_{\bar{A}-1} + \sum_{\bar{A}=1}^{\bar{A}} \bar{A}_{\bar{A}}\Delta\bar{A}_{\bar{A}-\bar{A}} + \bar{A}_{\bar{A}} \quad (2\text{-}13)$$

where:

β,φ = coefficients of the autoregressive model
p = number of lags in the autoregressive model
$\bar{A}_{\bar{A}}$ = is a Gaussian white noise process.

The AR model is said to have a unit root if one of the roots of the characteristic equation of the process is 1. For illustrative purposes, consider a

first order AR model (that is, a model with one lag). The process can be written as:

$$\bar{A}_{\bar{A}} = \bar{A}\bar{A}_{\bar{A}-1} + \bar{A}_{\bar{A}} \quad (2\text{-}14)$$

The first order AR process can be shown to have a characteristic equation of the following form:

$$\bar{A} - \bar{A} = 0 \quad (2\text{-}15)$$

If φ is equal to 1, then the root of the characteristic equation, m, also equals 1, and the AR process is effectively a random walk, which is nonstationary (Hamilton 1994). The ADF test is a hypothesis test to determine the likelihood that the AR model has a unit root. It tests whether φ=1 against the alternative of φ<1. A value of φ>1 is not considered because a coefficient of this type would manifest itself as an obviously explosive process.

Figure 7 illustrates the role of φ in an AR model by plotting three separate realizations of Equation 2-14 with 10,000 steps each. Plot A shows the first order AR model from Equation 2-14 with φ=0.5; Plot B shows φ=1.0; Plot C shows φ=1.001. When φ<1 (plot a) the process appears to fluctuate consistently around zero, without any prolonged periods above or below zero. In other words, when φ<1, the process appears to be, and in fact is, stationary. When φ=1.0, the process continuously grows, displays a consistent trend upwards, does not have a constant mean value, and is nonstationary. When φ=1.001, taking note of the orders of magnitude difference in the y-axis range, the process explosively grows and is obviously nonstationary. Plotting values of φ as small as 1.1 quickly become asymptotic lines shooting off towards infinity, and are not informative; thus, none are shown here.

The ADF test statistic is defined as:

$$\bar{A}\bar{A}\bar{A} = \frac{\hat{\bar{A}}}{\bar{A}\bar{A}(\bar{A})} \quad (2\text{-}16)$$

where:

$\hat{\bar{A}}$ = the estimate of φ
SE = standard error.

Figure 7. Visualization of first order AR model: (a) φ =0.5, (b) φ =1.0, c) φ = 1.001.

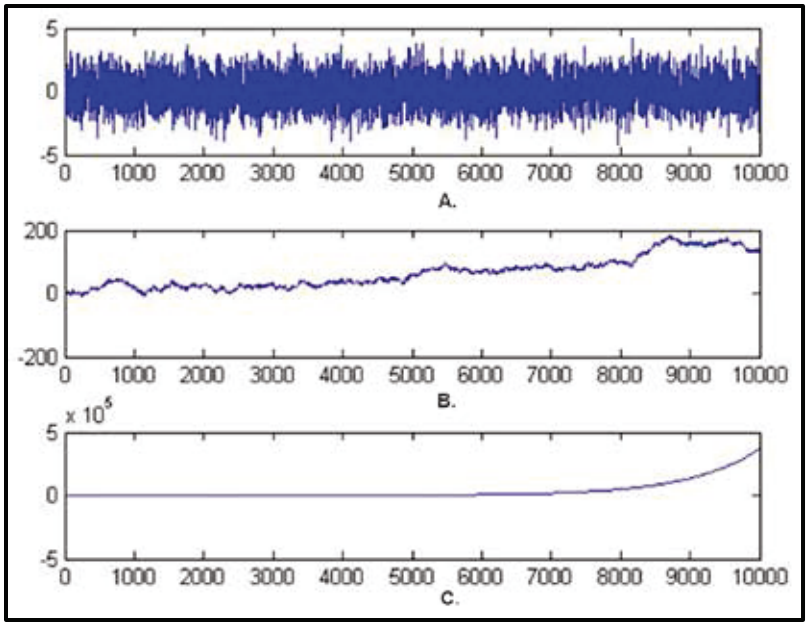

This statistic is compared to a critical value similar to a *t*-statistic. These values were tabulated by Dickey and Fuller, with a typical significance level of 0.05. The ADF test is a left-tailed hypothesis test, and so a test statistic less than the critical value will lead to a rejection of the null hypothesis of a unit root, in favor of the alternative stationary process. Effectively, the rejection of the null hypothesis with a 0.05 significance level states that, 5% of the time, the process will actually have a unit root if it is assumed not to have one.

2.2.2 Selection of number of lags for ADF test

The ADF test is dependent on the number of lags (past points) chosen for the AR model in Equation 2-13 and the test statistic will depend greatly on this selection. One approach is to test the statistical significance of the values of β in Equation 2-13 using *t*-statistics. Another approach is to use the Akaike Information Criterion (AIC), which is the method used in this research. The AIC concept is introduced briefly here; a more in depth treatment is given by Akaike (1974). The AIC is defined as:

$$\bar{A}\bar{A}\bar{A} = 2\bar{A} - 2\ln(\bar{A}) \tag{2-17}$$

where:

k = number of estimated parameters in the model
L = maximum value of the likelihood function of the model.

For the case of an AR model, k in Equation 2-17 can be seen as the number of lags in the model. The preferred AR model is the model with the number of lags that gives the minimum AIC value and thus provides a balance between model fit (e.g., small L) and model complexity (e.g., large k) (Akaike 1974). With the appropriate number of lags chosen, the values of parameters φ and β are estimated, the process of which can be found in textbooks on time-series analysis, such as Hamilton (1994). Finally, the ADF test is performed and used to classify the AR process as stationary or nonstationary. If the time series is well represented by the AR model, the time series itself is classified as stationary or nonstationary, which will further govern the selection of the appropriate analysis methods.

This section has shown one method for testing a time series for stationarity, the ADF test. The ADF test is performed by fitting the data to be tested to an auto-regressive model with an appropriate number of lags as determined by the Akaike Information Criterion. A hypothesis test is then performed on the coefficients of the AR model to test for a unit root of the process. A test statistic is found and compared against critical values tabulated by Dickey and Fuller, with a test statistic more negative than the critical value indicating rejection of the null hypothesis of a unit root in favor of the stationary alternative. Intuitively, a rejection of the null hypothesis states that, some percentage of time (the significance level chosen during the test, commonly 5%), one assumes there is not a unit root when the process actually has one. Conversely, it can be thought of as having 95% confidence that there is not a unit root in the process.

2.3 Statistical methods for analyzing multivariate time series

In this study, multiple time series are analyzed simultaneously as a single, multivariate time series. The time series are combined into a vector, $\boldsymbol{X}$, as:

$$\bar{\bar{A}} = \begin{bmatrix} \bar{\bar{A}}_{\bar{A}}^{(1)} \\ \bar{\bar{A}}_{\bar{A}}^{(2)} \\ \vdots \\ \bar{\bar{A}}_{\bar{A}}^{(\bar{A})} \end{bmatrix}_{\bar{A}\bar{A}\bar{A}} \tag{2-18}$$

where:

$\boldsymbol{X}$ = n x m data matrix
$\bar{\bar{A}}_{\bar{A}}^{(\bar{A})}$ = i^{th} m x 1 time series
m = number of observations for each time series
n = number of time series.

The analysis method chosen for the data matrix depends on the classification of the individual time series. Most time series analysis methods require a stationary series; however, methods do exist for analyzing nonstationary time series. PCA is the method chosen for this study and will be discussed in detail here. Subsequently, a brief introduction to the method of cointegration is presented as one option for analyzing nonstationary time series.

2.3.1 PCA for stationary time series

PCA is a statistical procedure for analysis of stationary time series. PCA is an orthogonal transformation of a set of n possibly correlated random variables or time series, to a set of n linearly uncorrelated variables known as the principal components of the data. The transformation is derived from the eigenvectors of the covariance matrix, where each eigenvector represents a "direction" of the data describing a certain percentage of the variance in the data. The associated eigenvalues correspond to the variance of the transformed time series. The percentage of the variance explained in a given principal direction can be determined as the ratio of the corresponding eigenvalue divided by the sum of the eigenvalues. That is:

$$\%\bar{A}\bar{A}\bar{A}\bar{A}\bar{A}\bar{A}\bar{A}\bar{A}\bar{A}\bar{A}\bar{A}_{\bar{A}} = \frac{\bar{A}_{\bar{A}}}{\sum_{\bar{A}=1}^{\bar{A}} \bar{A}_{\bar{A}}} \bar{A}\,100 \tag{2-19}$$

where:

$\lambda_i = i^{th}$ eigenvalue.

Thus, the largest eigenvalue corresponds to the direction (eigenvector) that "explains" the largest variance of the data.

PCA can be used to reduce the dimensionality of the data with a minimal loss of information. To this end, a certain percentage (say 90%) of the variance in the data to retain is first selected, PCA is applied, and the appropriate set of eigenvectors that represent this percentage is chosen. The data are then projected onto the corresponding eigenvectors, yielding a dimensionally reduced set of variables still containing the chosen percentage of the information. A brief treatment on the method of PCA is given here, and Chapter 3 introduces the application of PCA to structural health monitoring.

Much of the literature on PCA gives the first step of the process as normalizing the data by mean-centering each variable and forcing unit variance by dividing each variable by its sample variance. For example, normalizing is necessary for combining data that may have different units; however, for

the study at hand, the differing values in the mean of each random variable to be investigated is of critical importance to detect damage in the structure. Not performing this step does not invalidate the results of PCA, however, and so this step is not performed in this study. The first step then is to form a covariance matrix of the data. The covariance matrix, $\boldsymbol{\Sigma}$, of the data is defined as:

$$\bar{\mathrm{A}} = \begin{bmatrix} \bar{\mathrm{A}}[\left(\bar{\mathrm{A}}_{\bar{\mathrm{A}}}^{(1)} - \bar{\mathrm{A}}_1\right)\left(\bar{\mathrm{A}}_{\bar{\mathrm{A}}}^{(1)} - \bar{\mathrm{A}}_1\right)] & \cdots & \bar{\mathrm{A}}[\left(\bar{\mathrm{A}}_{\bar{\mathrm{A}}}^{(1)} - \bar{\mathrm{A}}_1\right)\left(\bar{\mathrm{A}}_{\bar{\mathrm{A}}}^{(\bar{\mathrm{A}})} - \bar{\mathrm{A}}_{\bar{\mathrm{A}}}\right)] \\ \vdots & \ddots & \vdots \\ \bar{\mathrm{A}}[\left(\bar{\mathrm{A}}_{\bar{\mathrm{A}}}^{(\bar{\mathrm{A}})} - \bar{\mathrm{A}}_{\bar{\mathrm{A}}}\right)\left(\bar{\mathrm{A}}_{\bar{\mathrm{A}}}^{(1)} - \bar{\mathrm{A}}_1\right)] & \cdots & \bar{\mathrm{A}}[\left(\bar{\mathrm{A}}_{\bar{\mathrm{A}}}^{(\bar{\mathrm{A}})} - \bar{\mathrm{A}}_{\bar{\mathrm{A}}}\right)\left(\bar{\mathrm{A}}_{\bar{\mathrm{A}}}^{(\bar{\mathrm{A}})} - \bar{\mathrm{A}}_{\bar{\mathrm{A}}}\right)] \end{bmatrix} \quad (2\text{-}20)$$

where:

$\bar{\mathrm{A}}_{\bar{\mathrm{A}}}$ = expected value of the i^{th} time series.

The eigenvalues and eigenvectors of $\boldsymbol{\Sigma}$ are found from the familiar eigenvalue decomposition. Because $\boldsymbol{\Sigma}$ is positive definite, there will be n eigenvalues and eigenvectors, and the eigenvectors will form an orthogonal basis. To proceed, the original data matrix $\boldsymbol{X}$, as explained in Equation 2-18, is projected onto the appropriate number of eigenvectors, so chosen to yield the desired amount of variance retained. If the first k eigenvectors account for the desired percentage of variance in the system, these eigenvectors are concatenated into a new matrix, such that:

$$\tilde{\bar{\mathrm{A}}} = [\bar{\mathrm{A}}_1 \quad \bar{\mathrm{A}}_2 \quad \cdots \quad \bar{\mathrm{A}}_{\bar{\mathrm{A}}}] \quad (2\text{-}21)$$

Then, the data matrix $\boldsymbol{X}$ is projected onto $\tilde{\bar{\mathrm{A}}}$ to form the dimensionally reduced data matrix $\tilde{\bar{\mathrm{A}}}$ as follows:

$$\tilde{\bar{\mathrm{A}}} = \tilde{\bar{\mathrm{A}}}^{\bar{\mathrm{A}}}\bar{\mathrm{A}} \quad (2\text{-}22)$$

where:

$\tilde{\bar{\mathrm{A}}}$ = n x k matrix of k retained eigenvectors, known as the "loadings"

$\tilde{\bar{\mathrm{A}}}$ = k x m reduced dimension data matrix, $k<n$.

For structural health monitoring, $\tilde{\bar{\mathrm{A}}}$ contains the critical information that is used to monitor for damage. How this method is applied to structural health monitoring will be introduced in Section 2.4. As noted, one of the implicit assumptions in PCA is that the time series to be analyzed is stationary. For nonstationary time series, other methods must be used, as explained in the next section.

2.3.2 Methods for nonstationary time Series

When a time series is nonstationary, many of the typical data analysis methods are no longer valid and are prone to yield seemingly statistically significant results that are actually meaningless. This phenomenon is known as spurious regressions and is due to the fact that the central limit theorem no longer applies to nonstationary time series (Panik 2009). Thus, other methods must be applied to handle nonstationary time series.

One simple method for analyzing a nonstationary time series is to difference the series enough times so that it becomes stationary. Recall the random walk model of Equation 2-14 has a unit root and φ=1. This equation then becomes:

$$\bar{A}_{\bar{A}} = \bar{A}_{\bar{A}-1} + \bar{A}_{\bar{A}} \tag{2-23}$$

As explained in Section 2.1, the above process is a random walk process, and is nonstationary. However, the first difference of this process will be a stationary Gaussian white noise process. To illustrate this point, the time series is differenced once by subtracting $\bar{A}_{\bar{A}-1}$ from both sides, then, the series can be rewritten as:

$$\Delta\bar{A}_{\bar{A}} = \bar{A}_{\bar{A}} \tag{2-24}$$

showing that the first difference of $\bar{A}_{\bar{A}}$ is a Gaussian white noise process. To reiterate the points in Section 2.1.3, the random walk process is thus considered an I(1) process, as differencing the series once produces a stationary, or I(0) process.

Differencing may result in loss of important information. However, methods that address nonstationary time series directly are often more complex than their stationary counterparts. One such method that has been developed to address nonstationary time series is known as cointegration.

Two or more nonstationary time-series are said to be cointegrated if there exists a linear combination of them that is stationary. Consider the following equation:

$$\bar{A}_{\bar{A}} = \bar{A}_{\bar{A}}^{\bar{A}}\bar{A} \tag{2-25}$$

The term $\boldsymbol{X}$ is an n x m matrix consisting of n nonstationary time series with m samples, β_i is an n x 1 vector, and z is a 1 x m vector. The subscript i is

used to indicate that β and z are not unique. If z is stationary, then β is said to be a cointegrating vector of $\boldsymbol{X}$. Intuitively, in the direction of β, the difference between the series in $\boldsymbol{X}$ is nominally constant, and z is a vector that describes long run relationships between the variables in $\boldsymbol{X}$.

The methods of determining whether or not the series in $\boldsymbol{X}$ is in fact cointegrated, and then finding β, are somewhat complex. For an in depth treatment on cointegration, the reader is directed to an advanced econometrics text book, such as Johansen (1996). For cointegration applied to structural health monitoring, Cross (2012) provides a good overview. Nonstationary methods will not be treated further in this report as the data under investigation appear to be stationary.

2.4 Change point detection and damage indicators

As it applies to structural health and condition monitoring, PCA is used to obtain a single, stationary time series that contains information from multiple time series. The single time series is created with data that are assumed to be from an undamaged structure. The time series from the undamaged condition is then used to indicate damage, which is assumed to occur if the statistics of the indicator change significantly. In what follows, the formulation of the damage indicator is first introduced, followed by the method for determining whether a change in the statistics is significant enough to be classified as damage.

2.4.1 Damage indicator using PCA

As mentioned in Section 2.2, PCA can be used as a method to reduce the dimensionality of the data. However, it remains to be seen how PCA can be used as a method of detecting anomalous behavior of the system (i.e., damage). Figueiredo et al. (2009) at Los Alamos National Laboratory used a method of finding the residual between the measured data and the dimensionally reduced data by using PCA eigenvectors formulated from an assumed undamaged dataset. The number of eigenvectors used depends on the amount of variance the user wishes to maintain in the system. Cross (2012) provides an example of PCA as a damage detector by projecting the data matrix $\boldsymbol{X}$ onto the eigenvector associated with the least amount of variance. Both approaches form a single time series that can be used as a damage indicator. The Cross method can be considered a special case of the Los Alamos approach in which enough variance in the system is maintained

such that all eigenvectors but the last one are used. As such, the Los Alamos method will be presented here.

Consider a data matrix, ***X***, consisting of information from a system under normal operating condition (i.e., no damage present). These data are referred to as the training data, as they "train" the PCA loading vectors based on the normal operating conditions of the system. Following the procedure set forth in Section 2.2.1, obtain the loadings in the system, $\tilde{A}$.

A damage index is then created by forming a residual of the dimensionally reduced, undamaged data $\tilde{A}$ (as defined in Section 2.2.1) and the original data ***X***. This is accomplished by projecting $\tilde{A}$ back to "original" coordinates. The residual, ***E***, is the error from projecting the reduced data back to original coordinates, and is found by subtracting this projection from the original data, i.e.:

$$\bar{A} = \bar{A} - \tilde{A}\,(\tilde{A}^{\bar{A}}\bar{A}) \tag{2-26}$$

Each point in time can be viewed an *n x 1* vector (see Section 1.1). To form a single time series, the Euclidean norm of this vector is taken at each point in time, i.e.:

$$\bar{A}_{\bar{A}} = \sqrt{\sum_{\bar{A}=\bar{A}}^{\bar{A}} \bar{A}_{\bar{A}}^{\bar{A}}}, \;\; \bar{A} = \bar{A}, \bar{A}, \ldots \bar{A} \tag{2-27}$$

As seen, $\bar{A}_{\bar{A}}$ is a vector consisting of the square-root of the sum of squares of the "error" in the PCA projection. Figueiredo then uses some percentage of the max value of $\bar{A}_{\bar{A}}$ as a threshold that, if a damage index created from tested data exceeds, damage will be indicated. He suggests that 90% of the max value is typically appropriate.

To test for damage, the same procedure is applied as in Equations 2-20 and 2-21, only with data from an unknown state (e.g., potentially damaged). The critical point is that *the same* loadings, $\tilde{A}$, from the trained data are used. If ***Xd*** represents the data to be tested, the procedure to test for damage is to find the residual of the tested data as follows:

$$\bar{A}_{\bar{A}} = \bar{A}_{\bar{A}} - \tilde{A}\,(\tilde{A}^{\bar{A}}\bar{A}_{\bar{A}}) \tag{2-28}$$

The Euclidean norm of the residual is taken at each point in time forming a new time series used as a damage index, or *DI*, i.e.:

$$\bar{A}\bar{A}_{\bar{A}} = \sqrt{\sum_{\bar{A}=\bar{A}}^{\bar{A}} \bar{A}_{\bar{A}\,\bar{A}}{}^{\bar{A}}} \quad , \quad \bar{A} = \bar{A}, \bar{A}, \ldots \bar{A} \tag{2-29}$$

DI from Equation 2-29 is compared with the threshold found from Equation 2-27 and damage is said to be present if any value of *DI* is above the trained threshold found from Equation 2-27, that is:

$$\bar{A}\bar{A}\bar{A}\ \bar{A}\bar{A}\bar{A}\,\bar{A}\bar{A}\,\bar{A}\bar{A}_{\bar{A}} > \bar{A}h\bar{A}\bar{A}\bar{A}h\bar{A}\bar{A}\bar{A} \tag{2-30}$$

2.4.2 Avoiding Type I and Type II errors

The choice of threshold in Section 2.4.1 is a critical step for damage detection, as it may lead to false positives or false negatives. A threshold that is too low may be too sensitive and lead to indication of damage when damage is not actually present (false positive, or Type 1 error). A threshold that is too high may be too insensitive and not indicate damage when damage is actually present (false negative, or Type 2 error). The selection of values at or near the maximum of the square-root-sum-of-squares of the trained residual is somewhat qualitative, and so this work suggests an alternative approach to classifying the significance of values in the damage index that exceed the threshold.

The data considered in this report, in general, follow a normal distribution, which will be explored in depth later. Because PCA performs a linear transformation on the data, the residuals from PCA will also follow normal distributions. However, the time series for damage detection, *DI*, found with Equation 2-29 is effectively a square root sum of squares of n normally distributed random variables. The sum of squares of standardized (mean centered and unit variance) normally distributed variables will follow a chi-squared distribution (NIST 2013). As mentioned previously, the variables of interest are not standardized; however, it will be shown that the distribution of the damage index can be well approximated by a lognormal distribution. Therefore, for the threshold of damage detection, the authors of this study use ±3 standard deviations from the mean of the natural log of the damage index. The motivation for this threshold is that, for normally distributed data, 99.7% of the data fall within 3 standard deviations, and thus, three out of every thousand observations will be significant outliers and potential false indicators.

To further reduce the potential for false indicators, an indication of damage is only considered when a certain number of consecutive observations are above or below the threshold of 3 standard deviations. To determine the number of consecutive observations required, the probability of an observation exceeding the threshold is modeled with a binomial distribution. The binomial distribution assumes that each observation is independent; it will be shown later that the data used in this study can be well approximated to be composed of independent observations. For a binomial process, the probability of *s* occurrences exceeding the threshold out of the next *q* observations is formally written as:

$$\bar{A}(\bar{A} = \bar{A}) = \binom{\bar{A}}{\bar{A}} \bar{A}^{\bar{A}}(1 - \bar{A})^{\bar{A}-\bar{A}} \tag{2-31}$$

where:

$$\begin{aligned} p &= \text{the probability of exceeding the threshold} \\ \binom{\bar{A}}{\bar{A}} &= \text{the binomial coefficient equal to } \frac{\bar{A}!}{\bar{A}!(\bar{A}-\bar{A})!} \end{aligned}$$

This study is interested in the case where $q = s$, i.e., to answer the question: At any point in time, what is the probability that all of the next *q* observances will exceed the threshold? For the case of $q = s$, Equation 2-31 simplifies to $\bar{A}^{\bar{A}}$, and *q* is chosen such that the probability of consecutive observations is less than a chosen acceptable rate of false alarms, $\bar{A}_{\bar{A}\bar{A}\bar{A}\bar{A}\bar{A}\bar{A}\bar{A}\bar{A}\bar{A}}$. That is:

$$\bar{A}^{\bar{A}} < \bar{A}_{\bar{A}\bar{A}\bar{A}\bar{A}\bar{A}\bar{A}\bar{A}\bar{A}\bar{A}} \tag{2-32}$$

Solving (2-32) directly for *q* will give the minimum consecutive observations required to indicate damage, and is found as follows:

$$\bar{A} \geq \frac{\ln(\bar{A}_{\bar{A}\bar{A}\bar{A}\bar{A}\bar{A}\bar{A}\bar{A}\bar{A}\bar{A}})}{\ln(\bar{A})} \tag{2-33}$$

where ln is the natural logarithm. For example, if the acceptable false alarm rate is 1 in 10,000, $\bar{A}_{\bar{A}\bar{A}\bar{A}\bar{A}\bar{A}\bar{A}\bar{A}\bar{A}\bar{A}} = 0.0001$ in Equation 2-33. Then, if the probability of an observation exceeding the threshold is 0.1, *q* will be at least four. That is, at least four consecutive observations above the threshold will be required to indicate damage is present. The probability of an observation exceeding the threshold is calculated from the training data by dividing the number of measured observations above the threshold by the number of total samples. That is:

$$\bar{A} = \frac{\#\,\bar{A}\bar{A}\bar{A}\bar{A}\bar{A}\,\bar{A}h\bar{A}\bar{A}\bar{A}h\bar{A}\bar{A}\bar{A}}{\#\,\bar{A}\bar{A}\bar{A}\bar{A}\,\bar{A}\bar{A}\bar{A}} \tag{2-34}$$

2.5 Summary

This chapter provides the mathematical tools necessary to analyze the data obtained from the SHM program implemented by the USACE. Appropriate data classification terminology was introduced, and methods to test for the classification were presented. Methods for analyzing the data based on the classification were then introduced along with methodology for avoiding false positives and false negatives. The next chapter will overview the type of data available in this study.

3 SMART Gate System

This chapter introduces and reviews the USACE's SMART Gate system, including the types of sensors deployed and the types of data available for damage detection. From the available data, strain is chosen as the best candidate for the task of monitoring for a gate/wall gap. The chapter concludes with a discussion of possible drawbacks to using strain as a solitary damage sensitive feature.

3.1 SMART Gate overview

In 2007, inspection of The Dalles Navigation Lock on the Columbia River in Oregon revealed extensive cracking at the bottom of the gate and loss of contact at the quoin wall. The USACE launched the Structural Monitoring and Analysis in Real Time for Lock Gates (SMART Gate) program at The Dalles to monitor the situation until repairs could be made. The goal of the program is to "provide engineering and operations professionals a real-time look at the condition of their structures" (Murray 2014). The system implemented at The Dalles consists of 176 gages measuring strain in structural members, temperature, water levels, and pressure on the gate. The data from these gages are uploaded to a web portal in real time to allow engineers and technicians to assess the performance of the structure. In late 2009, engineers noticed a marked change in the readings of some of the sensors, which led to the lock being shut down for an emergency inspection. The inspectors noticed substantial damage to the lower girders and the chamber wall, and emergency repairs were performed, preventing a catastrophic gate failure.

The success of the SMART Gate program in Oregon led the USACE to expand the monitoring campaign to include new lock and dam sites. The system is now employed on six gates in various locations, including on the Mississippi River at Lock and Dam 27, and on the Ohio River at the Greenup Lock and Dam. Each of the sites have instrumented gates with upwards of 300 total sensors measuring strain, temperature, tilt, and water levels. The data are sampled anywhere from $1/15^{th}$ to 50 hertz and are then uploaded to a database for processing. Table 1 lists the gate systems currently included in the SMART Gate program.

Table 1. SMART Gate system overview.

Lock and Dam Name	Location	Number of Sensors
Bonneville	Columbia River	84
Greenup	Ohio River	174
Lock and Dam 27	Mississippi River	289
Racine	Ohio River	125
Meldahl	Ohio River	157
The Dalles	Columbia River	177

3.2 Strain

For the problem of gap detection, the most useful information from the available sensors is strain. As noted in Section 1.1.2, the gates are designed to behave as three-hinged arches under load, with the girders transferring the load into the quoin block through compressive action. For lock gates, the load comes in the form of the differential head, that is, the difference in the upstream and downstream water levels. The strain in the girders should increase or decrease approximately linearly with an increase or decrease in load. As the load on the gate is directly related to the differential head (water levels), the strain should then linearly change with a change in water levels. The SMART Gate system has both strain and water level gages, so this relationship is tested and used to monitor for normal operating conditions of the gate.

3.3 Need for gage synchronicity

As discussed above, the strain for miter gates is expected to behave in an approximately linear fashion with respect to load. However, investigations into the strain behavior of different gates yielded unexpected behavior at some locations. The strain response with respect to water levels was either nonlinear, displayed hysteresis, or both. The hysteresis-like behavior was hypothesized to be caused by a time delay between water level sensors and the strain gages. Shifting the strain series in time to synchronize it with the measured water level aligned the data (Figure 8).

Figure 8. Strain response for a gage during 1 day at Greenup: (a) hysteresis-like behavior caused by temporal delay, (b) shifting strain in time aligns the plots.

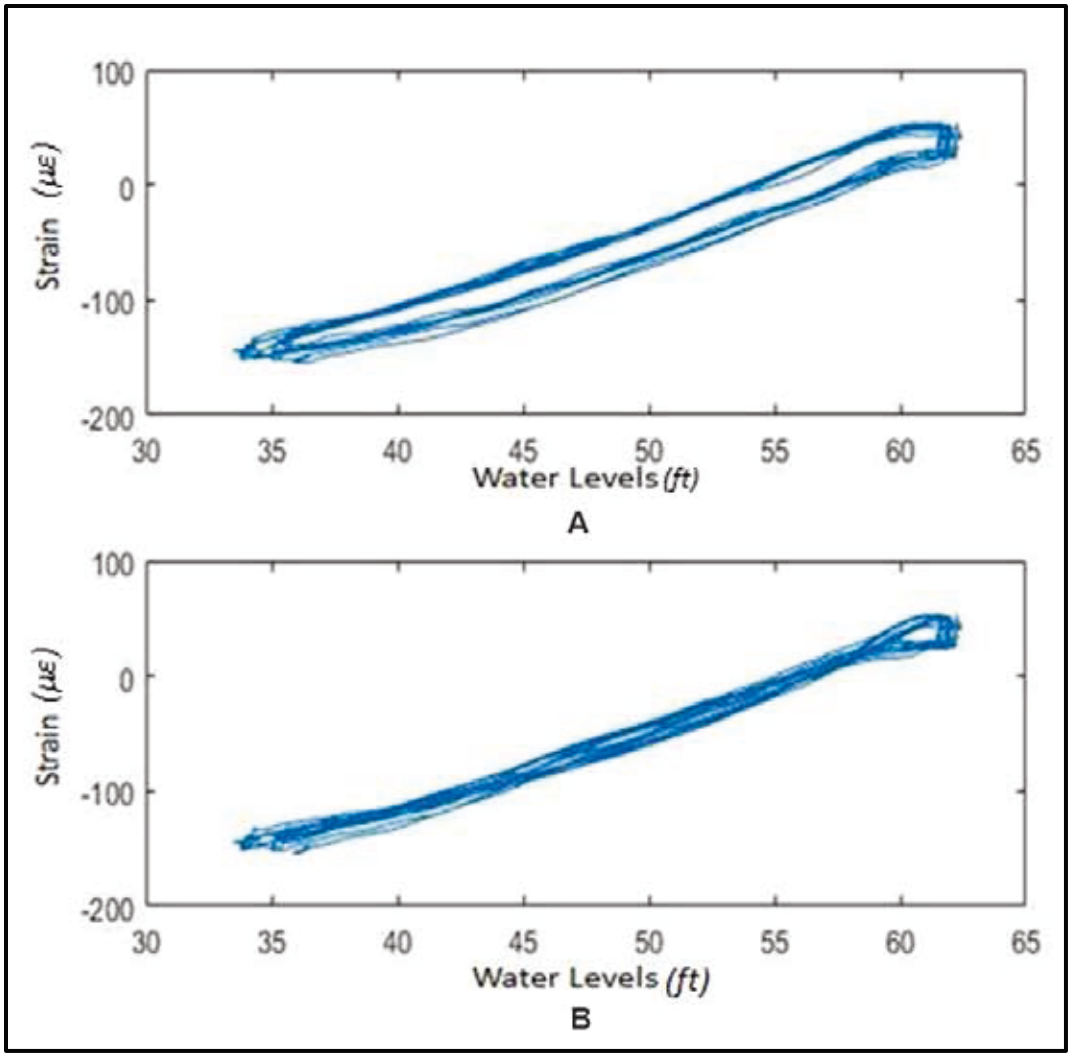

In Figure 8, the top plot shows the strain versus water levels for one gage on the Greenup gate. The two series, strain and water levels, are aligned in time as recorded, and an unexpected hysteresis-like loop is seen. If the loop is caused by a delay between the two recordings, then shifting one of the series in time would cause the two to overlap. This alignment is seen in the bottom plot, providing visible evidence that there is, indeed, a delay between the signals. Further investigation into the instrumentation on Greenup yielded that the water level sensors deployed on the gages are not designed to take dynamic measurements, and have a measurement time of 2 seconds. Thus, at any point in time, the water level measurement can be shifted by up to 2 seconds in time compared to the strain measurements.

The strain-water sampling discrepancy is more pronounced at Lock 27. Investigations into the strain behavior at this gate revealed highly non-linear and hysteresis-like response across multiple gages and varying locations on the gate. Figure 9 shows a typical example of this phenomenon. Inspection of the plot reveals that something more than a shift in time is occurring here, and so a further investigation was conducted. The investigation revealed that, on Lock 27, there were no water level sensors integrated with the strain sensors. That is, the water level readings come from a different data logger.

Figure 9. Non-linear response for a strain gage on Lock 27.

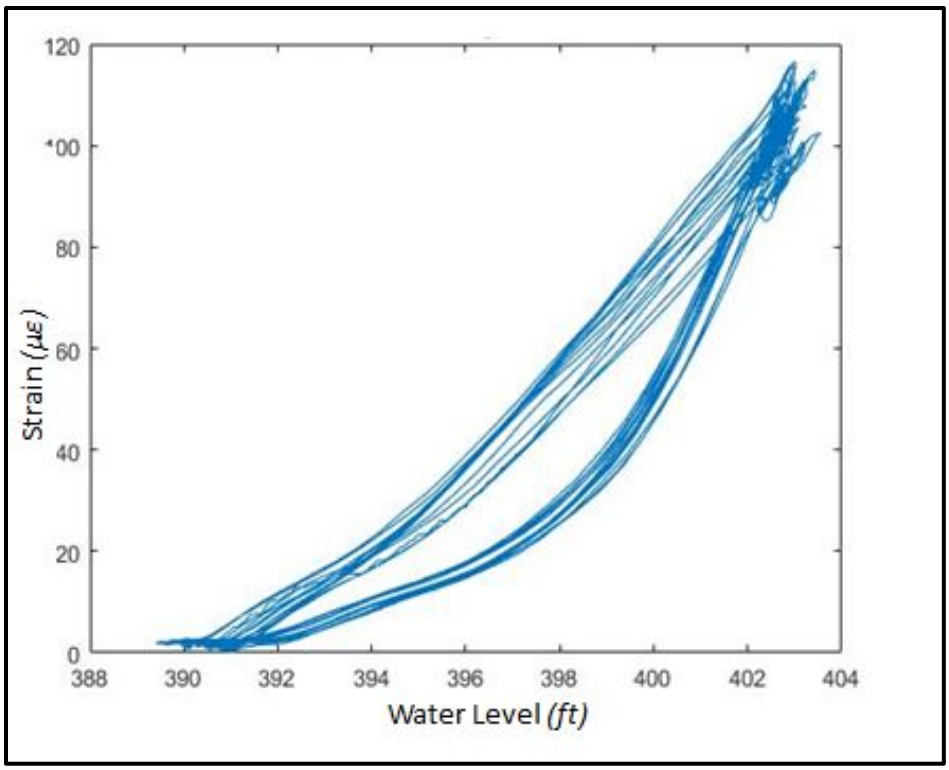

The above cases highlight the need for synchronized and integrated instrumentation with dynamic measurement capabilities. At Lock 27 the collected data were deemed unreliable and not suitable for inclusion in the study of gap detection. Chapter 4 of this report explains that the data of interest pertain to the rate of change of strain with respect to water level, eliminating concerns about offsets in the strain and water level. Therefore, for the Greenup site, the effect of the 2-second delay between strain measurements and water level measurements is eliminated.

3.4 Issues with strain

The strain response in the gate provides useful information for detecting a gap at the gate/wall interface; however, the strain response is only informative when the water levels in the lock chamber change. On a typical day at Greenup, about six lockage events occur, where the chamber water levels rise and fall. A typical lockage has a nominal duration of about 15 minutes; therefore, long periods of time exist in the data record where the strain gage data provide no useful information. Figure 10 shows these periods of inactivity in a plot of 1 day of strain response for a gage at Greenup. The sharp jumps in the data are times when the chamber is filling or emptying, and the long plateaus are periods of inactivity in the chamber.

Furthermore, strain is sensitive to temperature, which leads to a seasonal trend in the strain response. Figure 11 shows 6 months of strain response for the Greenup gate; the evidence shows that the mean value of the strain steadily increases as the weather gets warmer.

Figure 10. One day of strain response at Greenup with long periods of non-informative data.

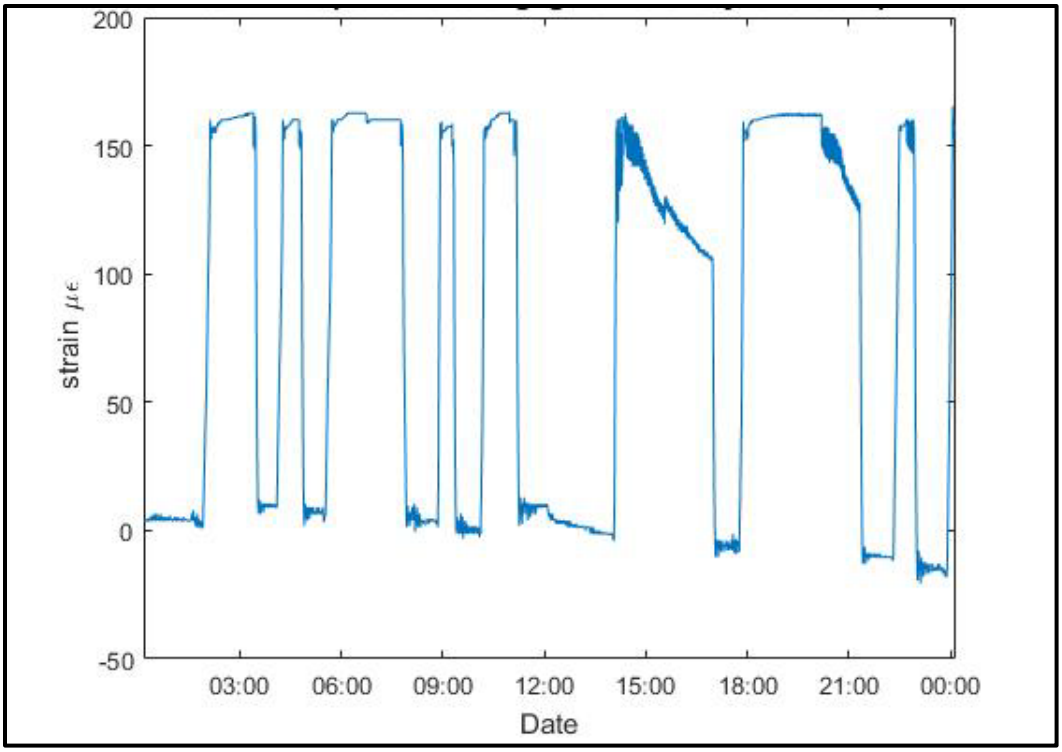

Figure 11. Strain response of one gage for 6 months, showing seasonal trend.

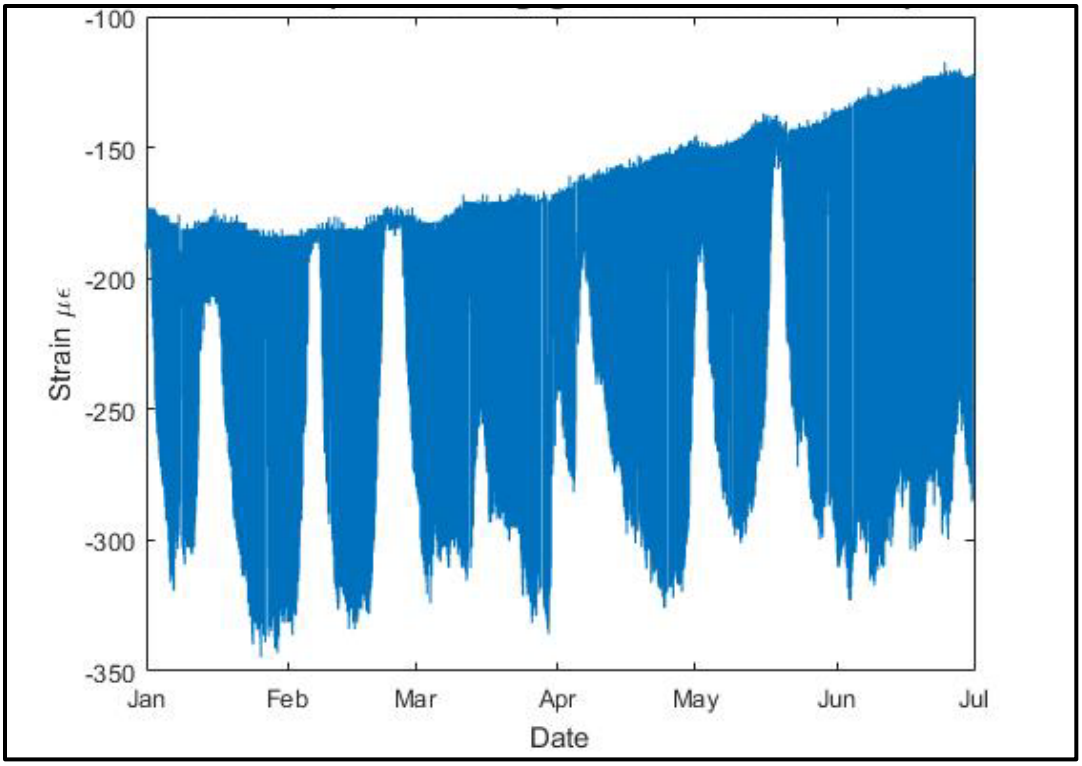

Temperature variations throughout the year can then be seen as causing the strain data to behave in a nonstationary manner. As explained in Chapter 2, nonstationarity is undesirable, as analysis of the data becomes more cumbersome. Moreover, the plan for detecting damage relies on assessing whether or not there is a significant change in strain behavior on the gate. The question arises then if any significant change in the strain data is caused by damage to the gate, or simply from temperature variations (or other environmental variables). Addressing these two problems with strain data, namely nonstationarity and overwhelming amounts of non-informative data from gate inactivity, will be explored in the next chapter.

3.5 Summary

The USACE SMART Gate system provides engineers with a wealth of information on lock gates such as strain, water levels, and temperature. Among the available data, strain is the most relevant to the problem of detecting a gap in the gate/wall interface. Strain itself is not infallible. It is sensitive to temperature variations and displays seasonal trends; and collected strain data tends to contain long durations of non-informative data. The next chapter explores the issues of nonstationarity and uninformative data from gate inactivity.

4 Proposed Gap Detection Methodology

As discussed in Chapter 3, the strain data supplied from the SMART Gate system represent the chosen candidate among the various data types available from the SMART Gate system for the detection of a gap. However, the nonstationarity of the data and the long periods of inactivity are a hindrance to its direct use as a damage feature. The most useful information in the strain data comes from times when the water level in the lock chamber is changing. Therefore, a method was developed to quantify the behavior of the strain gages during chamber events with a single value. The strain data are differentiated, which is seen to remove the seasonal variations in the data by effectively removing any constant thermally induced strain present during chamber events. The number of points to be analyzed is also significantly reduced. This chapter presents the approach to modifying the strain data by differencing.

4.1 Selection of damage sensitive feature

The strain response of a girder on the gate is expected to change approximately linearly with respect to load, or equivalently, with respect to water levels. Accordingly, the change in strain with respect to water level is expected to be useful as a damage sensitive feature that can be used to describe the strain behavior in the girder during chamber events. Thus, before proceeding, the expected linearity of strain is examined. Also examined is how strain can be used to detect the presence of a gap.

4.1.1 Linearity of strain

The linearity of the strain with respect to water is examined through visual inspection of the data before continuing on with the development of a methodology for detecting gaps in the gate/wall interface. The strain gage data for multiple gages was plotted against the water levels in the lock and the relationship was inspected on multiple days. Figure 12 shows a typical strain response for 1 day of activity at Greenup.

Figure 12. Strain response for 1 day at Greenup, showing linearity with respect to water level.

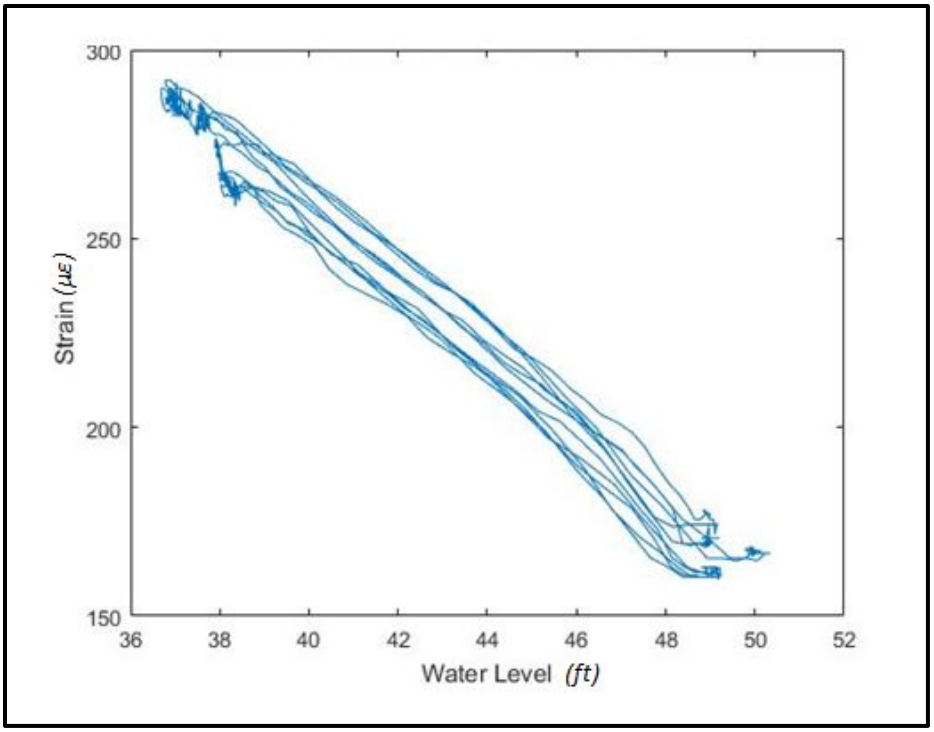

As seen, for this day at Greenup, approximately 10 fill and empty events occurred in the lock chamber, each represented by a long diagonal line on the plot. When there is no activity in the chamber, the strain generally hovers around the same value. For this day at Greenup, the downstream water level was around 38 ft., and the upstream water level around 49 ft. When the water level increases, the strain becomes less positive, indicating compression at this location. Most critically, as demonstrated in Figure 12, the change in strain occurs in a linear fashion, as hypothesized. This behavior was seen across multiple gages and multiple days.

4.1.2 Strain in the presence of a gap

When there is a gap between the gate and wall, the boundary conditions for the system change and the girders near the gap can no longer transfer load into the wall. The load that would have been transferred through the girders adjacent to the gap is now redistributed to other girders. This behavior manifests itself in the data as an increase or decrease in strain in the girders for the same differential head observed under normal operating conditions. This is a critical point in this report; when a gap is present at the gate/wall interface, the strain response in the girders near the gap will change, providing an indication of damage.

4.2 Slope as a damage sensitive feature

To address the issues with strain, namely nonstationarity and long periods of inactivity, the change in strain with respect to a change in water level is investigated as a potential damage sensitive feature. Algorithms were developed in MATLAB to detect a change in the water levels in the chamber significant enough to signify a chamber event (i.e., a lockage). Any data point that occurred outside of the lockage events was discarded. A line is fit to the strain data using ordinary least squares (OLS) for each gage during the entire chamber event. The change of the fitted line with respect to change in water level for a chamber event is referred to here as slope and is the metric that is used to describe the strain behavior at the gage location during chamber events. Figure 13 shows an example of the extracted strain and the least squares fit for strain data on one gage at Greenup for 1 day.

The gage represented in Figure 13 is located near the quoin at the bottom of the gate, and the behavior illustrated is for the lock chamber emptying. On this day at Greenup, five empty events occurred. The top plot in Figure 13 shows the noisy raw data from the strain gages for the empty events on that day. The bottom plot shows the least squares fit of the data. For all five events, the slopes of the line are nearly identical. This procedure was repeated for different gages with similar results.

Figure 13. Extracted strain during chamber empty events for 1 day at Greenup.

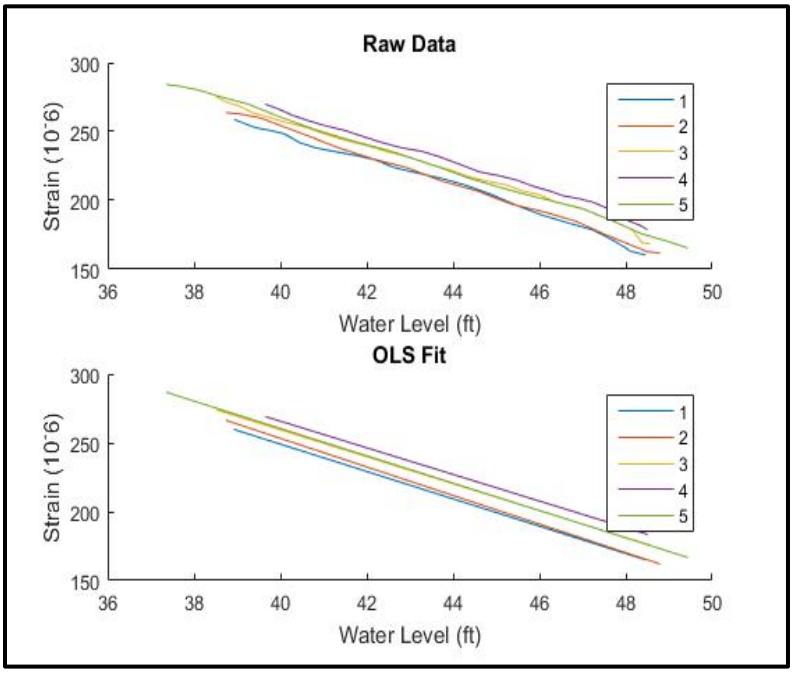

Thus, as hypothesized, the girders on the gate behave in a consistent and predictable manner. The small differences in intercept of the least squares lines can be caused by temperature variations throughout the day, or other noise in the system, and will not impact the slope estimates.

By using the slope as the metric by which to describe the gate's behavior, the number of data points to be analyzed is significantly reduced. For data sampled every 15 seconds, 5760 strain samples are taken every day for every gage on the gate. If only six empty and six fill events occur in the chamber in a day, the 5760 points are reduced to 12, making data analysis more computationally efficient. Moreover, in the presence of a gate/wall gap, the slope is expected to change in a similar manner as the strain, as explained in Section 4.1.2. The slope will henceforth be investigated as a damage sensitive feature.

4.3 Measured data processing: Slope extraction

The SMART Gate database has several years' worth of data across multiple lock sites, each with up to hundreds of sensors. Manually searching the data from each strain gage for lock-chamber fill or empty events and extracting the slope from each one would be impractical. To facilitate the processing of strain data, an algorithm was created in MATLAB that automates the extraction of slopes for each gage. The algorithm numerically differentiates the data from the lock chamber water level. Any significant change in the derivative signifies a chamber fill or empty event. When the derivative returns back to zero, the end of the event is signified. The time stamps from the beginning and end of a chamber event are then used to set a range of points over which to investigate the strain data in a similar way. In this way, water levels for each chamber event and the corresponding strain values for each gage were extracted from the data. Using these values, strain was linearly regressed onto the water level data using OLS regression. The slope of the line of best fit was then stored into a new time series to be used as the slope data of interest.

To ensure that the process was working appropriately, a small parcel of slope data were plotted for representative gages on the Greenup gate and inspected. In Figure 14, which shows the results for about 3 months of data, each colored line represents an individual strain series.

Figure 14. Processed slopes for 3 months at Greenup showing significant outlier.

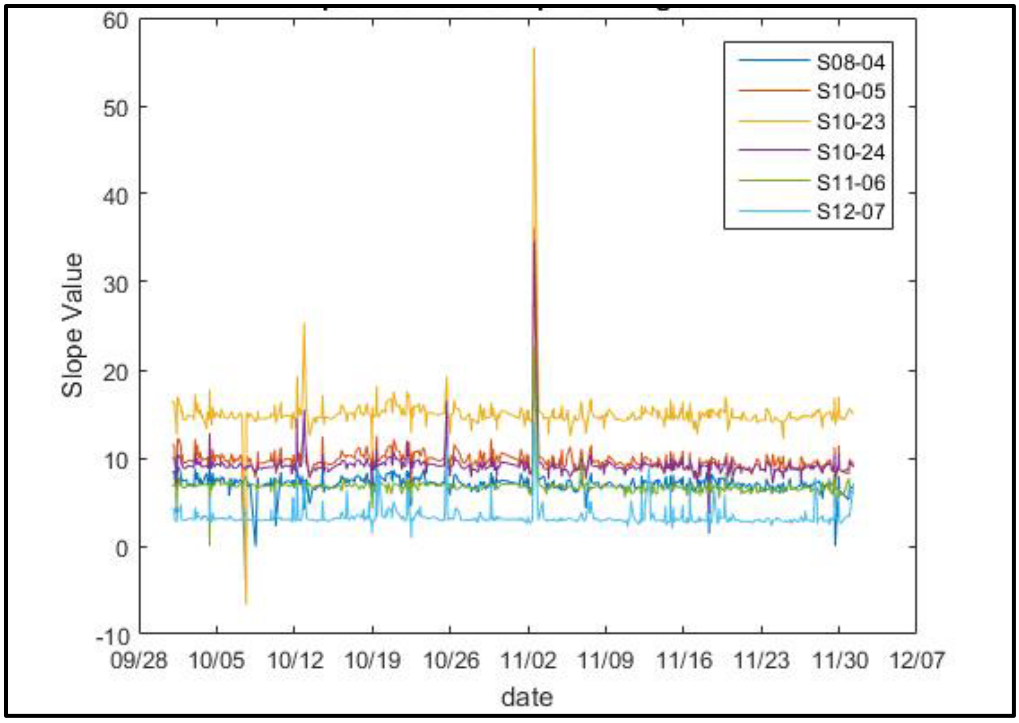

Several things of interest are to be gained from this plot. The slopes for each gage are relatively constant, validating their use as an appropriate damage identifier. The consistency is seen across 3 months, supporting the conjecture that, by differencing the strain data, the constant temperature offsets seen in Figure 11 are removed. Some significant outliers are also seen in the slope data. An outlier is considered significant if it lies far away from the mean. Plus or minus 5 standard deviations was determined to be significant for this study. The observed outliers provided the motivation for investigating the cause for the outliers, and eventual filtering these values out when justified.

4.4 Data cleansing

To begin cleaning the data of anomalous values, an investigation was performed into the cause of the occasional significant outlier in the slope data to see if there was some justification in excluding these points in the study (e.g., if there was a fault in the instrumentation). To start, 1 year of slopes were plotted for a gage and significant outliers were manually removed and inspected for patterns. Figure 15 provides a visualization of this process, with the blue crosses being slope values and the orange values being significant anomalies removed from the data.

Figure 15. One year of slopes for one gage, with removed outliers highlighted in orange.

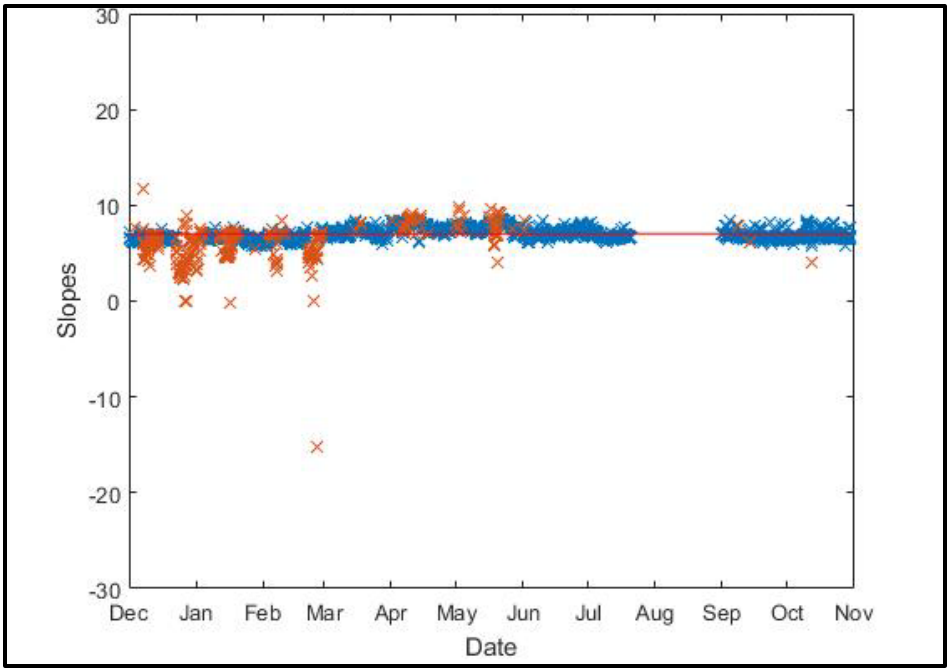

Figure 15 illustrates that significant outliers in the data tend to occur in clusters, suggesting that something occurred during the time period of these clusters to cause the data to be unusual. The strain measured by the gages should be directly related to the load applied to the gate, and hence, the water levels in the lock chamber. Accordingly, the chamber water levels were investigated for the periods where slope data had clumps of significant outliers. This investigation found that the clusters of significant outliers corresponded to periods when the water levels in the chamber changed very little. This is seen in Figure 16, where Figure 16A is identical to Figure 15, and Figure 16B is the corresponding chamber water levels for the same time period that the slopes were investigated.

Figure 16. (a) Slopes from the gage investigated;(b) the corresponding chamber water levels.

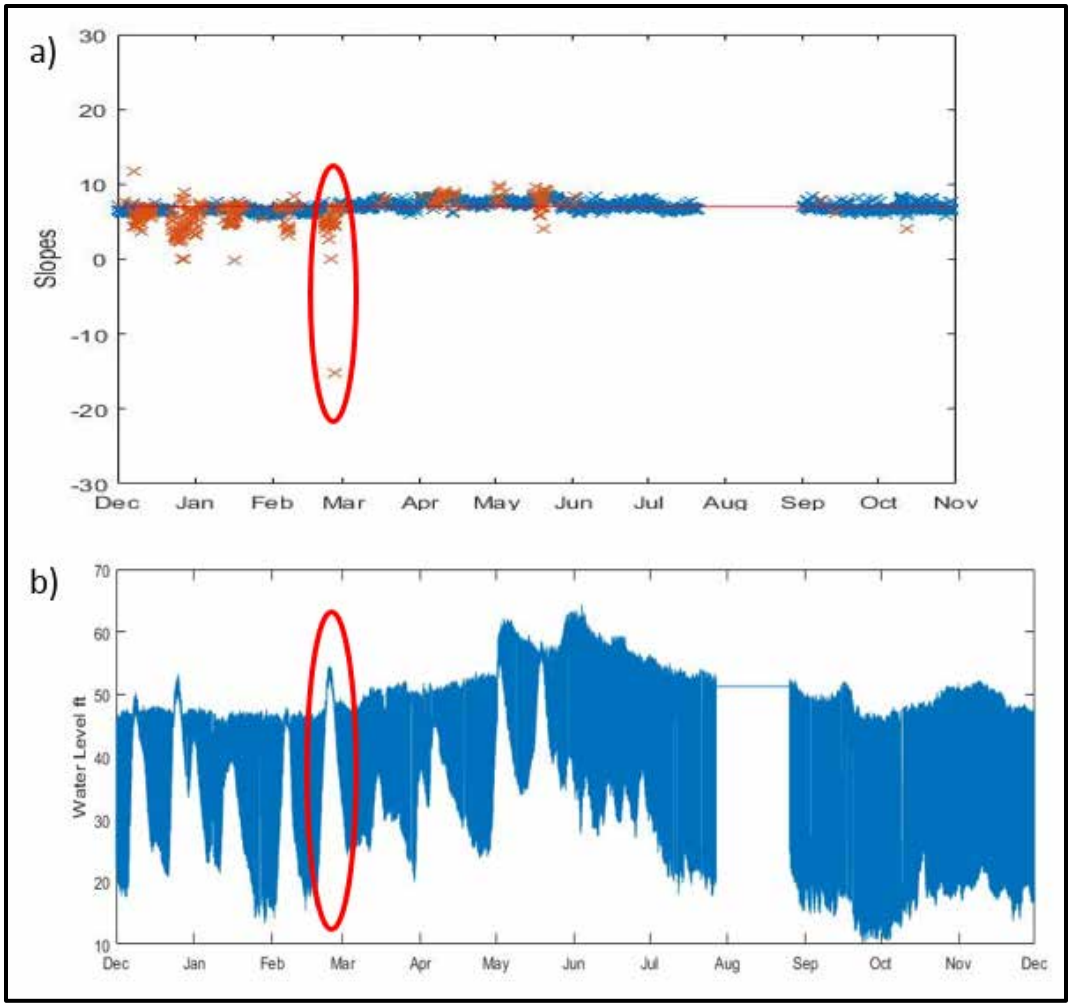

Figure 16B shows the chamber water levels, with the blue indicating how much the water levels in the chamber fluctuate throughout the year. For example, in September of the year investigated, the chamber water level typically fluctuated between around 20 and 50 ft. during a lockage, suggesting a differential head (difference between upstream and downstream water levels) of 30 ft. A period with a cluster of outliers, and the same period of water levels are circled in red in Figure 16 to highlight that the circled cluster, and indeed all other clusters, occurred when differential head was very low on the gate. Why low differential head might cause anomalous strain values was investigated. The findings were that, when differential head is very small, the load on the gate is proportionally small. Thus, the strain response in the gages is of a magnitude similar to the noise in the system.

Figure 17, which shows the response of a gage on Greenup for 1 day in October, illustrates this phenomenon. The plot on the left of Figure 17 shows the

chamber water levels for early October, with the red bars indicating the day the strain was investigated. For this period in October, the upstream water level was approximately 45 ft., and the downstream water level was around 15 ft., a differential head of 30 ft. The plot on the right shows the strain response with respect to water level for the same day. As seen in the plot on the right, the strain has a clear and approximately linear response to changes in water level (as hypothesized and desired). Figure 18 however, shows the strain response for a day in February where the differential head was less than 5 ft. The red bars on the left plot again signify the day in which the strain was investigated. The plot on the right shows the strain response for that day, and is circled in red for clarity. The two strain plots are on the same scale for easy comparison. For the day when the differential head is less than 5 ft., the strain response is indistinguishable from the noise in the system.

Figure 17. Strain response for S10-05 with differential head of 30 ft.

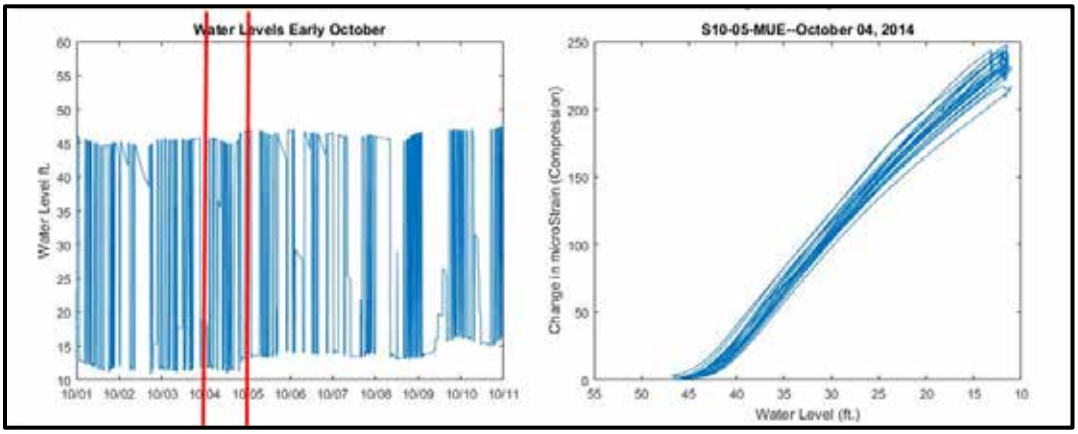

Figure 18. Strain response for S10-05 for differential head of less than 5 ft.

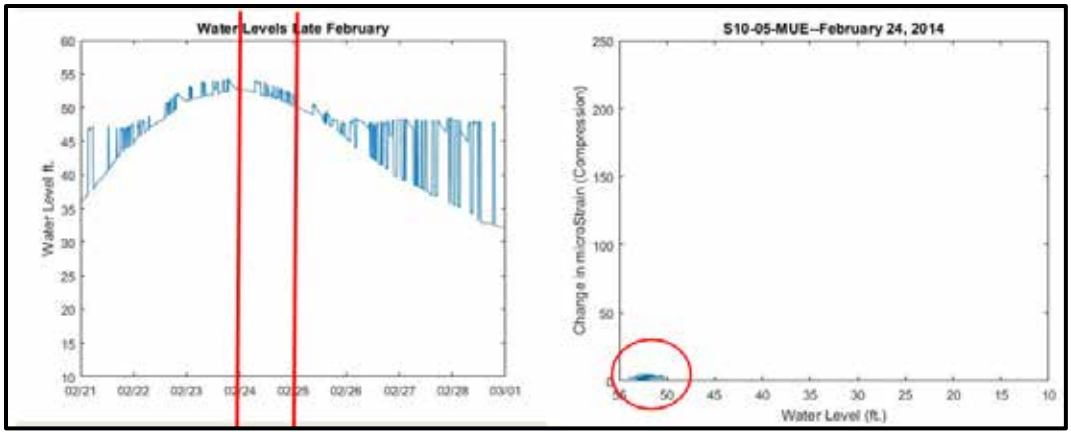

The results from this investigation led to updating the slope extraction algorithm to ignore any chamber events where the difference between the upstream and downstream water levels was less than 5 ft., as data from these events are uninformative.

Further outliers were seen to be caused by other anomalous events, such as the data logger shutting off in the middle of a fill event. Very significant outliers (greater than 5 standard deviations from the mean) were investigated and removed manually. These anomalies are almost always caused by a fault in the data logger (e.g., all gages shut off in the middle of a fill event). The manual removal of outliers is considered reasonable because, for normally distributed data, a point lying 5 standard deviations from the mean will occur once in 3.5 million observations. Furthermore, as mentioned in Section 2.4.2, only multiple consecutive outliers will be considered as an indication of damage.

The data were reprocessed using the event-based algorithm, and cleansed of significant outliers. Figure 19 shows the results for the same time period as shown in Figure 14 (p 37). These results show that the data are reliable and ready to be further analyzed.

Figure 19. Clean slopes for Greenup for 3 months, outliers removed.

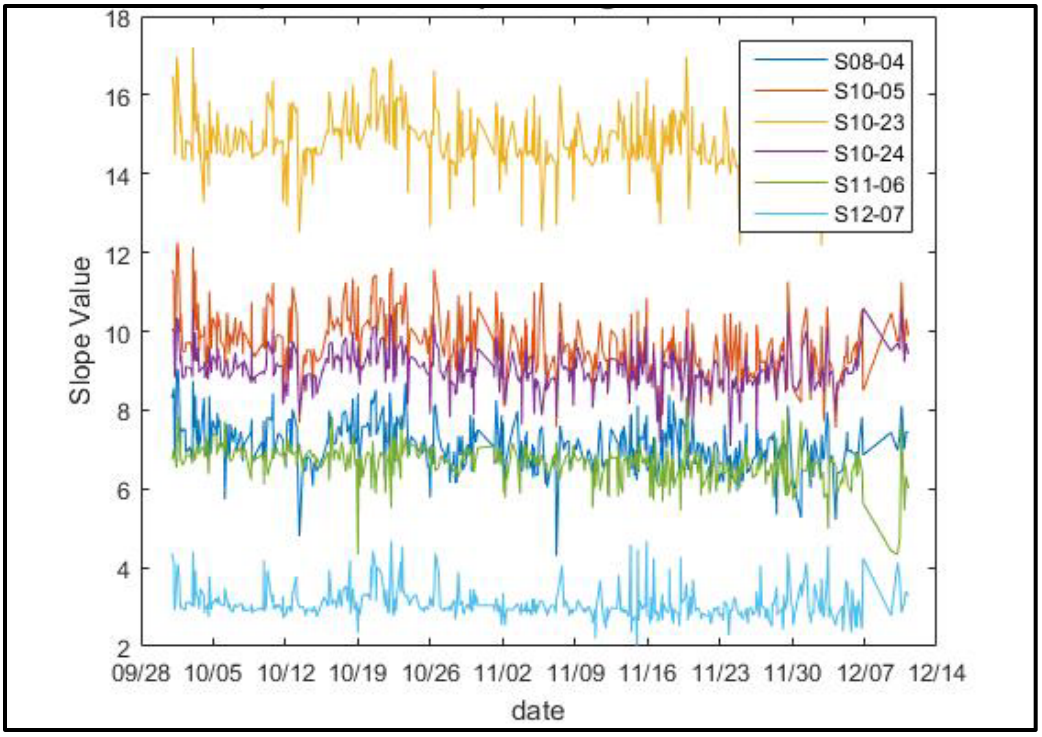

4.5 Stationarity of the damage sensitive feature

Using the slope has an added benefit in that it is expected to result in a stationary time series. As mentioned in Chapter 2, if a time series is nonstationary, differencing will often result in a stationary time series. The slope is effectively taking the first difference of strain with respect to the water level in the chamber, and the time series of the slope should be nominally stationary. An important distinction to be made is that, in the time series literature, differencing is typically done with respect to time. For the case of strain, engineering first-principles suggest that the strain data are dependent on the applied load, and are thus dependent on the water levels in the gate; therefore, differencing with respect to water levels is reasonable.

To visualize the stationarity, slope time series for various gages at three lock sites are investigated. The gates considered are The Dalles, Greenup, and Bonneville (Figures 20 through 22, respectively).

Figure 20. Time series for 6 months of slope values at The Dalles.

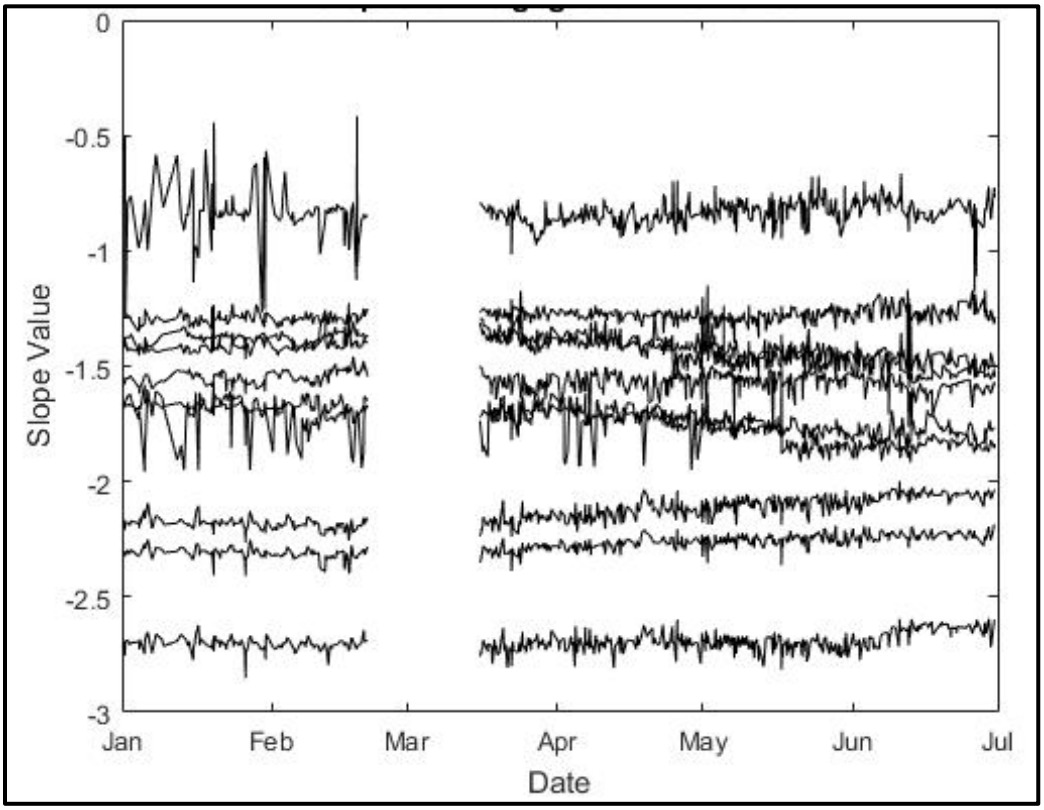

Figure 21. Time series for 1 year of slope data at Greenup.

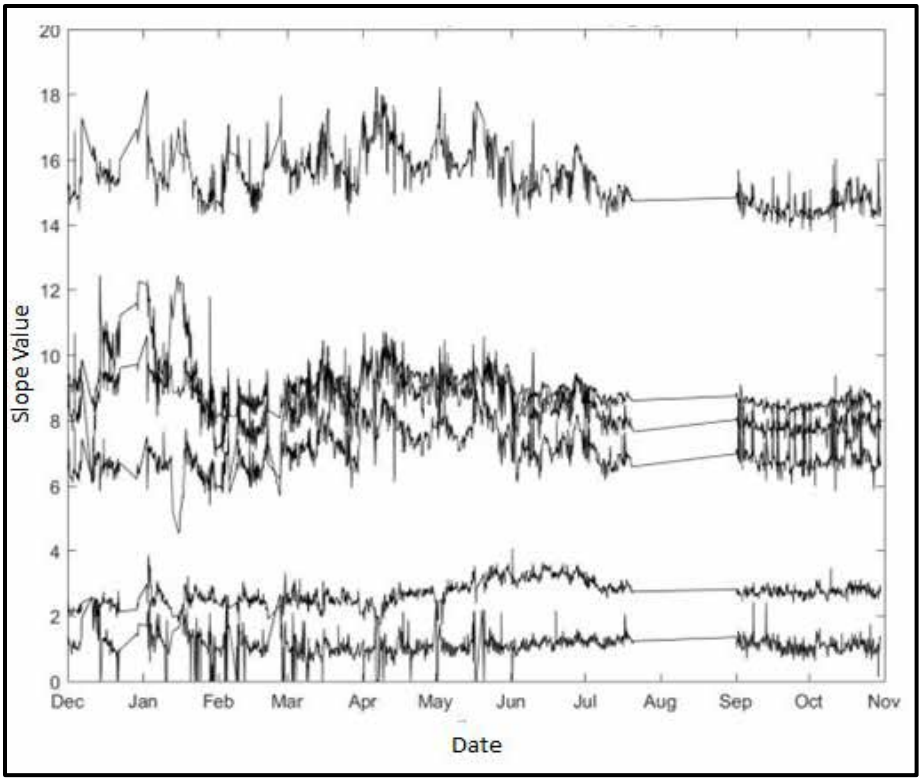

Figure 22. Time series for 6 months of slope data at Bonneville.

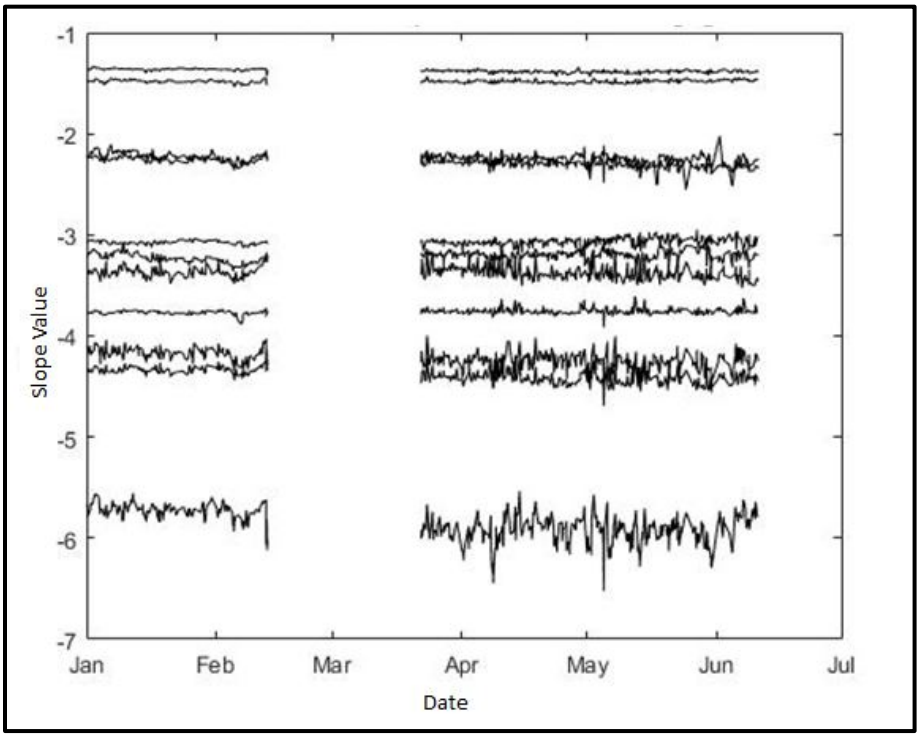

The long periods without data are due to the data logger being shut off due to operational issues such as a dead battery. Otherwise, the data display the qualities of stationarity. At each lock site and for each of the gages considered, no clear trend is seen and the data tend to fluctuate around a constant mean value with a consistent variance.

Inspection of the plots is a subjective method to assess the stationarity of the data. To rigorously quantify if the data is stationary or not, the methods described in Section 2.2 are used. First, the mean and variance of the data are checked for consistency across time. The consistency is checked in MATLAB by means of a moving average and moving variance approach. A moving average of each time series was taken with a 100-point window, meaning the average was first taken at the 100^{th} point of the time series, averaging across the previous 99 points. Similarly, the moving average was found at the remaining points in the time series, such that a vector of averages was obtained with a number of points equal to the length of the original time series minus 100. A similar process was repeated for the variance. For the time series investigated, the moving 100-point mean and variance were found to be relatively constant across the time interval investigated, with only minor fluctuations. Figures 23 through 25 show the consistency in the mean and variance. For simplicity, the coefficients of variation, defined as the square-root of the variance (the standard deviation) divided by the mean, are shown. The coefficient of variation (COV) contains information about both the mean and the variance; therefore, a change in either the mean or variance will cause a change in the COV, provided both are not changing at the same magnitude. For the slopes investigated, the variance and mean were not seen to change by the same magnitude.

Figure 23. Coefficients of variation for The Dalles, 100-point window.

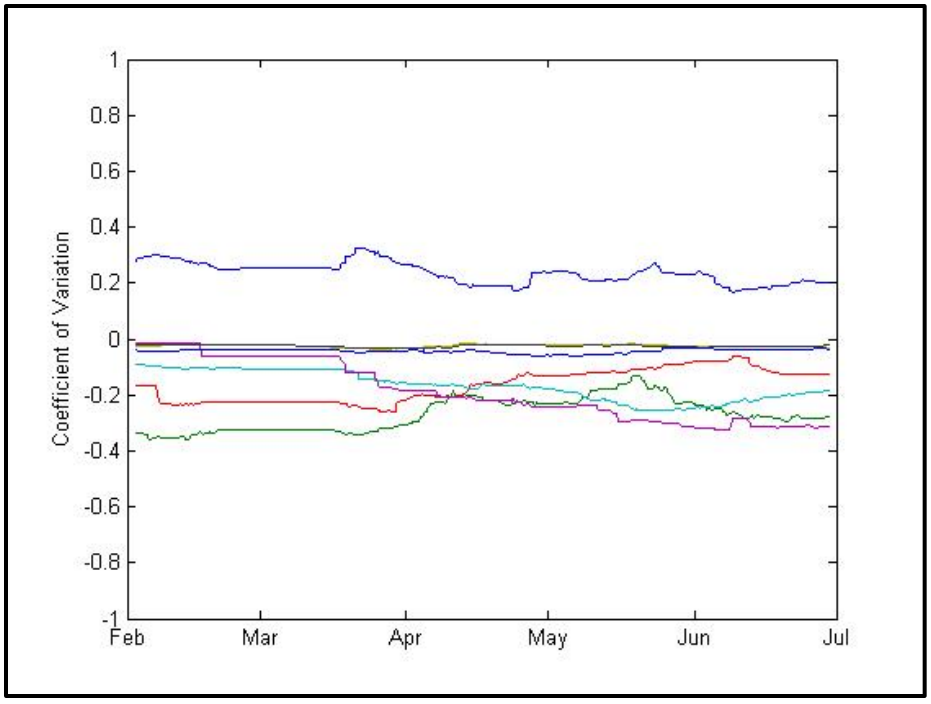

Figure 24. Coefficients of variation for Greenup, 100-point window.

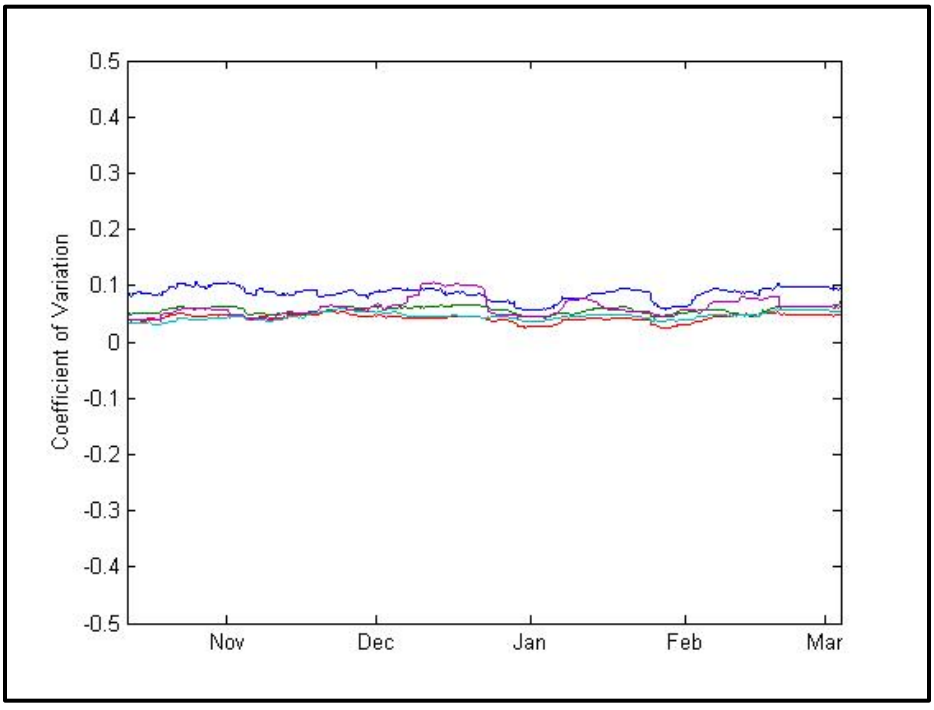

Figure 25. Coefficients of variation for Bonneville, 100-point window.

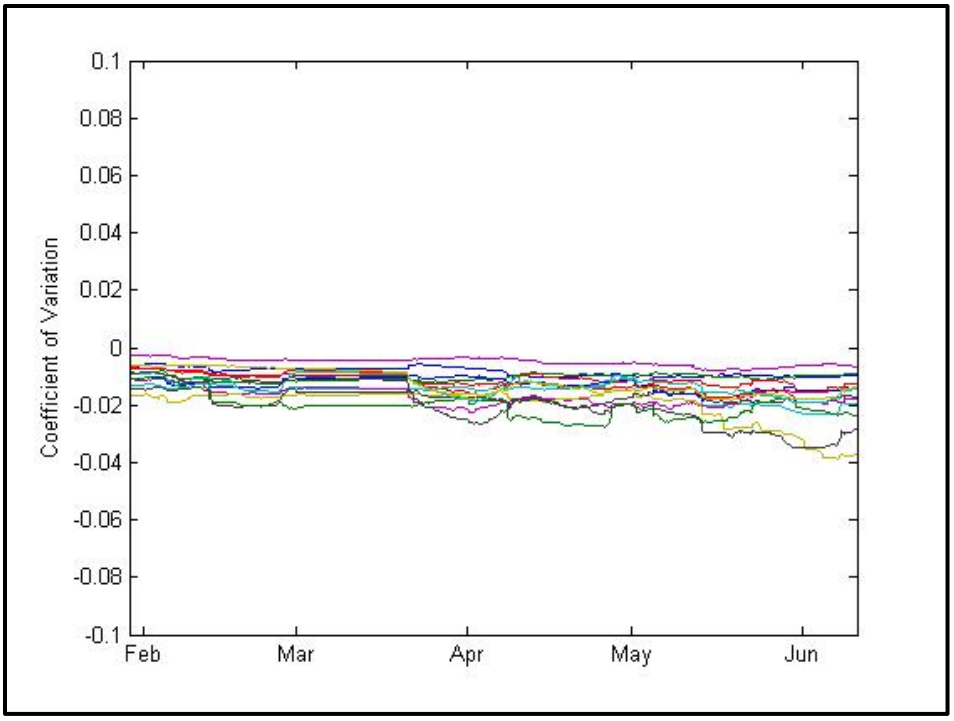

Figures 23 through 25 illustrate that the COVs, and by extension the mean and the variance, fluctuate slightly but are generally a consistent value. To further qualify the stationarity of the data, the ADF test is employed to test for a unit root, as described in Chapter 2. For the use of the ADF test, an assumption is made that the time series investigated can be well represented by an auto-regressive model. For the slope data, an autoregressive model is expected to be a reasonable fit as the behavior of the gate at any time is expected to be related to the behavior at previous times plus some random noise in the system. To visualize if the slope is well represented by an AR model, a predictive model is developed for a time series in MATLAB using AR model parameters, as outlined in MATLAB's documentation (MathWorks 2004). A plot is then created superimposing the AR predicted signal onto the measured signal (Figure 26).

Figure 26. (a) AR predicted model (red) superimposed on measured signal (blue); (b) same figure zoomed in for clarity.

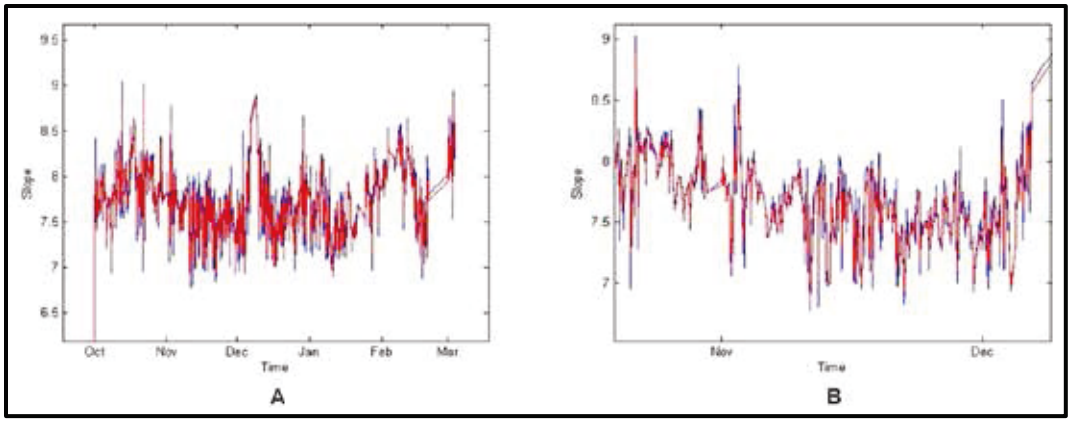

In Figure 26, the red line is the predicted model and the blue line is the measured signal, where Figure 26B shows a zoom of Figure 26A to better clarify 1 month of data. The plots illustrate that an AR model is able to readily describe the general behavior of the slope process, supporting the conjecture that slopes can be well represented by an AR model.

Applying the ADF test was done in MATLAB using the econometrics toolbox function *adftest* (MathWorks 2016). Applying *adftest* in MATLAB requires selection of an appropriate number of lags and an appropriate model. The model chosen was an Autoregressive model with a constant drift offset, labeled "ARD" in the MATLAB language. The constant drift offset accounts for the constant offset from zero that each of the series displays. The same results are obtained by choosing an autoregressive model without the constant drift parameter, and then mean-centering each series. The appropriate number of lags is chosen by the Akaike Information Criterion (AIC), as described in Chapter 2, which is a value included in the MATLAB results for the *adftest* function. The test was conducted for a wide range of lags, and the test with the smallest AIC value was chosen as the best option.

Recall that the ADF test is a left-tailed hypothesis test, meaning that values of the test statistic more negative than the critical value result in a rejection of the unit-root null hypothesis in favor of the stationary alternative. Table 2 lists the results of the ADF test for the time series shown in Figures 20 through 22. For simplicity, only the highest test statistic across all time series on each gate is shown, being the most critical case. That is, the highest test statistic is the one where there is the highest probability of rejecting the unit root hypothesis when a unit root is actually present. The test statistic for all other time series investigated for each gate is more negative. As seen,

in each case, the slopes are quantifiably stationary using the ADF test at 5% significance. Intuitively, what this means is that, if the test statistic was exactly the critical value, there would be a 5% probability of rejecting the null hypothesis of a unit root when a unit root was actually present. A more negative test statistic indicates a lower than 5% probability.

Table 2. ADF test results.

Gate	Critical Value	Maximum Test statistic
The Dalles	–1.94	–1.96
Greenup	–1.94	–3.08
Bonneville	–1.94	–2.15

The slope is well approximated as being stationary, and thus, it is assumed to be ergodic as well, and so statistical methods of analysis for stationary time series will be used and will be discussed in more detail later.

4.6 Implementation of SHM system

As discussed in Section 4.1.2, in the presence of damage, the load in the gate will redistribute leading to a change in strain in some of the girders under the same load. This in turn will lead to a change in the slope. Statistical analysis of the slope data is used to monitor for changes in the statistical parameters of the slope time series, with a significant and persistent change being an indication of damage (see Figure 27).

PCA is the method selected to combine the data from multiple gages into a single time series for statistical analysis. The combination of data from multiple gages is of interest, as opposed to simply using one slope series, because the location of gap formation is unknown. Moreover, the redistribution of load is expected to be a localized phenomenon in the gate, and so multiple gages need to be monitored simultaneously.

To begin the PCA process, an eigenvalue decomposition of the covariance matrix for the slopes of the undamaged structure is performed, and the associated eigenvectors are obtained. This study assumes that the data obtained from the SMART gate database is representative of a healthy structure. The authors are confident in this assumption as the instrumentation was deployed on new gates in the year 2011.

Figure 27. Flowchart of damage detection procedure.

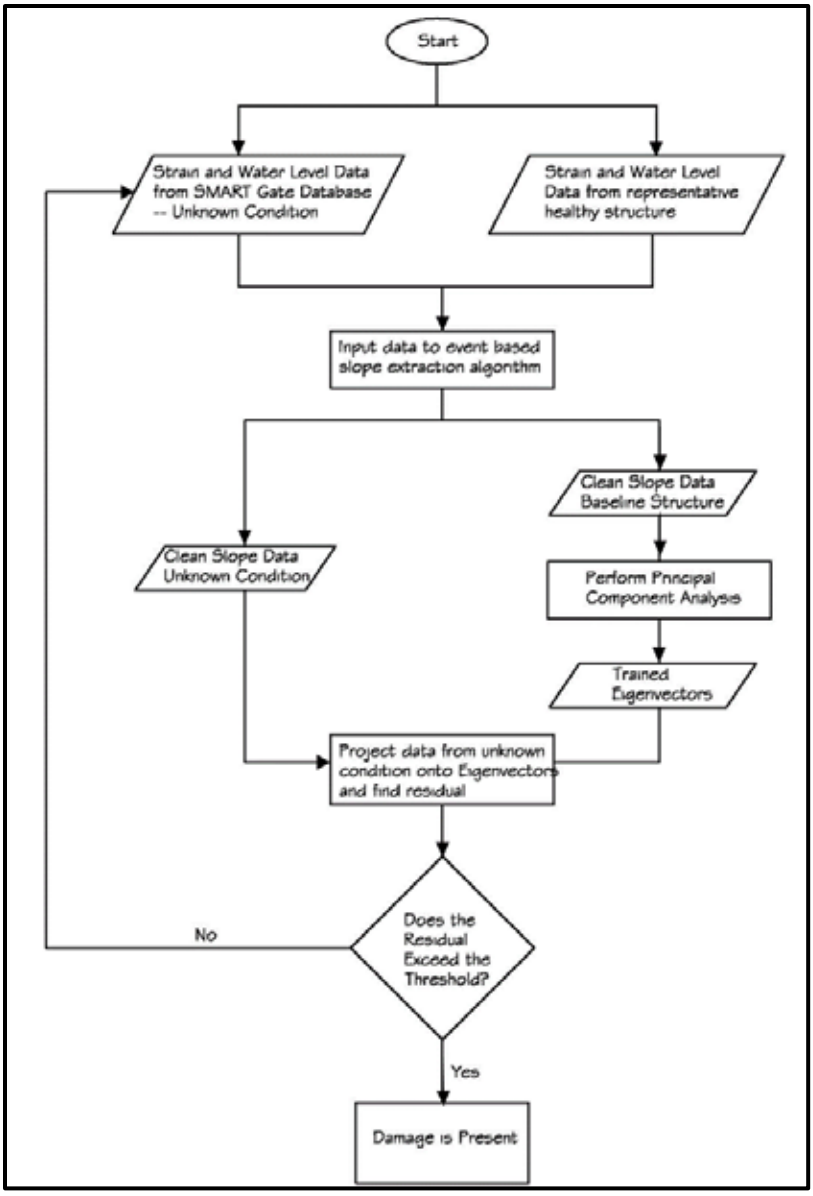

Subsequent data from the structure are projected onto the eigenvectors obtained from the training data and the damage index is found as explained in Chapter 2. If consecutive instances of the damage index being beyond the threshold are observed, damage is said to be present. Otherwise, the process is repeated.

To validate this study, damage is simulated in an FEM model and superimposed on the measured data to verify that the method works, since no observed data exist for a gate in the presence of a known gap. The details of the damage simulation are explained in the next chapter.

4.7 Summary

This chapter has shown that the "slope," defined as the change in strain with respect to water level, has been identified as a good candidate for a damage sensitive feature. Modifying the strain data by differencing them effectively removes any seasonal trends in the data and forces the data to be stationary. Using the slope significantly reduces the computational requirements for analysis by reducing the number of data points to be analyzed by three orders of magnitude, while still maintaining the information of interest. To facilitate the extraction of slopes from the strain data, an automated algorithm was created in MATLAB. After investigation, the algorithm was updated to exclude chamber events where head differential on the gate was less than 5 ft. The updated algorithm was shown to provide clean and reliable data for use in a damage detection algorithm. PCA was chosen as the method to combine information from multiple sensors into a single metric that can identify damage. Combining data from multiple sensors is critical because the location of a gap is unknown, and the redistribution of load is a localized phenomenon. To begin PCA, a reference dataset is used to train the PCA eigenvectors. Then the data of unknown condition are projected onto the eigenvectors and the PCA damage index is found. If the damage index consecutively exceeds a predefined threshold, damage will be said to be present. The next chapter presents an example of PCA of slope data from the Greenup lock and dam site to validate the methodology.

5 Validation of Methodology

To determine the effectiveness of the slope as a damage sensitive feature, a case study was performed using miter gates at Greenup lock and dam. Data were extracted from the SMART Gate database, processed, and cleansed. Many of the conjectures presented in the preceding chapters, such as slope stationarity and independence from temperature, are verified using 1 year of measured data from Greenup. To assess damage detection potential, a previously constructed, high-fidelity finite element model from a different, but geometrically similar, gate is used. The gap to be detected is modeled, and the change in strain under the same load is recorded. This change in strain is systematically superimposed onto the measured data. PCA is then applied, and the damage index is used as a method to indicate the presence of damage. The process is described in detail in the following sections.

5.1 Greenup Lock and Dam site

PCA was applied to the data collected from the SMART Gate system for the Greenup Lock and Dam, which is on the Ohio River near Greenup, KY. The lock gate is a horizontally framed miter gate, consisting of 12 horizontal girders of dimensions similar to those shown in Figure 2 (p 3).

5.1.1 Instrumentation

The sensors at Greenup are located on the upstream gate. The instrumentation on the gate consists of 115 strain gages, eight temperature sensors, four pressure transducers (to measure water levels), and a number of tilt meters and load sensors not used in this study. The strain gages used are 350 ohm, full-bridge, HiTec gages, model HBWF-35-125-6-150GP-NT. The gages are placed primarily on every other girder with a gage near the quoin, a gage near the miter, and three gages at mid-span to allow assessment of bending moments. A number of gages are also located on the vertical strut members of the gate. The temperature sensors are HiTec model TSW-00-D-150GP-RTD and are placed in a variety of locations on the gate and near the data logger. The pressure transducers are Campbell Scientific model CS450-L150-SA-2-9-NC and are intended to measure the upstream, downstream, and lock chamber water-levels. The sensors are all connected to a Campbell Scientific data logger model CR1000-ST-SW-NC. The data from each sensor are sampled every 15 seconds and are uploaded to a database by combination of wireless and wired communication.

Figure 28 shows a plan view of one leaf of the Greenup gate; Girders G1-G12 are labelled on the left; the red squares represent the locations of strain gages. Only one leaf on the gate is shown, and the squares that are located mid-span of the girders represent four separate gages.

5.1.2 Gage selection for investigation

The selection of gages was narrowed down to choices that would both exhibit a generally strong response under load and likely be affected by the presence of a gap. Gages near the bottom of the gate will carry more load than those near the top. Therefore, gages near the bottom of the gate are considered.

Figure 28. Strain gage locations on Greenup gate.

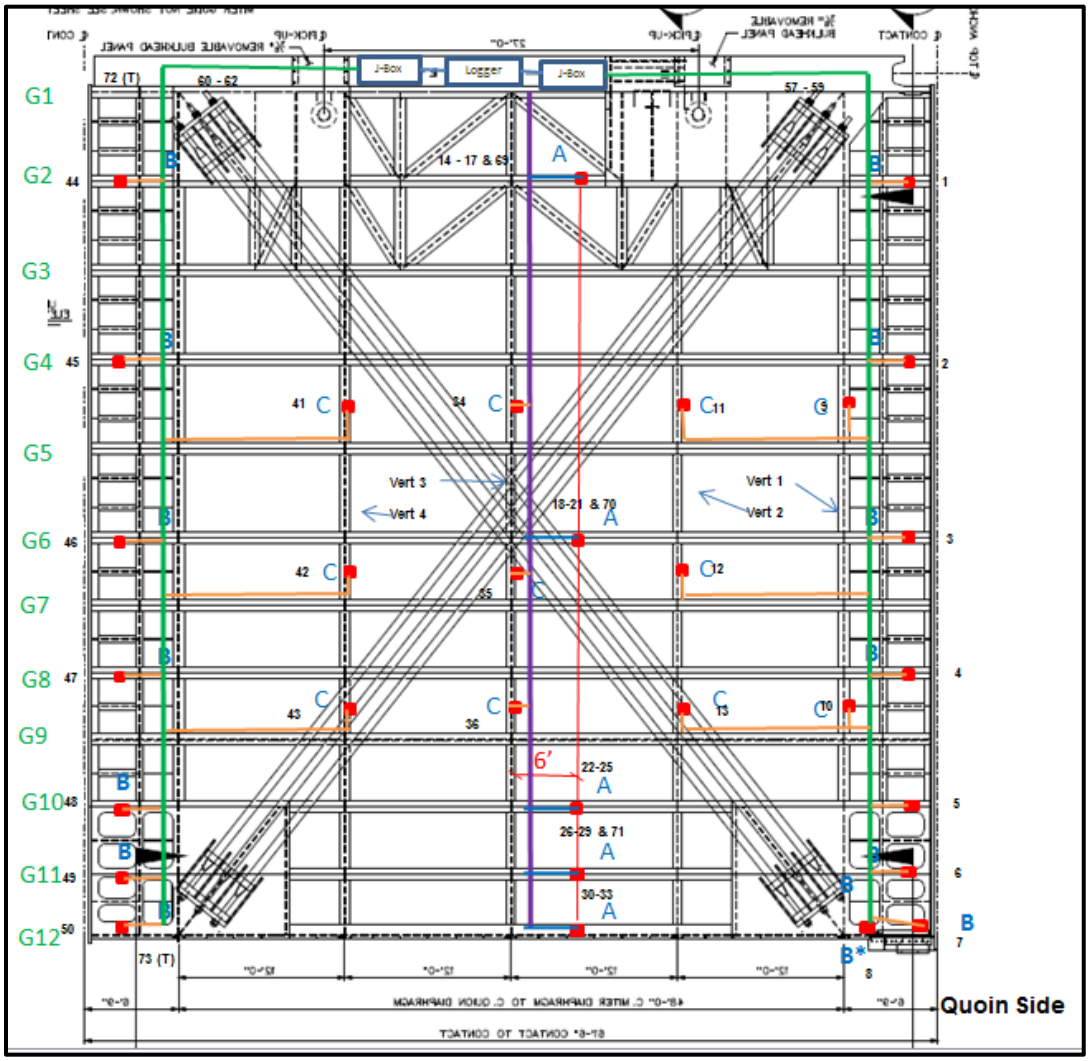

Furthermore, the gap will be in the gate/quoin interface, and thus gages near the quoin are affected the most. Accordingly, the final gages included in the study are those located near the bottom of the gate, and either at mid-span on the girder, or near the quoin. Figure 29 shows the areas where the gages are selected, boxed in bold red.

To facilitate extraction of the data from the database and for ease of future processing, a numbering convention has been implemented for the gages on the gate. Table 3 lists the location of gages selected for this study, and their assigned numbers.

Figure 29. Area with gages of interest for study.

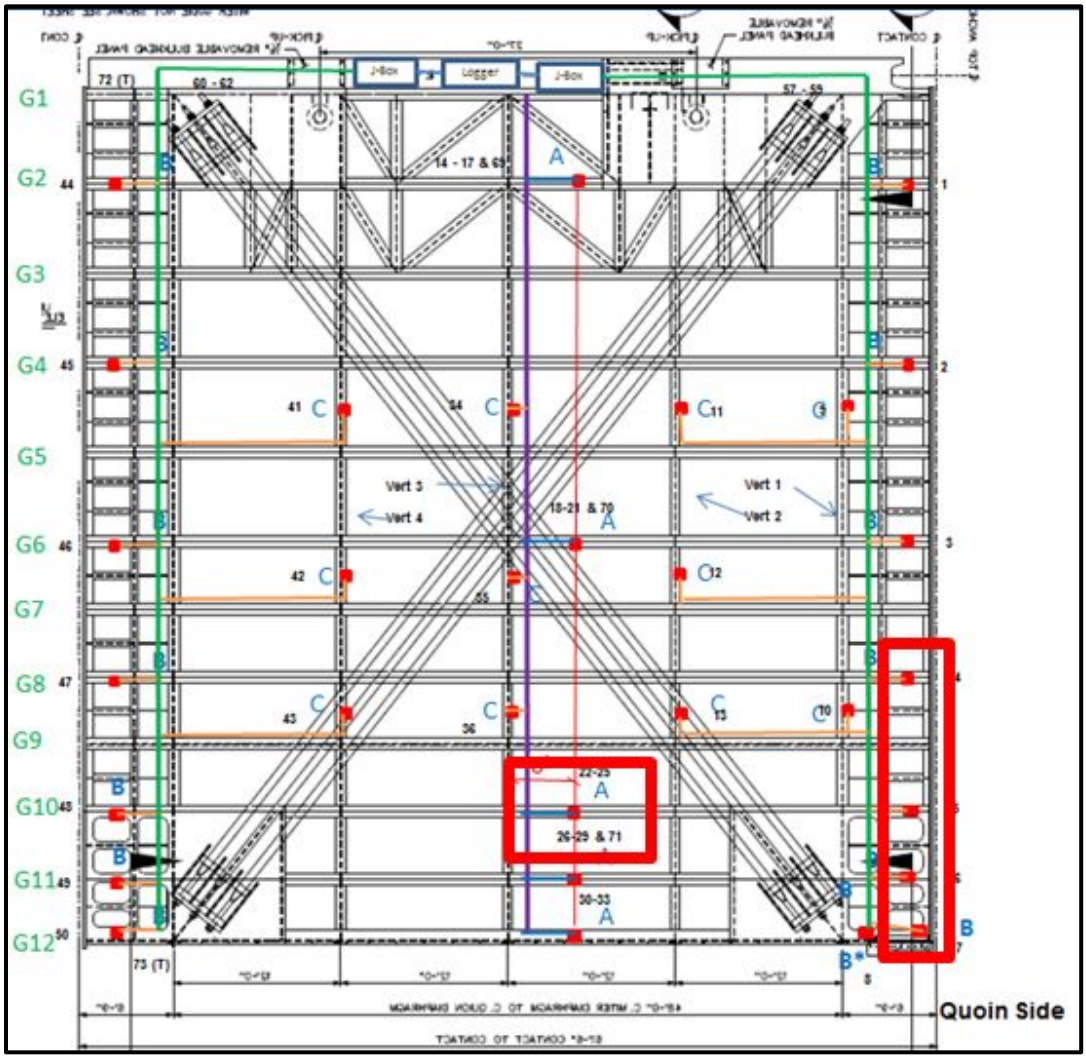

Table 3. Gage names and locations used in study.

Gage Number	Location Description
S08-04	Girder 8, near the quoin
S10-05	Girder 10, near the quoin
S10-23	Girder 10, mid-span
S10-24	Girder 10, mid-span
S11-06	Girder 11, near the quoin
S12-07	Girder 12, near the quoin

5.2 Data preprocessing

The data from the gages in Table 3 were preprocessed in the slope extraction algorithm as explained in Chapter 4. Chapter 4 presented the time series of clean slopes for verification of the algorithm; Figure 30 shows them again for the reader's convenience. These cleansed slopes are then used to further verify some of the underlying assumptions made in previous chapter, such as stationarity and temperature independence.

Figure 30. Clean slope data from Greenup.

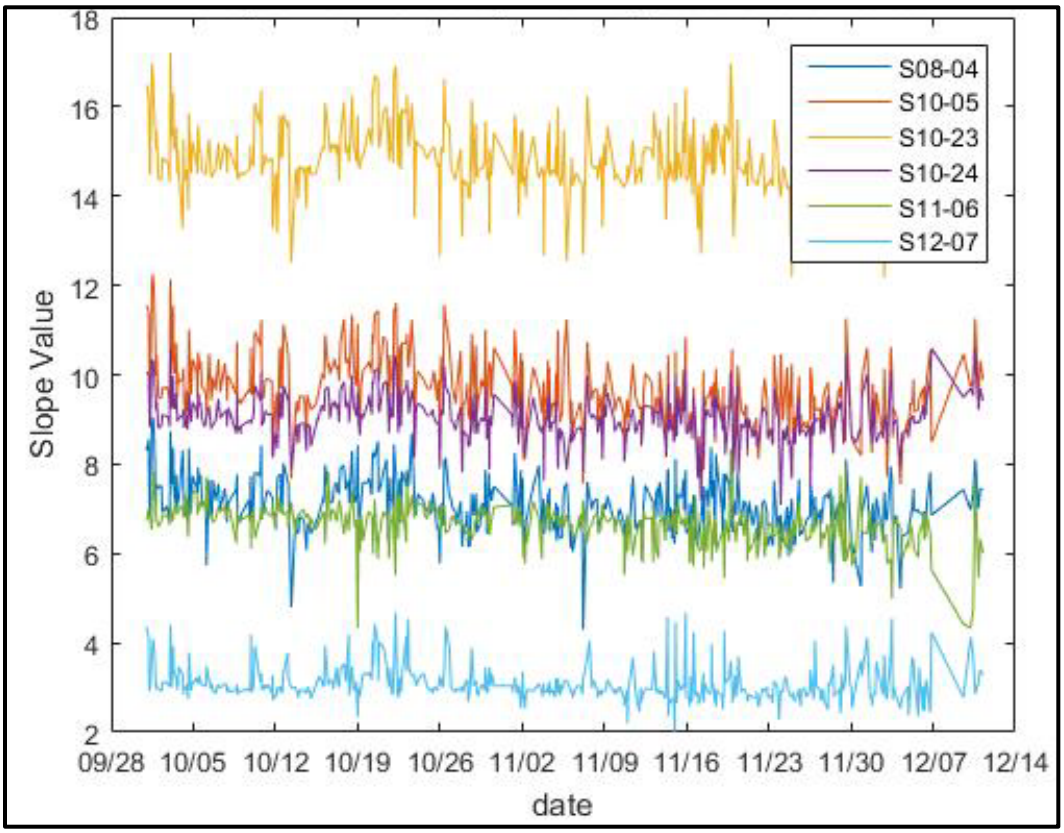

5.3 Verification of temperature independence

The slope data investigated appeared to be nominally free of the seasonal trends seen in the strain data; thus, the slopes are assumed to be free of any correlation with temperature. The motivation for this conjecture is that chamber events occur over a relatively short period of time (e.g., 15 minutes) and air or water temperatures will not vary significantly over this period. Accordingly, any thermal induced strain will be constant during chamber events and should be removed by the process of differencing. To support this conjecture, a correlation study was performed, testing the correlation of the slopes with both air temperature and water temperature. The first step in the process was extracting the temperature data for each fill and emptying event. Both the air and water temperatures were sampled at the start of each event. Using only one measurement for each event is reasonable because the chamber events are relatively short, as previously stated, and air or water temperatures would only change minimally within the event. The temperature data were plotted to ensure the readings were reasonable, with the data for air and water temperature from December 2013 through November 2014 shown in Figures 31 and 32, respectively.

Figure 31. Air temperature for Greenup.

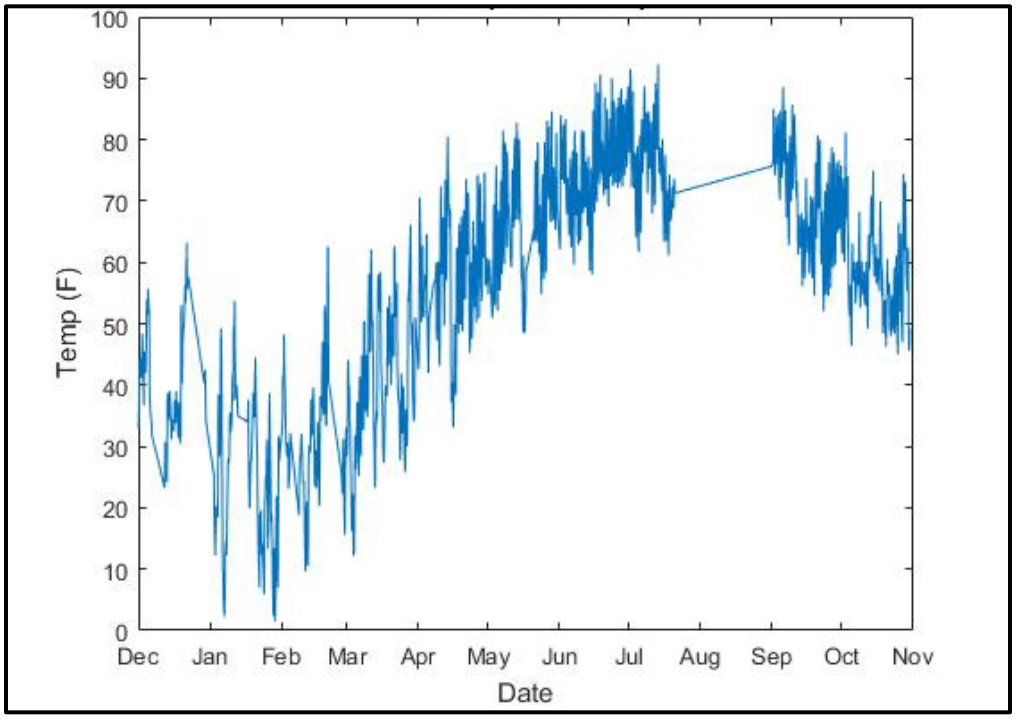

Figure 32. Water temperatures at Greenup.

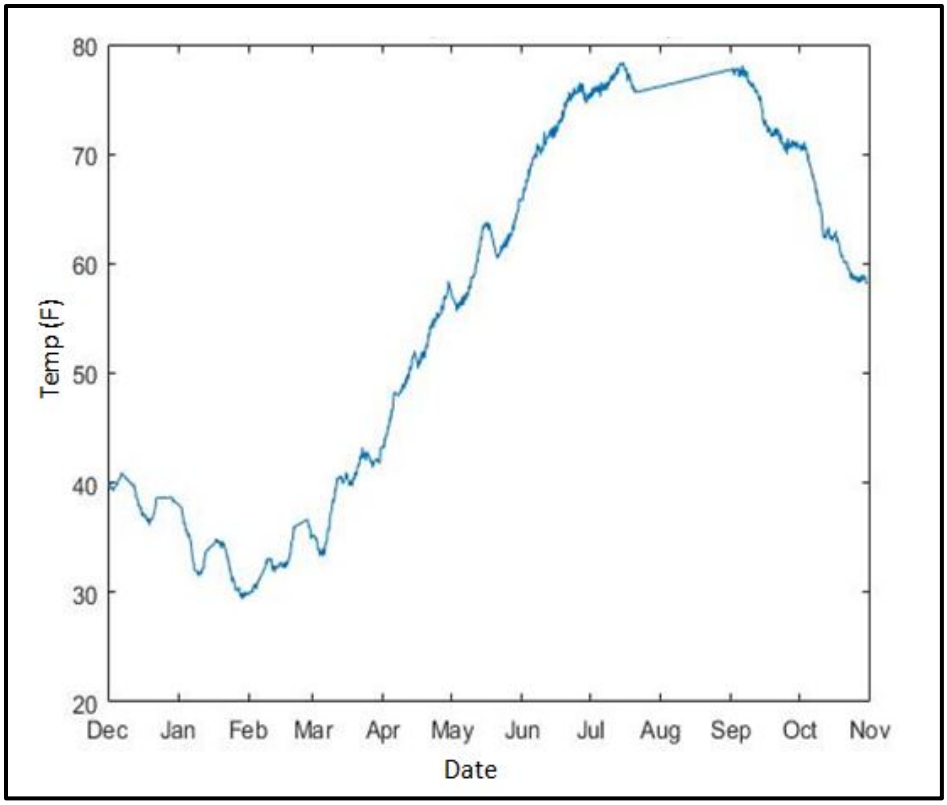

As seen in Figures 31 and 32, the air and water temperature follow a trend that is expected through the year; the temperatures are lower in the winter and higher in the summer. Critically, the water temperature rarely drops below freezing, which is expected, and thus, the temperature data are viewed as reasonable.

To investigate the correlation between slopes and temperature, the slopes were scatter plotted versus temperature to inspect for any obvious trends. Examples of the scatter plots are shown in Figures 33 and 34, which show little correlation.

Figure 33. Scatter plot of slope vs. air temperature for Gage S10-05.

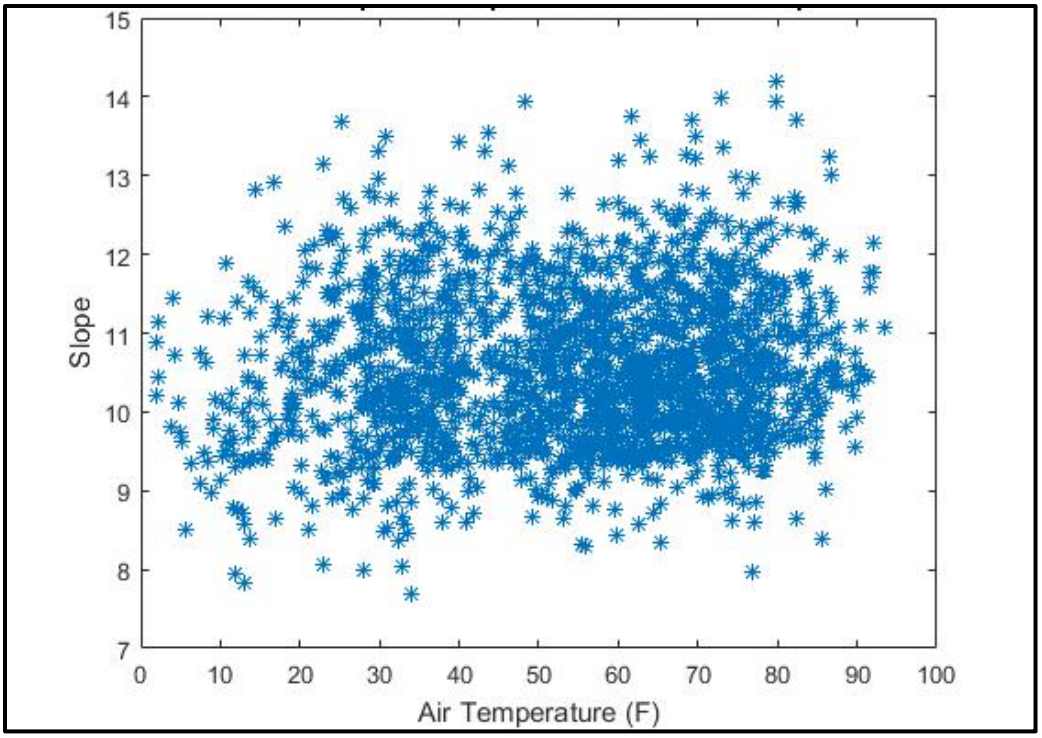

Figure 34. Scatter plot of slope vs. water temperature for Gage S10-05.

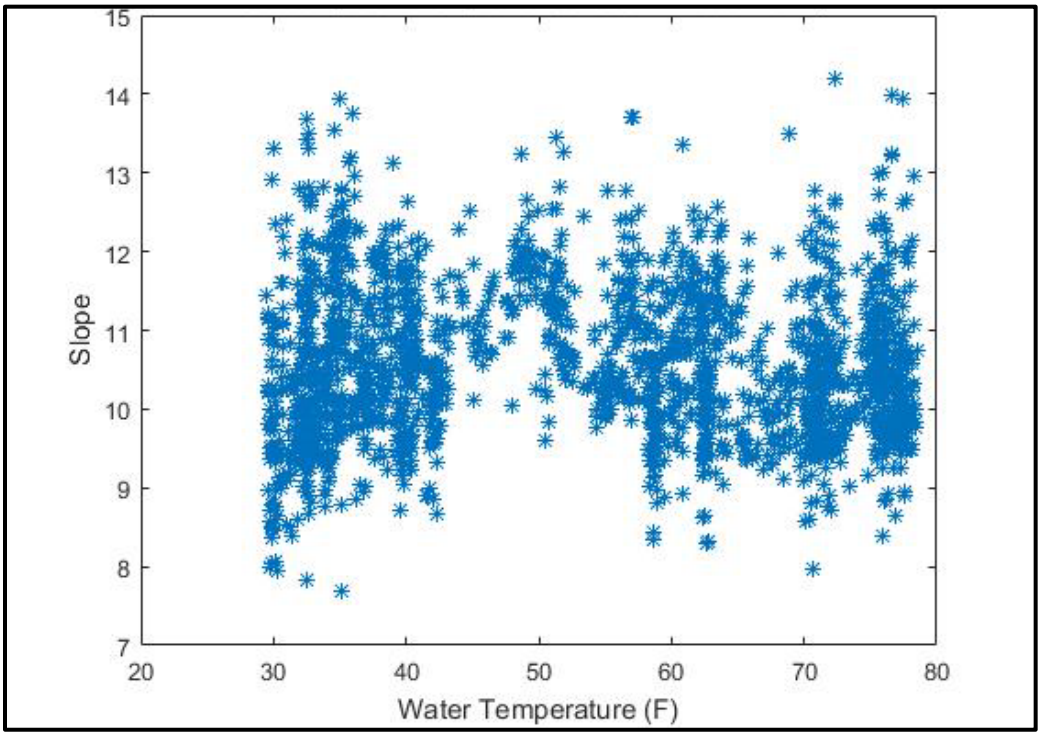

To quantify the relationship between slope and temperature, the correlation coefficients were calculated for each gage against each temperature. Table 4 lists the results.

Table 4. Correlation coefficients of slopes vs. temperature.

Gage Number	Correlation With Air Temperature	Correlation with Water Temperature
S08-04	−0.18	−0.05
S10-05	0.39	0.45
S10-23	−0.08	−0.08
S10-24	0.27	0.33
S11-06	0.26	0.24
S12-07	0.10	0.03

The correlation coefficients in Table 4 suggest that, in general, there is little to no correlation between slope data and temperature data. The highest correlation is found on Girder 10, but still the coefficient is less than 0.50. The moderate correlation seen is expected to be a product of an underlying driving factor, namely, the water levels in the river. The differential head on the gate is generally what drives the load in the girders. Through seasonal variations (summer rains, melting snow, etc.), the river levels fluctuate at a rate consistent with temperatures, and so, the moderate correlation between slopes and temperature may simply be a correlation between slope and water levels. Figure 35 shows this seasonal relationship of the water levels. Here, the chamber water levels at Greenup are plotted vs. time, where the water levels are seen to follow a similar trend as the temperatures. That is, the water levels for the time period investigated increase in the warmer months, and decrease in the colder months.

Figure 35. Chamber water levels for entire year at Greenup.

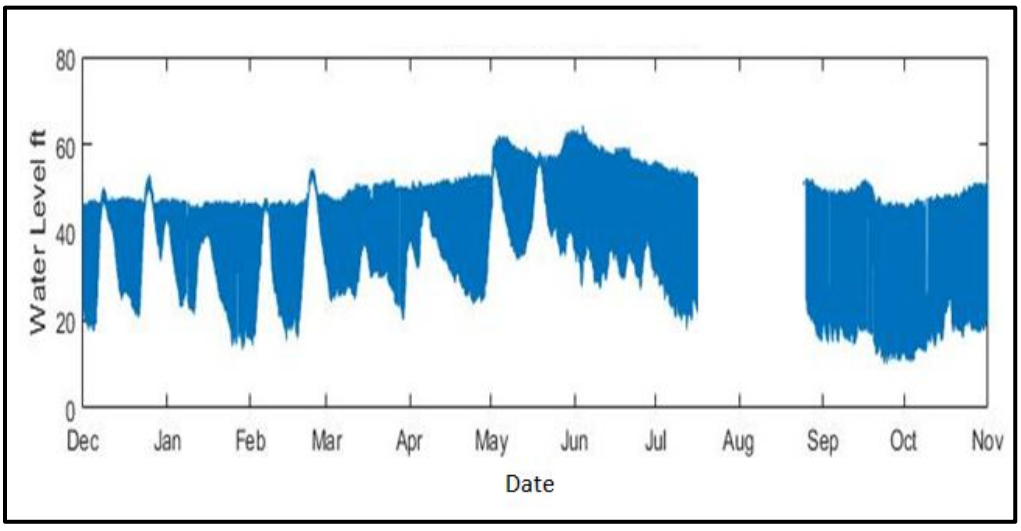

To further justify the conjecture that water levels are correlated with differential head, the correlation coefficients between differential head and temperature are calculated, as are the coefficients between slope and differential head. Table 5 lists these results, and shows the moderate correlation between temperature and differential head, and moderate to high correlation between slopes and differential head. The correlation coefficients support the conjecture that slopes are uncorrelated with temperature, and that any correlation seen is actually being driven by a similar trend between temperature and water levels. Furthermore, the coefficients support the conjecture that differential head is the driving force in the gate.

Finally, an unexpected but beneficial outcome of this correlation study is that it showed that the slope time series in each gage are very highly correlated with one another, particularly those at the bottom of the gate. Correlation coefficients between gages on Girders 10, 11, and 12 ranged from 0.7 to 0.86. This result further justifies the selection of slope as a damage detector, and the use of a multivariate approach to testing for damage.

Table 5. Correlation coefficients with differential head.

Scenario	Corr. With Diff. Head
Air Temperature	0.30
Water Temperature	0.47
S08-04	0.42
S10-05	0.44
S10-23	0.52
S10-24	0.54
S11-06	0.59
S12-07	0.63

5.4 Stationarity of slope

As seen in Section 4.5, the time series of the slopes are seen to be generally stationary across different gages and different gates. For completeness, the slopes are also shown to be stationary for the gages used in this study. The plots shown in Figure 30 (p 54) appear to be generally stationary, with perhaps the potential of a trend downward, but the data shown are only a portion of the data included in the study. To quantify whether or not the series are stationary, the ADF test is implemented on the full datasets as described in Section 2.2. As discussed, the *adftest* function was used in MATLAB, with the number of appropriate lags dependent on the series being investigated and determined according to the AIC criteria. Table 6 lists the results for

each gage. Note that the critical value for each test is determined by the number of samples and the model chosen, both of which are identical for each case; thus, the critical value never changes.

Table 6. ADF Test results for slope time series.

Gage Number	Critical Value	ADF Test Statistic
S08-04	−2.87	−3.00
S10-05	−2.87	−3.23
S10-23	−2.87	−5.29
S10-24	−2.87	−5.14
S11-06	−2.87	−2.91
S12-07	−2.87	−5.32

Recall that the ADF test is a left-tailed probability test, so a test statistic more negative than the critical value will reject the null hypothesis of a unit root process in favor of the stationary alternative. As seen, the slope time series for each gage can be shown as quantifiably stationary, and thus, PCA is an ideal candidate for damage detection.

5.5 Normal distribution of slope data

For the sake of setting thresholds for damage detection, recall the argument for using a threshold of 3 standard deviations from the mean. The motivation for this threshold is that, 99.7% of the time, normally distributed data should fall within 3 standard deviations of the mean. It remains to be shown that the slope data do approximately follow a normal distribution. To support the conjecture of normal distribution in the data, graphical methods are used. The first method is done by plotting a histogram of the slope data, and fitting a normal distribution to points.

The procedure for performing this type of graphical inspection can be gleaned from any statistics textbook, such as Ang and Tang (2007). For this study, the *histfit* command in MATLAB is employed with the "normal" model chosen. The slope data are normalized for easy comparison. Figure 36 shows exemplary results.

The goodness of this fit can be further supported by performing a Chi-squared goodness of fit test, such as by using the MATLAB function *chi2gof*. For the data presented here, the data are seen to acceptably fit the normal probability distribution because the null hypothesis of the chi-squared goodness of fit test cannot be rejected.

Figure 36. Data from Gage S10-05 fit to a normal distribution.

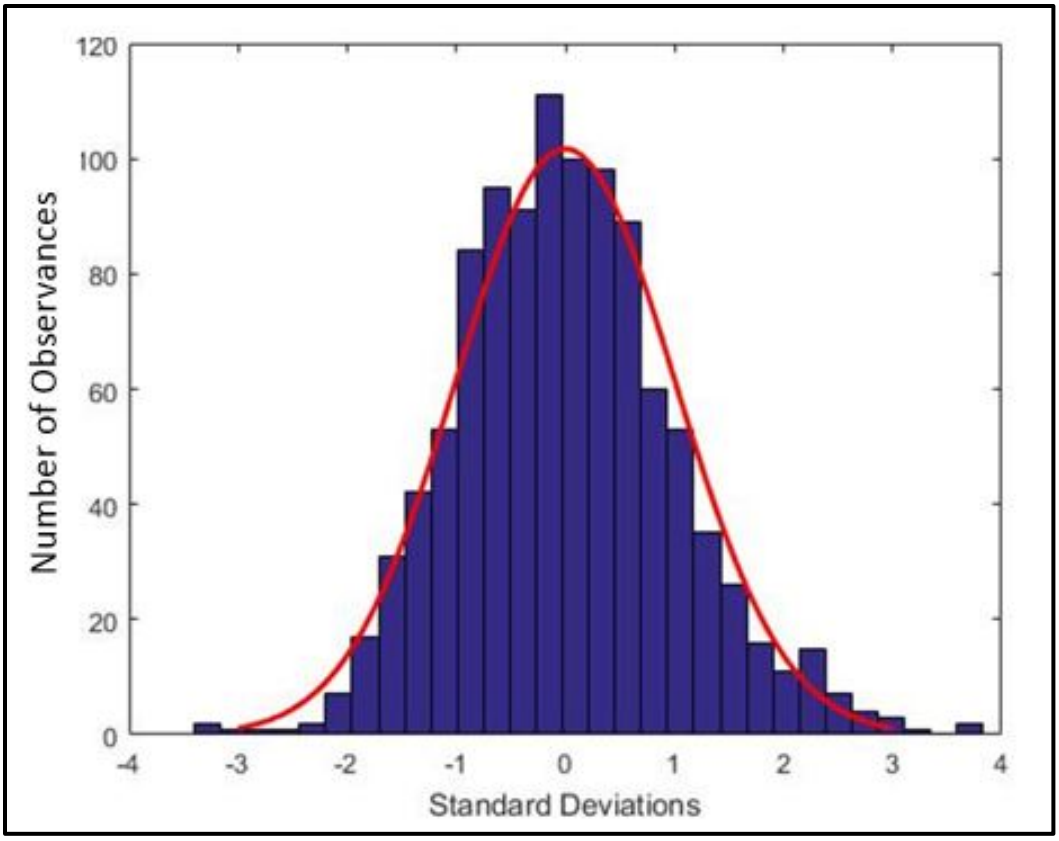

Another method to determine if the slopes are normally distributed is to plot the time series on probability paper. This process effectively plots the empirical cumulative distribution function (CDF) of the data and compares it to an actual normal CDF. If the data are normally distributed, the empirical plot should exactly overlap the actual normal CDF. Figure 37 shows the same data from histogram fit. The dashed line in the figure represents the actual normal CDF, and the blue data points represent the empirical CDF evaluated at each data point. There is very good agreement between the data and a normal CDF.

The above examples indicate that the data can be well approximated as normally distributed, lending credence to the threshold parameters of ±3 standard deviations.

Figure 37. Probability plot for data on Gage S10-05.

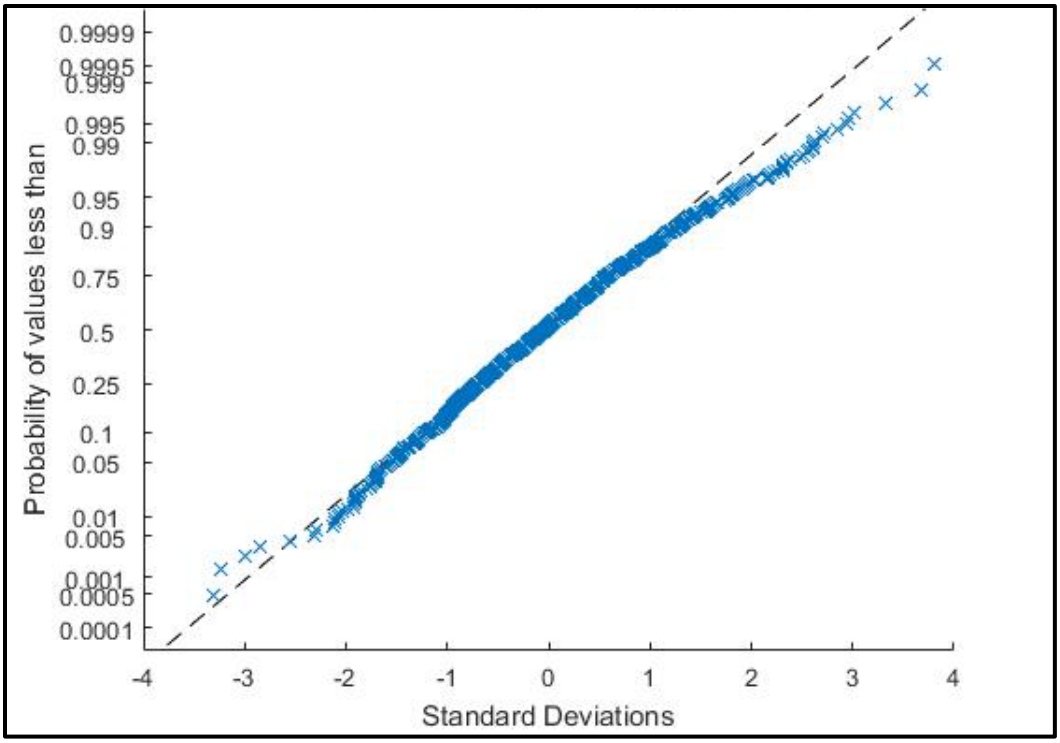

5.6 Training PCA with the measured slope data

The preceding sections illustrate that the previous assumptions about the slopes are consistent with the data, i.e., the slopes are nominally stationary, normally distributed, and independent of temperature. Thus, the study proceeded by applying PCA to the data as explained in Chapter 2. First, 5 months of data, from May 2014 through September 2014, were used as training data. To compare the sensitivity to the amount of variance to keep in the data when performing the PCA method, two scenarios are considered:

1. Keep 92% of the variance – use the first three eigenvectors
2. Keep 98% of the variance – use all but the last eigenvector.

The eigenvectors obtained from the training data for both cases were stored and the residuals were found using data from October 2014 through March 2015, as shown in Equation 2-29. The data from October through March are expected to indicate no damage, and thus, the damage index of this data is inspected for Type 1 errors, that is, false positive. The nature of the damage index being a squared value, as seen in Equation 2-29 (p 24), the plot of *DI* takes the form of a bar graph (Figures 38 and 39). In these plots, the red

line in the middle represents when the algorithm training was stopped. Everything to the left of the red line represents the damage index of the training data, and everything to the right represents the damage index from projecting the untrained data onto the trained eigenvectors. The blue horizontal line represents the threshold of 3 standard deviations away from the mean value of the trained damage index.

As mentioned in Chapter 2, damage will be indicated when consecutive observations above the threshold are observed. If the number of consecutive observations required to indicate damage is equal to 2, consecutive observations above the threshold for Case 1 are never observed. For Case 2, there is one occurrence of consecutive observations on December 18th. If the number of consecutive observations above the threshold required is 3, a false positive never occurs.

To formalize the probability of false positives, first Equation 2-34 is used to find the probability of an observation exceeding the threshold of ±3 standard deviations of the mean. For this dataset, there were 27 observations above the threshold and a total of 2028 samples, yielding a probability of exceedance of 0.0133. For a binomial distribution to be valid, the observations in the data must be independent.

To test this, the correlation coefficient was found between a time series consisting of the damage index, and another time series consisting of the same damage index shifted one point in time. The data consisted of 2,028 points, so the correlation was found between a time series consisting of $[\bar{A}\bar{A}_1,\bar{A}\bar{A}_2,\ldots\bar{A}\bar{A}_{2027}]$ and a time series consisting of $[\bar{A}\bar{A}_2,\bar{A}\bar{A}_3,\ldots\bar{A}\bar{A}_{2028}]$; the results indicated that the correlation coefficient was 0.07. This supports the conjecture that the observations in the damage index are independent. Now, Equation 2-31 is used to calculate the probability for the case of $q = s = 2$ and $q = s = 3$, with the results listed in Table 7.

Figure 38. Plot of PCA damage index for undamaged case w/ 92% variance retained.

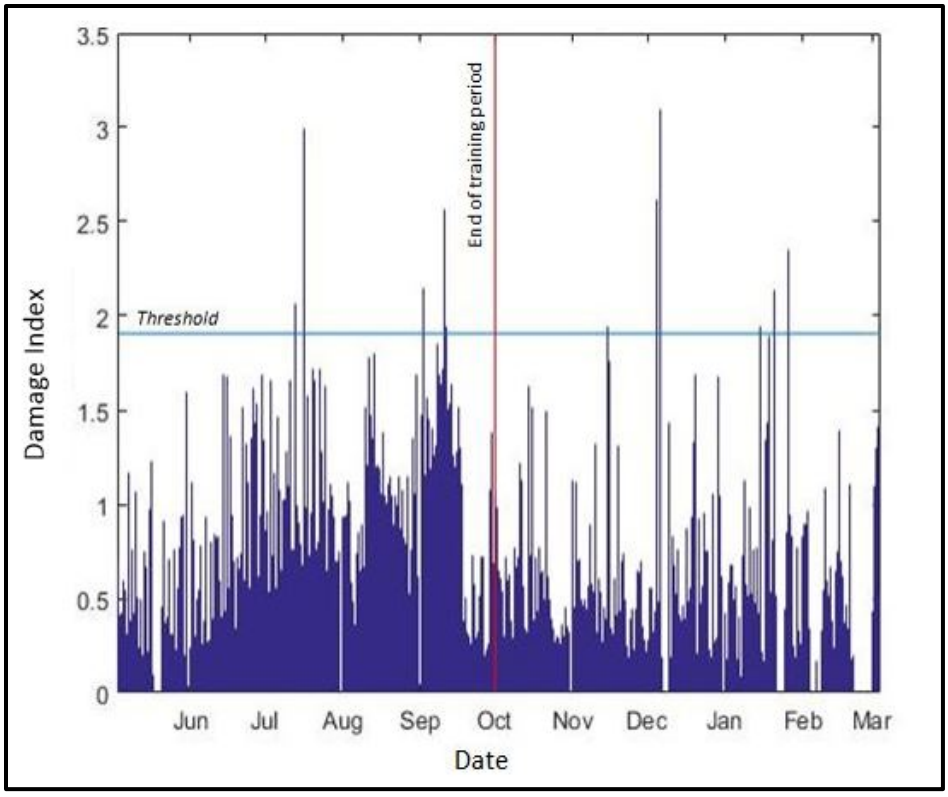

Figure 39. Plot of PCA damage index for undamaged case w/ 98% variance retained.

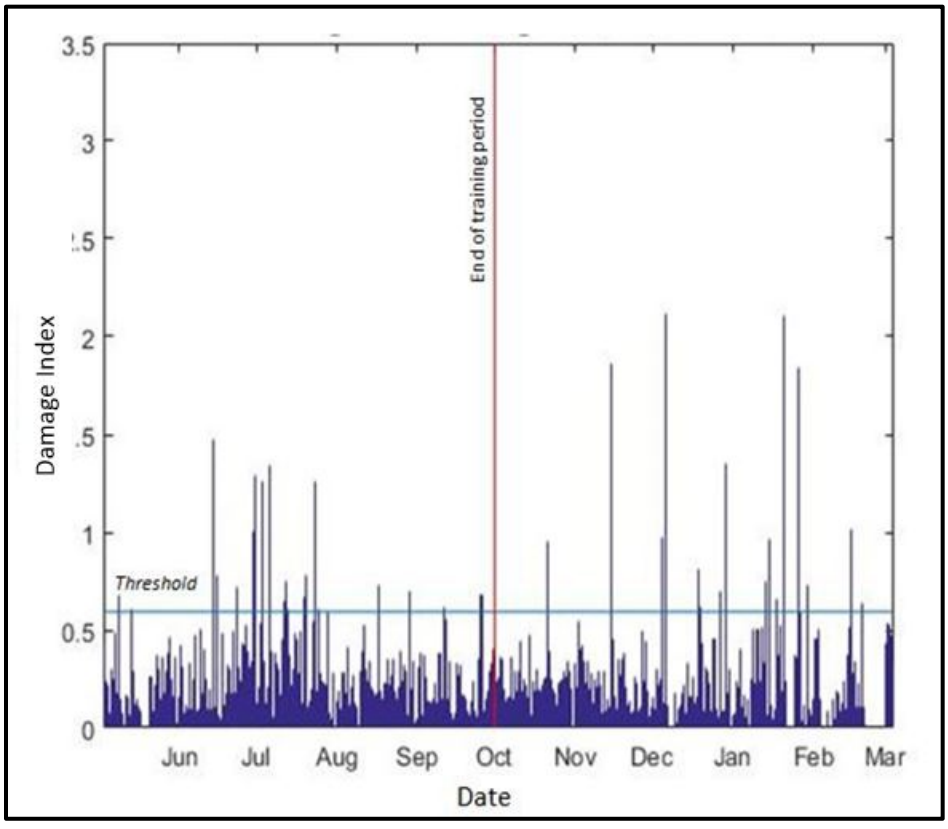

Table 7. Probability of false positives.

No. of Consecutive Observations for Damage Indication	Probability of occurrence	False Alarm Rate
2	1.77×10^{-4}	1 in 5,653 events
3	2.35×10^{-6}	1 in 425,000 events

As seen, the PCA damage index is a good feature for monitoring the healthy state of the structure, as the occurrence of false positives is small for two consecutive observations, and highly improbable for three observations. If there is an average of 10 lockages per day, the use of two consecutive observations to indicate damage would be expected to yield a false alarm once every 18 months for this gate. For three consecutive observations, a false alarm would be expected once every 116 years. To fully characterize the effectiveness of PCA, damage will be simulated in the FEM model and superimposed on the measured data. This simulated damage is then run through the PCA algorithm to check the efficacy of the proposed approach

5.7 FEM model for damage simulation

An existing ABAQUS finite element model created for a different gate of similar geometry was used to simulate damage on the Greenup gate. The model consists of approximately 500,000 reduced integration, linear Q4 shell elements per leaf. Figure 40 shows a visual representation of the model.

Figure 40. ABAQUS finite element model of a miter gate.

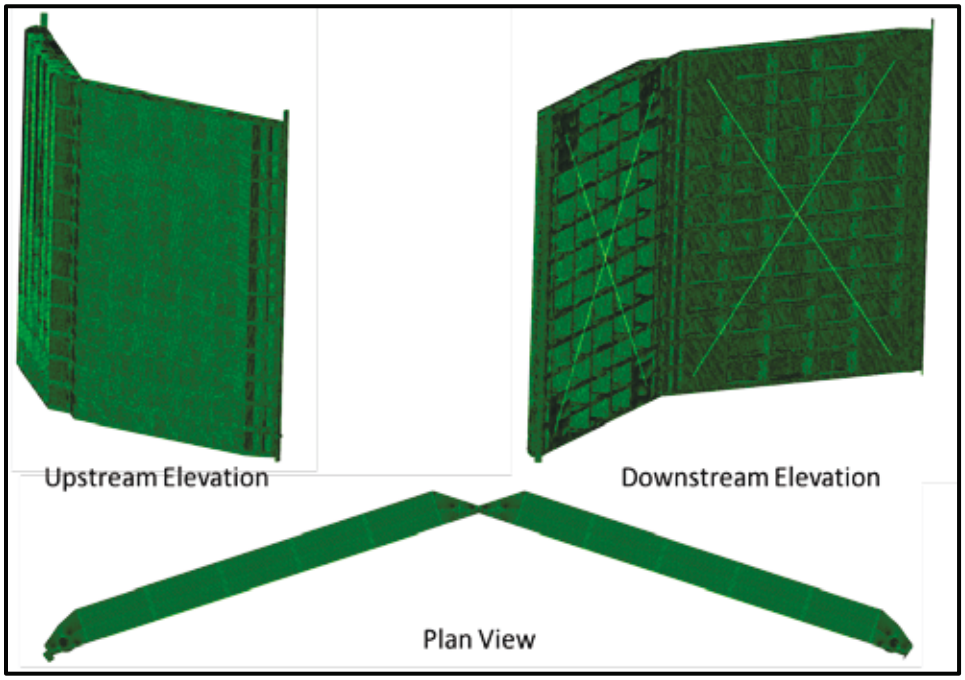

This model was designed using geometry specific to a different gate, namely Lock and Dam 27 on the Mississippi River. However, the difference in geometry between Greenup and Lock and Dam 27 is minimal. The gates are designed to transfer load in the same manner, and changes in behavior in one gate will be similar in the other gate under the same damage scenario.

5.8 Damage simulation using the FEM model

Locations in the FEM model that corresponded to the physical strain gage locations were selected for investigation of gate behavior. The strain at these locations was investigated for the undamaged case and the simulated damaged cases. Damage, in the form of a gate/wall gap, was simulated by removing a portion in the contact wall that forms a boundary condition in the model at the quoin near the pintle region. Figure 41 shows a schematic representing the location and reference dimensions for the gap; Table 8 lists the dimensions for the two cases considered.

Figure 41. Layout of where a gap was simulated, with reference dimensions "A" and "B."

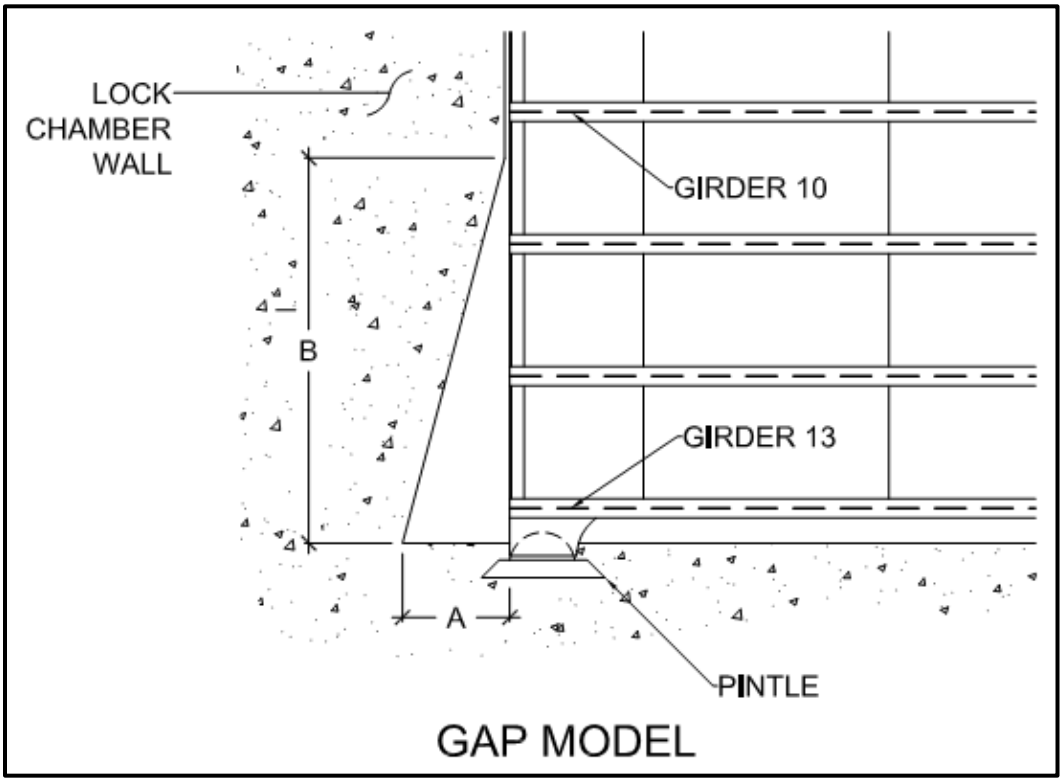

Table 8. Simulated gap dimensions.

Damage Case	"A" dimension	"B" dimension
1 – Small Gap	1/8 in.	7 ft.
2 – Large Gap	1/4 in.	12 ft.

Two differential head scenarios were used in the ABAQUS model for this study, one with an upstream water level of 70 ft. and downstream level of 14 ft., and one with an upstream water level of 50 ft. and downstream of 14 ft. Figure 42 shows a schematic showing the meaning of the differential head for the case of 14 to 50 ft.

Figure 42. Representation of differential head.

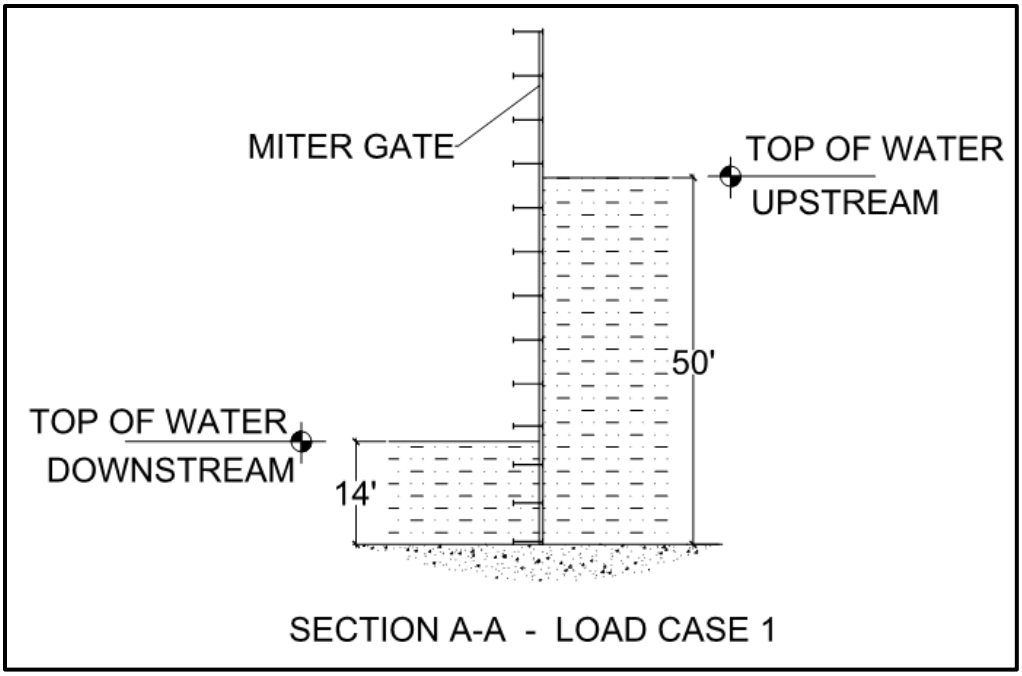

For the two cases, the ABAQUS model was manually inspected and the strain at each location of interest was recorded. As mentioned previously, the strain in the system is well approximated to behave linearly with respect to the water levels, so a line can be fit between the strain at one differential head case to arrive at the strain in the other. Accordingly, the reader can assume that the strain at an upstream water level of 14 ft. is zero at all gages. Table 9 lists the corresponding strain for the undamaged and two damage scenarios for the upstream level of 70 ft.

Table 9. Strain values taken from ABAQUS for upstream water level = 70 ft.

Gage Number	Undamaged Strain x 10^{-6}	Small Damage Strain x 10^{-6}	Large Damage Strain x 10^{-6}
S08-04	-667	-677	-711
S10-05	-775	-832	-1,092
S10-23	-72.6	−72.0	−74.4
S10-24	-72.6	−72.0	−74.4
S11-06	−869	−902	−186
S12-07	−1,590	−1,512	−1,806

Strain values from ABAQUS were recorded for only two differential head scenarios; however, infinitely many differential head scenarios are possible in practice. Thus, a systematic method was developed to superimpose the damaged strain onto the measured data in MATLAB. Because the difference in strain occurs approximately linearly with respect to water level, a linear relationship for the change in strain based on water levels was developed. The calculated slope for the change in strain was found by taking the difference in strain at 14 ft. to be zero, and using the absolute difference between the damaged scenario and undamaged scenario at 70 ft. to be the second point of the line. For example, consider Gage S08-04. For the large damage case, the absolute difference in strain between undamaged and damaged cases is -711με – (-667με) = -54με. The calculated value is used to create the slope of the linear relationship, knowing the range in water-levels to be 70 - 14=56 ft., and the intercept of the line was taken as the negative of this slope times 14 ft. Thus for Gage S08-04, the linear relationship between difference in damaged strain and water levels was found to be:

$$\Delta\bar{A} = \frac{-54\bar{A}\bar{A}}{56\bar{A}\bar{A}} h_{\bar{A}\,\bar{A}\bar{A}\bar{A}} + 11\bar{A}\bar{A} \qquad (5\text{-}1)$$

Thus, damage was able to be systematically added to the measured data. As an illustrative example, consider a hypothetical chamber event, with chamber water levels raising from 30 to 50 ft., and the strain ranging from -300με to -400με. The sampled water levels are input into Equation 5-1 to obtain the appropriate change in strain for the simulated damaged case. This change in strain is then added to the measured strain to get the simulated damaged response of the gage. Table 10 lists the hypothetical values.

Table 10. Example of simulated strain implementation.

Sampled water levels for fill event (ft.)	Measured strain (με)	Δε (Eq. 5-1) (με)	Simulated damaged strain (με)
30	–300	–17.93	–317.93
34	–320	–21.79	–341.79
38	–340	–25.64	–365.64
42	–360	–29.50	–389.50
46	–380	–33.36	–413.36
50	–400	–37.21	–437.21

Equation 5-1 is specific to Gage S08-04, and a similar linear relationship was developed for all other gages and implemented on the measured data as described above. The process was repeated considering four cases:

1. Difference in strain from small, sudden gap
2. Difference in strain from small, gradual gap
3. Difference in strain for large, sudden gap
4. Difference in strain for large, gradual gap.

For the gradual gap, the absolute difference in strain was linearly increased from zero to full measured intensity for the time during which damage was to be simulated. Thus, if damage is to be simulated on data from October through March, the change in strain was zero on October 1st, full intensity on March 31st, and linearly increasing between. Now that damage has been simulated, it remains to assess the ability of the PCA method to detect it.

5.9 Damage detection

To test the damage detection sensitivity, the two damage scenarios each for the large and small gap were superimposed on the real data using the dimensions listed in Table 8. The damage was added to the system by adjusting the strains using the location specific equations, such as Equation 5-1. The trained PCA eigenvectors, as found in Section 5.6, were used and the four cases listed in Section 5.8 for damage simulation were tested. For the sudden formation of a gap, the data were left undamaged until December 1st, when the full extent of change in strain was implemented on the measured data. The gradual gap was imposed over the full period from October to March as noted in Section 5.8. Note that in the following plots, the gaps seen in the data are a byproduct of the "event-based algorithm" noted in Section 4.4. Flood events occurred at these times leading to insufficient differential head on the gate, so no valuable data were collected during these periods.

5.9.1 Case 1: Small, sudden gap

For case 1, the change in strain caused by the small gap was imposed on the measured data suddenly and at full intensity on December 1st. Figures 43 and 44, respectively, show the results for retaining both 92 and 98% of the variance in the PCA algorithm. In the plots, the red vertical line represents when training the algorithm stopped, and the blue vertical line represents when damage was introduced. The horizontal line represents the threshold, above which damage will be indicated.

As seen, for the case using 92% variance, one false positive in the untrained, undamaged data is observed in the middle of November if two consecutive observations are considered as damage indication. If three consecutive observations are required, no false positives are observed. After damage is introduced, multiple indications of its presence are observed, however, a wealth of false negatives are also present.

Figure 43. Small, sudden gap detection, 92% variance.

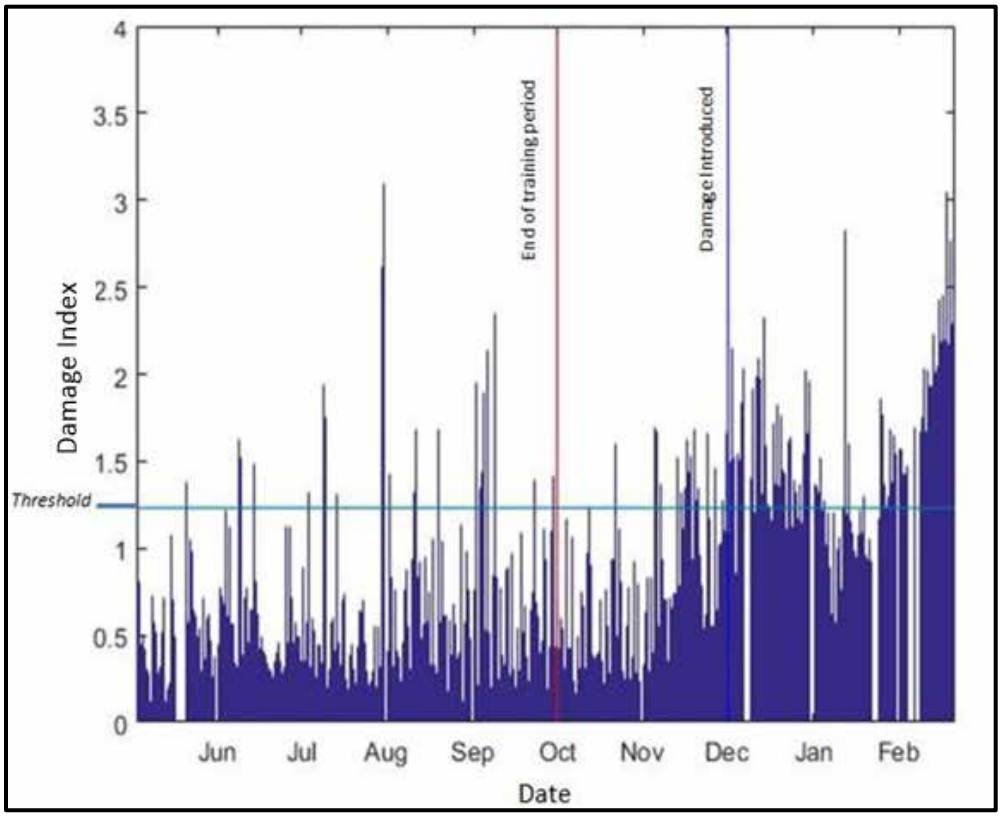

Figure 44. Small, sudden gap detection, 98% variance.

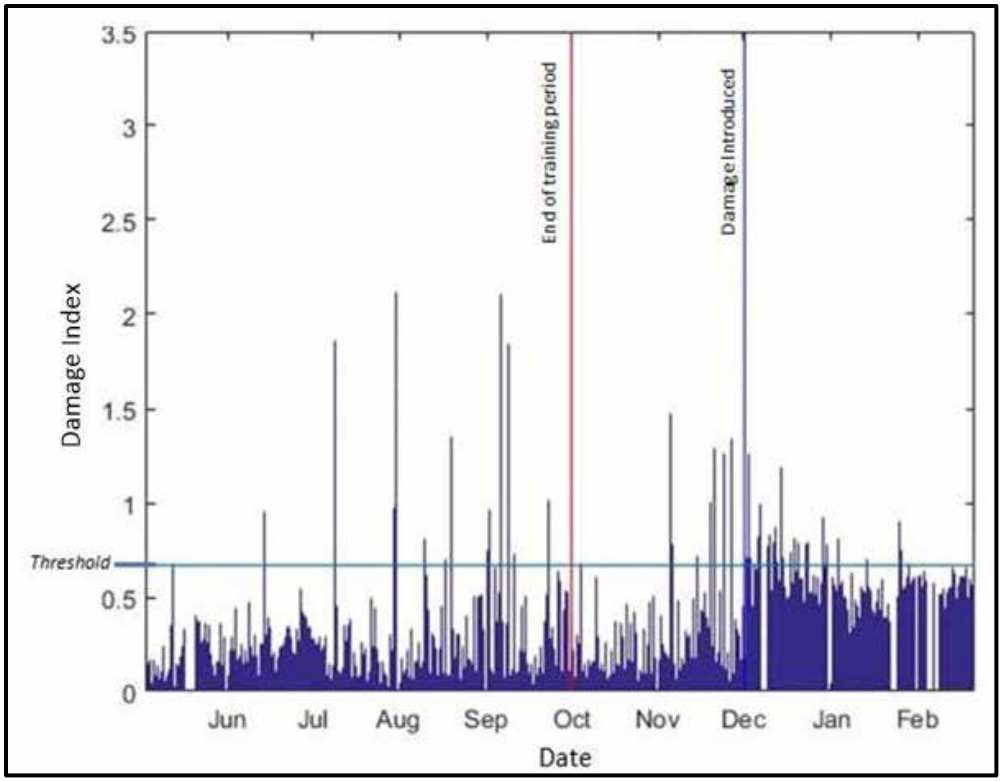

For 98% variance maintained, no false positives in the untrained, undamaged data are observed. However, once damage is introduced, only four occurrences of two consecutive observances above the threshold are present and only two occurrences of three consecutive observations. Thus, the 98% variance case is almost exclusively false negatives.

5.9.2 Case 2: Small, gradual gap

For this scenario, the change in strain caused by the small gap case was superimposed gradually on the data, starting at the point where the training data stopped, and increasing the change in strain to full magnitude at the end of the sampled data. Figures 45 and 46, respectively, show the plots for 92 and 98% variance retained.

Figure 45. Small, gradual gap detection at 92% variance.

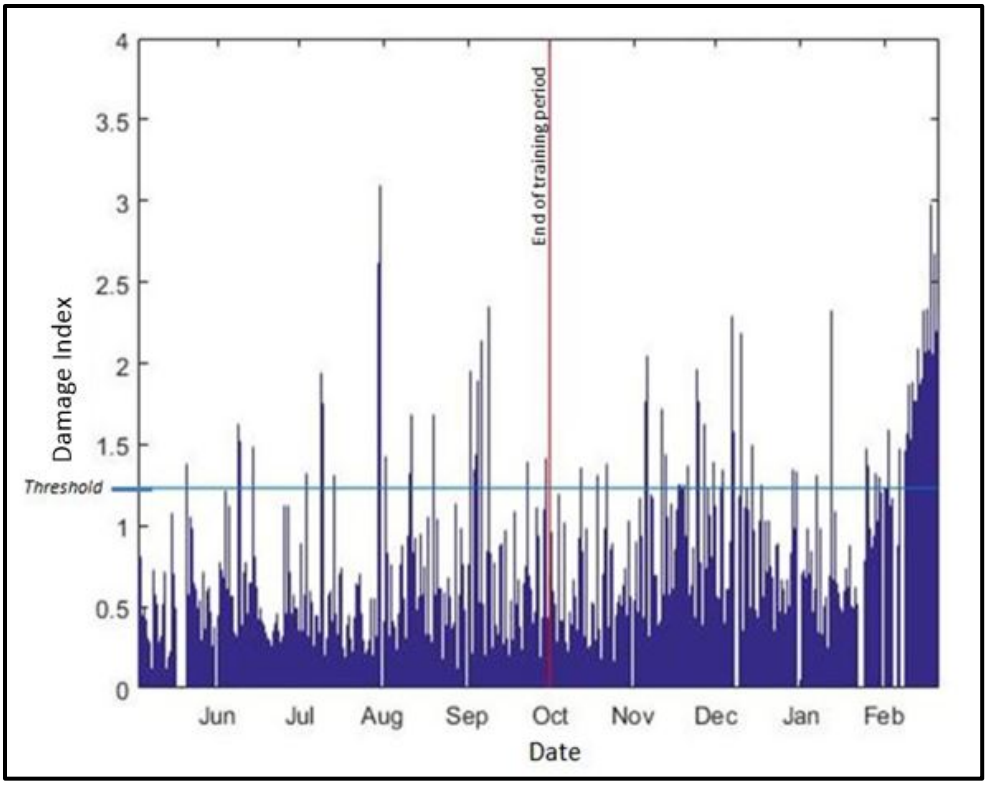

Figure 46. Small, gradual gap detection at 98% variance.

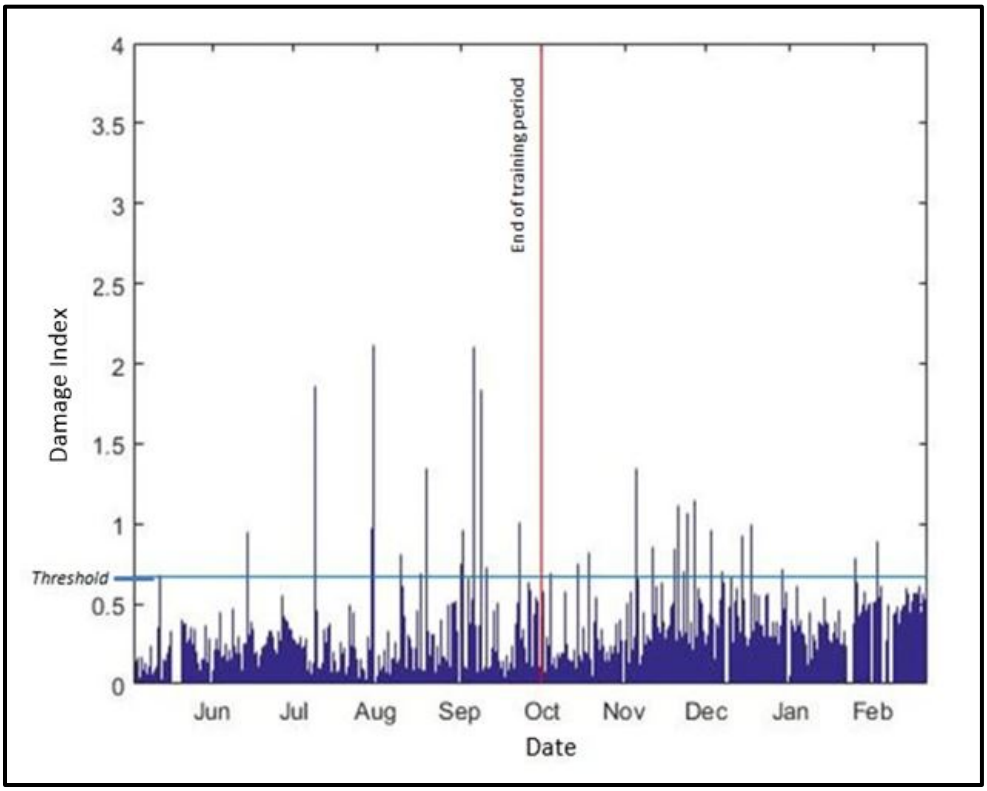

For this case, after the training data, some damage is always imposed on the gate; therefore, false positives are not possible. For the 92% variance case, damage is not indicated until the damage is almost at full intensity, at which case, damage is readily indicated. For the 98% variance case, damage is never indicated; therefore, the threshold for this case is too insensitive for this damage scenario

5.9.3 Case 3: Large, sudden gap

Case 3 is identical to Case 1 with the exception that the damage that is suddenly imposed is the simulated large gap. Figures 47 and 48, respectively, show the results using 92 and 98% variance.

As seen, the large gap is readily detected by both PCA cases. Before damage occurs, a false positive for the 92% variance identical to that seen in Case 1 is observed. After damage is introduced, no false negatives for either case are observed.

Figure 47. Large, sudden gap detection at 92% variance.

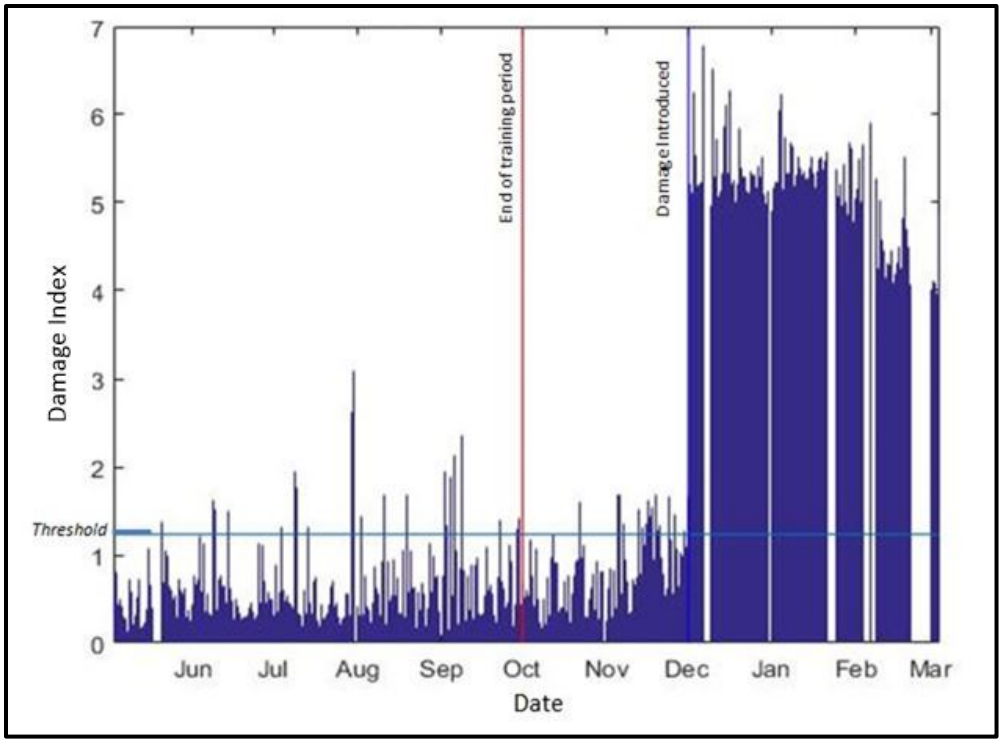

Figure 48. Large, sudden gap detection at 98% variance.

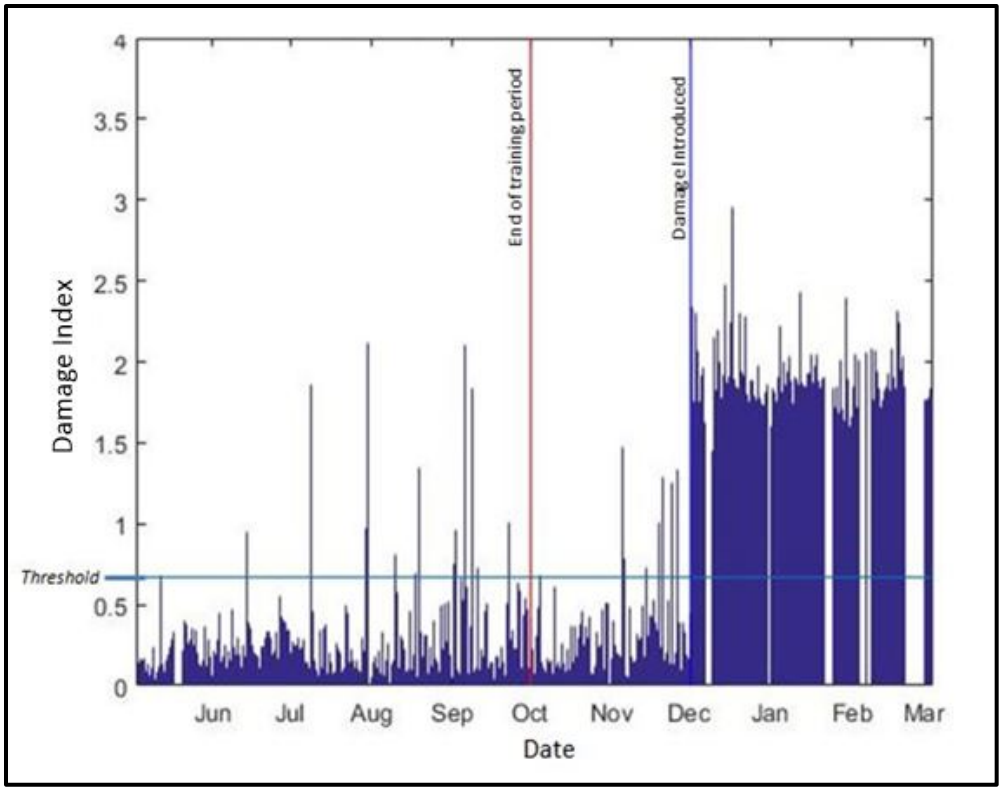

5.9.4 Case 4: Large, gradual gap

Case 4 is identical to Case 3 with the exception that the change in strain from the large gap is gradually imposed on the measured data. Figures 49 and 50, respectively, show the results for retaining 92 and 98% variance.

As seen, both PCA approaches perform similarly for the large, gradual gap case. Damage is readily and consistently indicated after about a quarter of its intensity is introduced.

Figure 49. Large, gradual gap detection at 92% variance.

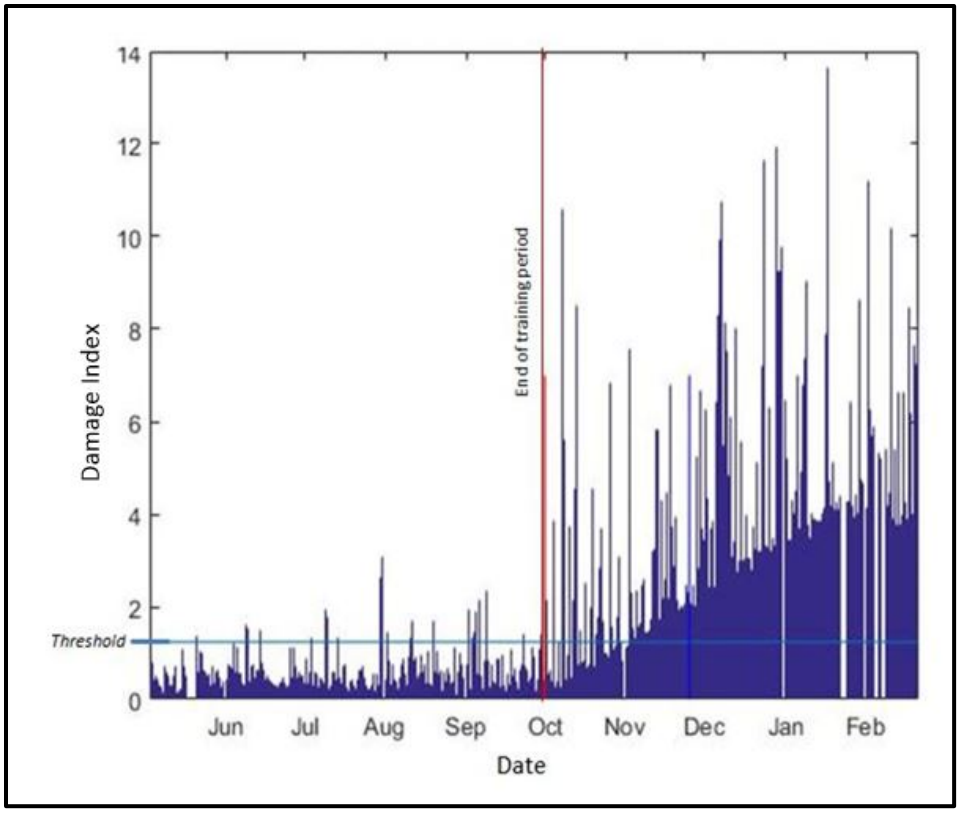

Figure 50. Large, gradual gap detection at 98% variance.

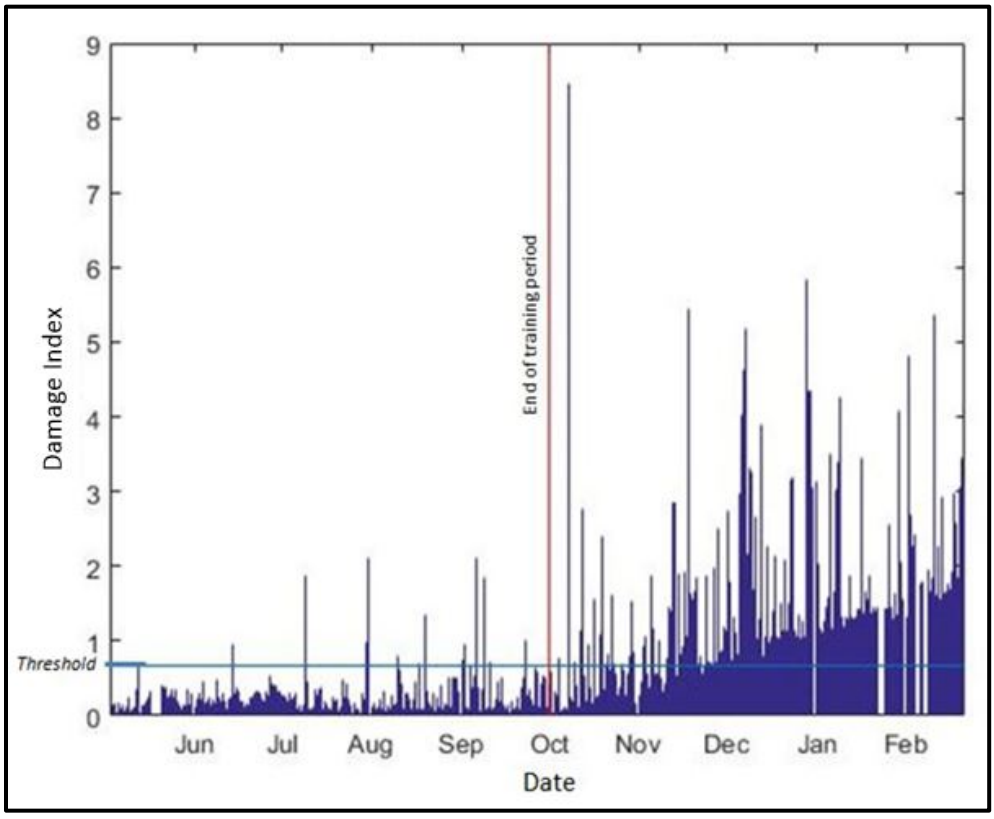

5.10 Summary

This chapter provided an example of gap detection between the gate and wall for the lock and dam located at Greenup. The instrumentation at Greenup was labeled, and the data acquisition parameters were presented. The method of processing and cleaning the data was explained. The measured Greenup data were shown to support the assumptions taken here of slope stationarity, and of the lack of correlation with temperature and normal distribution. An existing FEM model for a similar gate was used to simulated gate behavior and strain response under load for both damaged and undamaged cases. The method of imposing damage on the measured data was explained as were the two different damage scenarios considered. Finally, the damage indices from the PCA method were used as a method to detect damage. Two PCA approaches were used to compare the sensitivity of the method: a damage index formed by retaining 92% variance in the system, and one by retaining 98% variance. The PCA damage indices were seen to readily indicate the presence of a large gap in the gate/wall interface. They were less sensitive to the presence of a small gap, but the 92% variance approach was able to provide indications of damage present.

6 Conclusions

This study presented initial efforts to develop the necessary knowledge and understanding required for the monitoring of miter gates of navigational locks. Waterway navigational locks are an important part of the national infrastructure that enable the flow of billions of dollars of commerce and support efforts for flood control. The gates of the navigational locks are one of the most vulnerable and maintenance intensive parts of the lock and have been the leading cause of scheduled and unscheduled lock maintenance events.

Miter gates are the most widely found lock gate type in the inventory of USACE locks. Gaps at the gate/wall interface are of critical importance in that they cause a redistribution of loads, which is known to lead to premature fatigue failure in critical gate components. To circumvent the need for costly dewatering or underwater inspections to determine the condition of gates, a structural health monitoring program, known as SMART Gate, has been implemented on six sets of lock gates maintained by the USACE. This research first identified a new damage sensitive feature for detecting gaps at the gate/wall interface; subsequently, appropriate sensors were selected for gap detection, and finally PCA was applied as the method to detect damage. The results demonstrate the efficacy of the PCA method for detecting even small gaps at the gate/quoin interface. The main findings of this research are summarized in the remainder of this chapter.

6.1.1 Selection of a damage sensitive feature

Among the wealth of data available in the SMART Gate database, strain data are the most applicable to the task of detecting a gap in the gate/wall interface. However, multiple issues related to the direct use of strain were identified, such as nonstationarity, long periods of non-informative information, environmental effects, etc. The derivative of the strain data with respect to the water level in the gate chamber, slope, was identified as an effective damage sensitive feature. The time series comprised of slope data was shown to be nominally stationary and independent of temperature effects. Moreover, the slope time series has significantly fewer samples than the strain time series, reducing computation time. Therefore, for the task of gap detection, slope is selected as the damage sensitive feature to be analyzed.

6.1.2 Selection of gate instrumentation

The sites being monitored by the SMART Gate system have up to hundreds of gages scattered about the different gates providing an overwhelming amount of data. To facilitate and simplify a damage detection strategy, the gages exhibiting strains that are sensitive to the presence of gaps at the gate/wall interface were selected. A correlation study showed that gages near the top of the gate are generally uncorrelated to any of the other data available in the database, suggesting that their behavior is somewhat unpredictable. In contrast, gages near the bottom of the gate are highly correlated to water levels and to other gages near the bottom. This correlation suggests that gages near the bottom will behave in a predictable manner and are the ideal candidates to include in a damage detection algorithm. Finally, the damage simulation in the FEM model showed that the effect of a gap attenuates quickly the further away a gage is from the gap.

Gaps can occur anywhere along the quoin area. However, the gaps of most concern are those located near the bottom of the gate because the gate is subjected to larger loads at this location. Thus, the selection of gages was further narrowed down. For the detection of a gate/wall gap, gages need to be both near the bottom of the gate and near the quoin. An additional finding in this study was that, for these findings to be implemented, all of the gages in the gate must be synchronized in time. The investigation into the strain behavior of Lock 27 revealed that a time delay in between strain readings and water level readings may produce results with an apparent nonlinear behavior and/or hysteresis in the system. Thus, for the success of this methodology, the instrumentation on the gate must be time synchronized.

6.1.3 Development of a gap detection algorithm

Chapter 5 showed that the damage indices of the PCA method are sensitive to the presence of a gap. The sensitivity of the algorithm is dependent on the amount of variance retained in the system when training the eigenvectors as well as the selection of an appropriate threshold. Among the two training schemes tested, the 92% variance (that is, using the eigenvectors corresponding to the three directions with the three highest variances) was more sensitive to the presence of damage than was the 98% variance (using all but the eigenvector that describes the least variance). This makes sense, as the model with less information of the system would be more sensitive to small changes in the system. The optimal choice of variance to retain in the system should be seen as a parameter to be chosen based on the specific

requirements of the system to be monitored. Also important is that, as seen in Section 5.6, the PCA method works well in monitoring the gate in the absence of damage in that no false positives are shown when damage was not imposed on the gate.

False positives occasionally occur and need to be addressed. For example, the threshold can be raised for indicating damage. Raising the threshold will make the algorithm less sensitive, but the threshold can be determined based on a qualitative assessment of what "critical" damage is. A different method would be to increase the number of consecutive observations required above the threshold to be considered an indication of damage. For this study, there was never a false positive consisting of more than three consecutive observations. False negatives were a bigger problem, particularly for the 98% variance approach with a small gap. For this approach to work, the threshold would have to be lowered, but then, the false positives would likely increase in the absence of damage.

Once the gap reaches a certain level, just above the size of the small gap considered, the damage index is able to readily and reliably detect the damage, as seen in the results for the large, gradual gap. Thus, this study concludes that PCA is an effective algorithm for detecting gaps in miter gates.

The success of this study provides a firm foundation on which to build practically deployable structural health monitoring systems for miter-gates operated by USACE.

7 Future Work

SHM is to be the backbone of a larger *consequence model* being developed by USACE-ERDC. SHM will provide the data necessary to assess the current state of a structure and determine possible repair or maintenance alternatives. Combining the data with probabilistic degradation and future loading models, a probabilistic assessment of the future condition of the structure is made. A value metric is then imposed on each action alternative, and in this way, maintenance and repair of structures is prioritized and use of available funding is optimized. Next steps for realizing an SHM program to fully characterize the state of a lock gate include developing methods for damage localization, determining the extent of damage, and determining the remaining life in the structure.

7.1 Damage localization

It is expected that the PCA method will be able to determine the location of a gap. As discussed, the effects on strain caused by a gap attenuate quickly the further the gage is from the gap. Thus, the expectation is that the location of a gap can be determined by inspecting the gage that is causing the highest change in variance in the system. This will likely manifest itself as a higher value in the residual for that degree of freedom before taking the square root sum of squares. To investigate damage localization, more FEM simulations of gaps at various locations are needed.

7.2 Damage intensity

As seen, the change in the PCA residual is very sensitive to the size of the damage on the gate. For a larger gap, a larger deviation from normal behavior is observed manifesting itself as a larger PCA residual. Thus a correlation between PCA residual magnitude and size of damage will be made. More FEM simulations of gaps of different sizes are needed to identify damage intensity.

7.3 Remaining service life

Assessing the remaining life in the structure may be perhaps the most challenging question to solve using this approach. To accomplish remaining life estimations, a detailed investigation of design practices will be done. Of particular interest will the investigation into the design approach for fatigue, and the particular S-N curves used in miter gate design. Then,

the extent and location of damage will be used to determine the new expected cycles before failure in fatigue critical components. The number of cycles will be correlated to remaining life based on average number of lockages in a day.

References

Akaike, H. 1974. A new look at the statistical model identification. *IEE Transaction on Automatic Control*.

American Society of Civil Engineers (ASCE). 2013. *2013 Report Card for America's Infrastructure*. Reston, CA: ASCE.

Ang, A. H.-S., and W. H. Tang. 2007. *Probability Concepts in Engineering: Emphasis on Applications to Civil and Environmental Engineering*. Hoboken,NJ: Wiley.

Chapman, B. 2010. *Markland and Greenup Gate Failures*. Springfield, VA: USACE.

———. *2013 Tough Challenges Ahead: The Navigation Infrastructure'*. Huntington, WV: USACE.

Commander, B. C., J. X. Schulz, and G. G. Goble. 1994. *Detection of Structural Damage on Miter Gates*. Vicksburg, MS: USACE Waterways Experiment Station.

Cross, E. J. 2012. *On Structural Health Monitoring in Changing Environmental and Operational Conditions*. Sheffield, UK: University of Sheffield.

D. Murray. 2014. Chickamauga lock shut down for emergency repairs. *The Waterways Journal Weekly*.

Estes, A. C., D. M. Frangopol, and S. D. Foltz. 2004. Updating reliability of steel miter gates on locks and dams using visual inspection results. *Engineering Structures* 26:319-333.

Farrar, C. R. 2012. *Structural Health Monitoring: A Machine Learning Perspective*. Hoboken, NJ: Wiley and Sons.

Figueiredo, E., G. Park, J. Figueiras, C. Farrar and K. Worden. 2009. *Structural Health Monitoring Algorithm Comparisons Using Standard Datasets*. Los Alamos,NM: Los Alamos National Laboratory.

Fuller, W. 1995. *Introduction to Statistical Time Series*. Hoboken, NJ: Wiley and Sons.

Gillerman, M. 2013. Barge traffic moving again on Mississippi River. *St. Louis Post Dispatch,* 23 January 2013.

Greimann, L., J. Stecker, and K. Rens. 1991. Inspection and rating of miter lock gates: Repair, evaluation, maintenance, and rehabilitation research program. *Journal of Performance of Constructed Facilities* 5(4)226-238.

Hamilton, J. D., 1994. *Time Series Analysis*. Princeton, NJ: Princeton University Press.

James, R. J., and L. Zhang. 1996. *Fatigue Cracking Evaluation of the Markland Miter Gates*, San Diego, CA: ANATECH Corp.

Johansen, S. 1996. *Likelihood-Based Inference in Cointegrated Vector Autorregressive Models*. Oxford, UK: Oxford University Press.

MathWorks. 2004. Linear prediction and autoregressive modeling. *MathWorks*. Web site. Accessed 15 June 2016, http://www.mathworks.com/help/signal/examples/linear-prediction-and-autoregressive-modeling.html

———. 2016. Econometrics toolbox user's guide. *MathWorks*. Web site. Accessed 15 June 2016, http://www.mathworks.com/help/pdf_doc/econ/econ.pdf

McAllister, T. P., and B. R. Ellingwood. 2001. Reliability-based condition assessment of welded miter gate structures. *Journal of Infrastructure Systems* 7:95-106.

Missouri Department of Natural Resources (MDNR). 2004. *Locks and Dams and River Navigation - History of the Mississippi River Navigation System*. Jefferson City, MO: MDNR.

National Institute of Standarads and Technology (NIST). 2013. *Engineering Statistics Handbook*. Web page. Accessed 21 June 2016, http://www.itl.nist.gov/div898/handbook/eda/section3/eda3666.htm

Panik, M. 2009. *Regression Modeling: Methods, Theory, and Computation with SAS*. Boca Raton, FL: CRC Press.

Prado, R., and M. West. 2010. Notation, definitions and basic inference. *Time Series: Modeling, Computation, and Inference*. Ch. 1. Boca Raton, FL: CRC Press, pp 3-88.

Rankin, M. 2014. Maintenance makeover drains Wheeler Lock. *Distric Digest*. 29 October 2014.

Rytter, A. 1993. *Vibration Based Inspection of Civil Engineering Structures*. Aalborg, Denmark: Aalborg University.

Steigerwald, D. G. 2009. *241B Lecture, Ergodic Stationarity*. Accessed 09 June 2016, http://econ.ucsb.edu/~doug/241b/Lectures/10%20Ergodic%20Stationarity.pdf

U.S. Army Corps of Engineers (USACE). 2014. *Lock Characteristics General Report*. Vicksburg, MS: USACE.

———. 2015. *Upper Mississippi River Locks and Dams*. Vicksburg, MS: USACE.

———. 2016. *Technologies to Extend the Life of Existing Infrastructure*. Vicksburg, MS: USACE.

Zivot, Eric. 2015. Time Series Concepts. Ch 1. Accessed 8 June 2016, http://faculty.washington.edu/ezivot/econ424/timeseriesconcepts.pdf

Acronyms and Abbreviations

Term	Definition
ADF	Augmented Dickey-Fuller (test)
AIC	Akaike Information Criterion
ANSI	American National Standards Institute
AR	Autoregressive
ASCE	American Society of Civil Engineers
CDF	Cumulative Distribution Function
CEERD	U.S. Army Corps of Engineers, Engineer Research and Development Center
CERL	Construction Engineering Research Laboratory
COV	Coefficient of Variation
DI	Damage Index
ERDC	U.S. Army Engineer Research and Development Center
ERDC-CERL	Engineer Research and Development Center, Construction Engineering Research Laboratory
FEM	Finite Element Model
GDP	Gross Domestic Product
HQUSACE	Headquarters, U.S. Army Corps of Engineers
IEE	Institution of Electrical Engineers
MDNR	Missouri Department of Natural Resources
NIST	National Institute of Standards and Technology
NSN	National Supply Number
OLS	Ordinary Least Squares
OMB	Office of Management and Budget
PCA	Principal Component Analysis
SAR	Same As Report
SAS	Statistical Analysis Software
SF	Standard Form
SHM	Structural Health Monitoring
SMART	Structural Monitoring and Analysis in Real Time
TR	Technical Report
USACE	U.S. Army Corps of Engineers

REPORT DOCUMENTATION PAGE

Form Approved
OMB No. 0704-0188

1. REPORT DATE (DD-MM-YYYY)	2. REPORT TYPE	3. DATES COVERED (From - To)
04/11/2018	Final	

4. TITLE AND SUBTITLE
Miter Gate Gap Detection Using Principal Component Analysis

5a. CONTRACT NUMBER

5b. GRANT NUMBER

5c. PROGRAM ELEMENT
Navigation Systems Research Program

6. AUTHOR(S)
Brian A. Eick, Zachary R. Treece, Billie F. Spencer Jr., Matthew D. Smith, Steven C. Sweeney, Quincy G. Alexander, and Stuart D. Foltz

5d. PROJECT NUMBER

5e. TASK NUMBER

5f. WORK UNIT NUMBER

7. PERFORMING ORGANIZATION NAME(S) AND ADDRESS(ES)
U.S. Army Engineer Research and Development Center (ERDC)
Construction Engineering Research Laboratory (CERL)
PO Box 9005,
Champaign, IL 61826-9005

8. PERFORMING ORGANIZATION REPORT NUMBER
ERDC TR-18-2

9. SPONSORING / MONITORING AGENCY NAME(S) AND ADDRESS(ES)
Headquarters, U.S. Army Corps of Engineers (HQUSACE)
41 G St., NW
Washington, DC 20314-1000

10. SPONSOR/MONITOR'S ACRONYM(S)
CEERD-HT

11. SPONSOR/MONITOR'S REPORT NUMBER(S)

12. DISTRIBUTION / AVAILABILITY STATEMENT
Approved for public release; distribution is unlimited.

13. SUPPLEMENTARY NOTES

14. ABSTRACT

The U.S. Army Corps of Engineers (USACE) operates and maintains 236 lock chambers at 191 lock sites on 41 waterways throughout the contiguous United States. Waterway navigational locks are important parts of the nation's infrastructure. Locks enable the flow of billions of dollars of commerce and support efforts for flood control. Proper maintenance of the locks and early detection of damage is crucial; however, due to shrinking budgets, adequate funding to apply traditional scheduled maintenance and visual inspection is not available. Structural health monitoring (SHM) systems have been considered to assist in establishing more efficient maintenance, repair, and replacement priorities for navigational locks. This work was undertaken to develop and implement a real-time methodology that provides lock operators with a robust, accurate warning system of gap(s) at the gate-to-wall interface. This initial effort, which focused on horizontally framed miter gates and on damage that is assumed to take the form of a gap at the gate/wall interface (quoin), developed a methodology to identify the occurrence of damage in miter gate structures using data from strain and water level gages that is collected continuously from the SHM system deployed by USACE.

15. SUBJECT TERMS
Hydraulic structures--Maintenance and repair, Locks (Hydraulic engineering), Hydraulic gates, Structural analysis (Engineering), Structural failures--Mathematical models

16. SECURITY CLASSIFICATION OF:			17. LIMITATION OF ABSTRACT	18. NUMBER OF PAGES	19a. NAME OF RESPONSIBLE PERSON
a. REPORT	b. ABSTRACT	c. THIS PAGE			19b. TELEPHONE NUMBER (include area code)
Unclassified	Unclassified	Unclassified	SAR	95	